ZfK – 562

# PROCEEDINGS

## of the XIV-th International Symposium on the Interaction of Fast Neutrons with Nuclei

**– Neutron Generators and Application –**

organized by

**the Technical University of Dresden**
**November 19–23, 1984 in Gaussig (GDR)**

edited by

D. Seeliger and U. Jahn

Juli 1985

Postanschrift: Akademie der Wissenschaften der DDR
Zentralinstitut für Kernforschung Rossendorf
8051 Dresden
Postfach 19 Deutsche Demokratische Republik

Diese Publikation wurde in der Abteilung Literatur und Information des Zentralinstitutes für Kernforschung hergestellt

AKADEMIE DER WISSENSCHAFTEN DER DDR

Z E N T R A L I N S T I T U T  F Ü R  K E R N F O R S C H U N G

R O S S E N D O R F  B E I  D R E S D E N

ZfK - 562

# PROCEEDINGS

of the XIV-th International Symposium

on the Interaction

of Fast Neutrons with Nuclei

- Neutron Generators and Application -

organized by

the Technical University of Dresden

November 19 -23, 1984 in Gaussig (GDR)

edited by

D. Seeliger and U. Jahn

Juli 1985

## Preface

The traditional international symposia on the interaction of fast neutrons with nuclei are organized every year by the Section of Physics of the Technical University in Dresden. The XIV$^{th}$ Symposium was devoted to current problems of intense fast neutron sources, especially 14 MeV DT-neutron generators, and their broad spectrum of application in nuclear physics. 56 participants from 12 countries and the IAEA demonstrate the high interest on this selected topics. The submitted contributions can be divided into two general parts. The first one gives a review about the different possibilities of the technical and technological solution in development, the present status of operation and also the problems connected with the use of intense neutron sources. Various experimental arrangements for neutron spectroscopy, determination of nuclear data and theoretical aspects are the content of the second part. The participation in this meeting of designer and operators on the one hand and users of neutron sources on the other hand was a good choice and stimulated productive discussions during the conference. The editors hope that the publication of more than thirty contributions on the XIV$^{th}$ Gaussig-Symposium is useful for further works.

The editors

Organizing Committee: D. Seeliger
D. Schmidt
U. Jahn
E. Paffrath
U. Kaiser

Technical University Dresden
Section of Physics
Division of Nuclear Physics

ACKNOWLEDGEMENTS

The organizing committee would like to thank all participants especially the lecturers and chairmen for their effort and active discussions during the symposium. The committee expresses the thanks to the International Department of the Technical University Dresden for the valueable support and to the staff of the rest home in Gaussig for the comfortable conditions. Moreover, the committee is obliged to the Central Institute of Nuclear Research in Rossendorf for the publication of the Proceedings of the XIV$^{th}$ Symposium.

Organizing Committee

TABLE OF CONTENTS

Page

LIST OF PARTICIPANTS 1

I. INTENSE NEUTRON SOURCES

Комплекс источников нейтронов на основе протонных пучков московской мезонной фабрики 3
Ю.Я. Стависский

KARIN - a sealed high power generator tube of 14 MeV neutrons for radiotherapy , activation analysis and neutronic applications 8
K.A. Schmidt

Rotating target neutron source-II: Facility and experimental program x)
J.C. Davis

Design of a $10^{12}$ n/s compact neutron generator 9
Sun Biehe

The intense neutron generator concept in Debrecen 10
T. Sztaricskai

Intense neutron generator development at the institute of physics 15
J. Pivarč

*Design of a multi-purpose intense neutron generator* 24
D. Schmidt

II. ION BEAM HANDLING

Ионно-оптические свойства ускоряющей трубки нейтронного генератора 30
С.В. Бажал

A Duoplasmatron source for the production of intense d ion currents 33
Sun Biehe

A 300 ke compact neutron generator 40
Sun Biehe

Ionoptical calculations of the intense neutron generator INGE-1 46
U. Jahn

Extraction-process calculation for a duoplasmatron ion source 50
J. Dietrich

Experimental investigations of duoplasmatron ion source 52
A. Tunia

Beam monitor developments at the Rossendorf Cyclotron 56
H. Büttig

III. TECHNICAL EQUIPEMENT AND COMPONENTS RELATED TO INTENSE NEUTRON GENERATORS

The vacuum system of the intense neutron generator INGE-1 — 59
E. Paffrath

Computer control of the neutron generator INGE-1 — 63
P. Eckstein

Radiation protection problems with tritium in high flux neutron generators (HNG) — 68
B. Lorenz

An evaluation of neutron yields from thick titanium-tritium-targets under deuteron bombardment — 71
H. Helfer

Isolating transformer IT 300 for 300 kV and 10 kVA — 74
J. Pivarč

The current stabilizer for analyzing magnets in small accelerators — 78
A. Bieńkowski

Transmission of 14 MeV neutrons by shielding slabs — 80
O. Pentchev

IV. NEUTRON PHYSICS INVESTIGATIONS

Транспорт нейтронов никелем сравнение экспериментального и расчетного решения — 82
И. Буриан

Measurement of neutron leakage spectra from a lead sphere fed with 14 MeV neutrons — 85
K. Seidel

Lead slowing down neutron spectrometer — 90
A. Górski

Применение интенсивных фильтрованных пучков нейтронов для физических исследований — 93
В.П. Вертебный

Аномальные значения моментов инерции ядер, получаемые при анализе спектров нейтронов из реакций (p,n ) и (n,n' ). — 95
О.А. Сальников

Some questions of composition of neutron spectra and their solution — x)
KH. YA. Bondars

Selection of optimal sets of activation detectors for investigation of a 14 MeV neutron source — x)
KH. YA. Bondars

Мгновенные нейтроны низкоэнергетического деления атомных ядер 103
В.А. Рубченя

Evidence of the instable super heavy isotope 6-hydrogen in the reaction $^{7}Li(^{7}Li,^{8}B)$ x)
D.V. Aleksandrov

Measurement and interpretation of double-differential neutron emission cross sections from lead at 14 MeV 110
S. Unholzer

Complexity of angular dependence of scattered fast neutrons - consequences and recommendations for measurement and application of data 113
D. Hermsdorf

Analysis by radioactivation using 14.8 MeV neutrons applied to exploration of mineral resources 122
I. Gârlea

Neutron cross sections measured at 14.8 MeV 126
I. Gârlea

Fast neutron sources for therapy 129
J. Vincour

x) contribution not submitted

LIST OF PARTICIPANTS

| | | |
|---|---|---|
| Albert, D. | ZfK Rossendorf | GDR |
| Aleksandrov, D. | IAE Moscow | USSR |
| Bach, L.B. | IAEA Vienna | VIETNAM |
| Bazhal, S. | PEI Obninsk | USSR |
| Berkes, I. | Kossuth Univ. Debrecen | HUNGARY |
| Biehe, S. | Lanzhou Univ. | P.R. China |
| Bienkowski, A. | INR Warsaw | POLAND |
| Bondars, H. | Latvian State Univ. Riga | USSR |
| Burian, J. | INR Rez | CSSR |
| Büttig, H. | ZfK Rossendorf | GDR |
| Davis, J.C. | LLNL Livermore | USA |
| Desdin, L.F. | INR Havana | CUBA |
| Dietrich, J. | ZfK Rossendorf | GDR |
| Eckstein, P. | TU Dresden | GDR |
| Elfruth, T. | TU Dresden | GDR |
| Förster, H. | FNE Freiberg | GDR |
| Gandarias, D. | IAEA Vienna | CUBA |
| Garlea, I. | CIP Bucharest | ROMANIA |
| Gerhardt, K. | MKD Dresden | GDR |
| Gleisberg, F. | TU Dresden | GDR |
| Gorski, A. | Univ. Lodz | POLAND |
| Guratzsch, H. | ZfK Rossendorf | GDR |
| Helfer, H. | TU Dresden | GDR |
| Hentschel, R. | ZFTM Dresden | GDR |
| Hermsdorf, D. | TU Dresden | GDR |
| Jahn, U. | TU Dresden | GDR |
| Janssen, D. | ZfK Rossendorf | GDR |
| Kaminski, E. | INR Warsaw | POLAND |
| Krause, R. | TU Dresden | GDR |
| Letz, B. | ZfI Leipzig | GDR |
| Lohse, H. | ZFTM Dresden | GDR |
| Lorenz, B. | SAAS Berlin | GDR |
| Märten, H. | TU Dresden | GDR |
| Meinel, R. | ZfK Rossendorf | GDR |
| Paffrath, E. | TU Dresden | GDR |
| Pilz, W. | TU Dresden | GDR |
| Pivarc, J. | SAS Bratislava | CSSR |
| Pentschev, O. | INRNE Sofia | BULGARIA |
| Ramirez, E. | Kossuth Univ. Debrecen | HUNGARY |
| Rosu, H.N. | CIP Bucharest | ROMANIA |
| Rubchenya, W. | RI Leningrad | USSR |
| Salnikov, O. | PEI Obninsk | USSR |
| Schaefer, I. | FNE Freiberg | GDR |
| Schmidt, D. | TU Dresden | GDR |
| Schmidt, K.A. | KfK Karlsruhe | FRG |
| Schwierz, R. | TU Dresden | GDR |
| Seeliger, D. | TU Dresden | GDR |
| Seidel, K. | TU Dresden | GDR |

| | | |
|---|---|---|
| Stavisski, I. | INR Moscow | USSR |
| Streil, T. | TU Dresden | GDR |
| Szatariczkai, T. | Kossuth Univ. Debrecen | HUNGARY |
| Thiem, S. | ZFTM Dresden | GDR |
| Tuuia, A. | TU Dresden | POLAND |
| Unholzer, S. | TU Dresden | GDR |
| Vertebni, V.I. | INR Kiev | USSR |
| Vincour, J. | INR Prague | CSSR |

# КОМПЛЕКС ИСТОЧНИКОВ НЕЙТРОНОВ НА ОСНОВЕ ПРОТОННЫХ ПУЧКОВ МОСКОВСКОЙ МЕЗОННОЙ ФАБРИКИ

Грачев М.И., Колмычков Н.В., Казарновский М.В., Лебедев С.Г., Лобашев В.М., Сережников С.В., Сидоркин С.Ф., Стависский Ю.Я., ИЯИ АН СССР

Булкин Ю.М., Кочнов Я.К., Мацнев А.Е., Трушкин Р.И., Хмельщиков В.В., Хрястов Н.А., НИКИЭТ

## АННОТАЦИЯ

Дается описание комплекса источников нейтронов для физических исследований на основе протонных пучков Московской мезонной фабрики. Ожидаемая интенсивность нейтронов в $4\pi$ в режиме резонансного селектора $\sim 3.10^{16}$ нейтр/с (25 нсек, 400 гц), пиковая плотность потока тепловых нейтронов на светящей поверхности замедлителя $\sim 5.10^{15}$ нейтр/см$^2$с при длительности импульса $\sim 50$ мкс.

Сооружаемая в ИЯИ АН СССР, в Троицком научном центре мезонная фабрика - сильноточный ускоритель протонов и ионов $H^-$ на энергию 0,6 ГэВ с током 0,5-I ма (рис.I). Интенсивные пучки протонов, в том числе поляризованных, пучки $\pi$, $\mu$ -мезонов и нейтрино, получаемые при взаимодействии протонов с веществом мезонных мишеней и ловушек протонных пучков позволят развить широкий круг исследований - от фундаментальных проблем строения материи I) до таких важнейших прикладных направлений, как, например изучение радиационного поведения материалов для атомной энергетики и установок термоядерного синтеза 2).

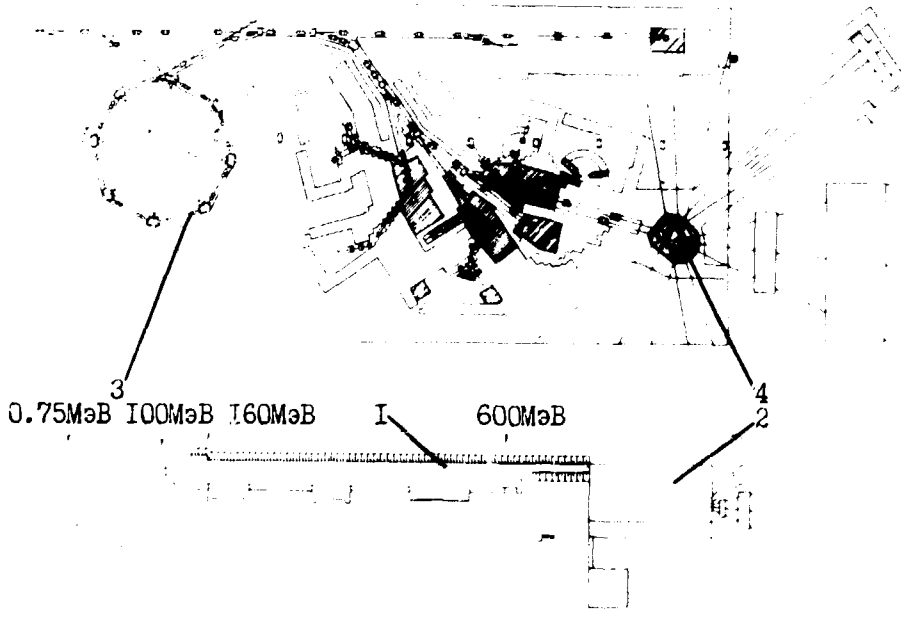


Рис.I. Московская мезонная фабрика.
I - линейный ускоритель протонов.
2 - экспериментальный комплекс.
3 - накопитель протонов.
4 - комплекс источников нейтронов.

Протоны средних энергий позволяют получать и интенсивные потоки нейтронов. Действительно, при взаимодействии протона с энергией 0,6 ГэВ с веществом протяженной мишени из тяжелых ядер (вольфрам, свинец) испускается 10–12 нейтронов, из них более 90% – испарительные, со средней энергией 2–3 МэВ. В случае мишени из $U$-238 число вторичных нейтронов около 25, примерно половина – нейтроны деления. При доступных ныне интенсивностях протонных пучков от сильноточных ускорителей протонов – мезонных фабрик средние интенсивности нейтронов пока еще ниже чем достигнутые в современных исследовательских реакторах, однако возможность изменения в широких пределах временной структуры протонного пучка, и соответственно, временной структуры потока нейтронов открывает уникальные экспериментальные возможности 3).

Формирования коротких импульсов протонов средних энергий опирается на использование перезарядной инжекции ионов $H^-$ в накопители. Перезарядная инжекция, предложенная в свое время Альварецом 4) и осуществленная впервые Г.И.Будкером с сотрудниками 5), открывает пути накопления в кольцевых магнитных системах больших циркулирующих токов протонов (десятки ампер 6)). Быстрый вывод протонов из накопителя Московской мезонной фабрики на внешнюю мишень позволит генерировать импульсы нейтронов длительностью 5-200 нсек со средней интенсивностью нейтронов в $4\pi$ до $6.10^{16}$ нейтр/с.

На основе сгруппированного таким образом пучка протонов могут быть получены импульсные потоки тепловых и резонансных нейтронов для исследований по физике конденсированных сред (изучение упругого и неупругого рассеяния холодных и тепловых нейтронов в конденсированных средах), уникальные по интенсивности импульсные потоки резонансных нейтронов. Спектрометры резонансных нейтронов на основе импульсного источника Московской мезонной фабрики позволяют развить широкий круг исследований парциальных процессов взаимодействия нейтронов с ядрами в изолированных резонансах и в области перекрывающихся уровней.

Импульсный характер нейтронного потока при малом выходе нейтронов между импульсами (в случае $U$-238 этот выход $\sim 1\%$, $Pb \sim 0,1\%$, а для мишеней среднего веса, например из $Mo < 10^{-5}\%$ /3/) позволит, применяя временную селекцию событий, получать в хороших замедлителях ( $D_2O$ , $Be$ , $C$ ) квазистационарные потоки тепловых и холодных нейтронов с малым вкладом надтепловых и быстрых ("временная тепловая колонна"). Это открывает возможность постановки таких уникальных экспериментов как прямое изучение рассеяния нейтрона на нейтроне, обнаружение нейтрон-антинейтронных осцилляций 7).

Комплекс интенсивных источников нейтронов создается на основе двух пучков протонов (см.рис.2), которые могут быть использованы одновременно. Первый пучок – пучок протонов из ускорителя со средним током до 1 ма, имеющий временную структуру ввиде последовательности макроимпульсов длительностью 100 мкс, следующих с частотой повторения 100 герц. Этот пучок попадает в нейтронную мишень квазистационарного источника тепловых и холодных нейтронов (рис.2,3). Второй пучок, сгруппированный в накопителе с перезарядной инжекцией и однооборотным выводом (рис.1), в виде последовательности импульсов длительностью 5-200 нс (100–400 герц) при среднем токе до 500 мка, попадает в нейтронную мишень импульсного источника нейтронов (рис.2,4).

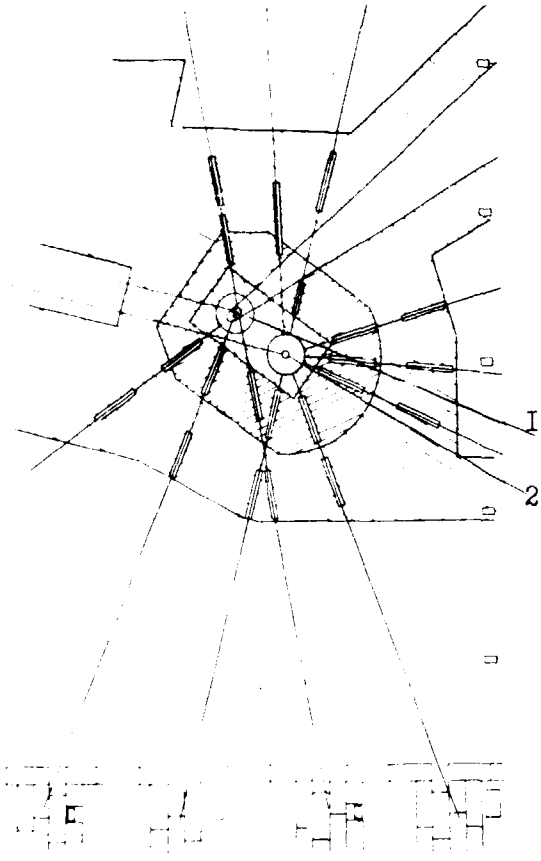


Рис.2. Комплекс источников нейтронов.
I - квазистационарный источник. тепловых и холодных нейтронов.
2 - импульсный источник нейтронов.

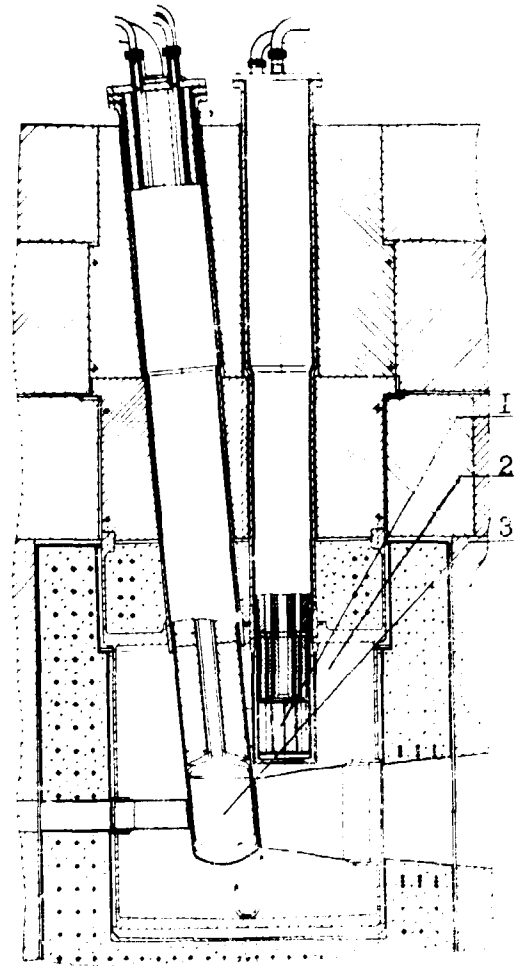


Рис.3. Квазистационарный источник тепловых и холодных нейтронов. I-нейтронная мишень. 2-тяжеловодный замедлитель.3-жидкодейтериевый замедлитель.

В импульсном источнике нейтронов наряду с импульсами протонов, сгруппированными в накопителе может использоваться микроструктура протонного пучка, формирующаяся в линейном ускорителе. Импульсы микроструктуры имеют длительность 0.2-0.3 нс и следуют с частотой 200 мгц в пределах импульса макроструктуры. Для время-пролетных исследований они могут быть использованы после селекции, при частоте повторения до 200 кгц, что, естественно приводит к соответствующей потере средней интенсивности.

Оба источника располагаются в цилиндрических боксах радиационной защиты из стали и бетона (рис.5) и "просматриваются" системой каналов, снабженных шиберами гильотинного типа.

Квазистационарный источник тепловых и холодных нейтронов (рис.3) включает водоохлаждаемую нейтронную мишень ввиде плотной упаковки стержней из естественного урана в алюминиевых оболочках, тяжеловодный замедлитель в алюминиевом баке, жидкодейтериевый замедлитель. Жидкодейтериевый замедлитель просматривается широкоапертурным каналом эксперимента по обнаружению осцилляций нейтрон-антинейтрон, каналами для исследований с холодными и ультрахолодными нейтронами. Сквозной тангенциальный канал позволит проводить исследования в интенсивных полях тепловых нейтронов в тяжеловодном замедлителе.

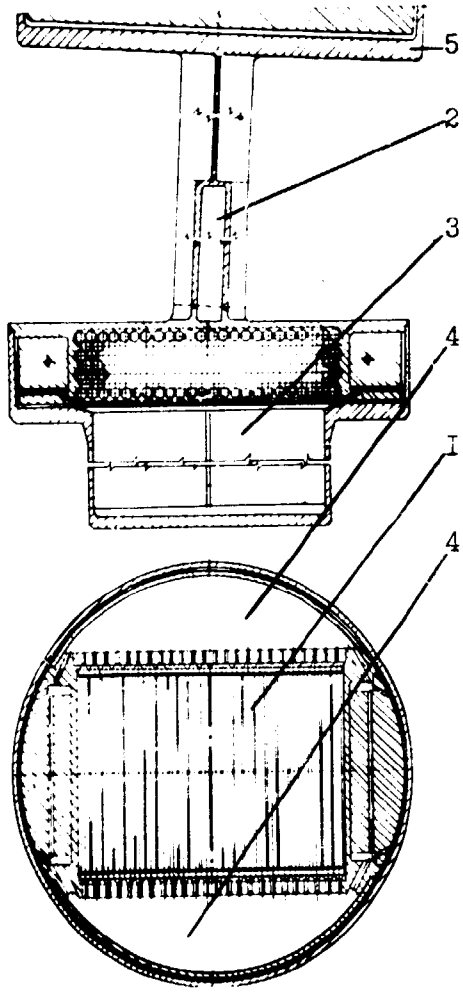


Рис.4. Импульсный источник нейтронов. I-сборка стержней из U-238 (вольфрама).2-верхний замедлитель.3-нижний замедлитель. 4-водяные коллекторы.5-защитная пробка.

При токе протонов 0,5 ма расчетное значение плотности потока тепловых нейтронов на дне экспериментального канала $\sim 3.10^{13}$ нейтр/см$^2$с, плотность потока холодных нейтронов на светящей поверхности холодного замедлителя $\sim 10^{13}$ нейтр/см$^2$с при эффективной температуре $\sim$30К.

При этом полное тепловыделение в нейтронной мишени I МВт, в тяжелой воде $\sim$ 40 квт, в холодном замедлителе $\sim$0,5 КВт.

Тепло,выделяемое в мишени отводится водой с входной температурой $\sim 30^{o}$С, передающей тепло воде второго контура. Мгновенная активность воды первого контура определяется взаимодействием протонов и нейтронов с кислородом и складывается из активности трития (12,3 лет) $Be^{7}$ (53 дня), $C^{11}$ (20,5мин), $^{13}$ (10 мин), $O^{15}$ (126 с) и $N^{16}$ (7,4 с). Суммарная насыщенная активность воды при номинальной мощности установки $\sim$ 0,85 кюри/литр для объема I-го контура $\sim$ 2 м$^3$, примерно половину вносит тритий.

Тепло,выделенное в тяжелой воде отводится во внешнем теплообменнике. Холодный дейтериевый замедлитель охлаждается за счет конденсации паров дейтерия в теплообменнике, обдуваемым 15К-гелием от холодильной установки, работающей в рефрижераторном режиме.

Импульсный источник нейтронов 8) включает мишень-сборку из урановых (вольфрамовых) стержней в алюминиевых оболочках, охлаждаемую водой, и систему замедлителей. Легководные замедлители примыкают к "верхней" и "нижней" поверхности мишени (рис.4). Тонкий ($\sim$ 2 см) "верхний" замедлитель светит в каналы и нейтроноводы резонансных и быстрых нейтронов с максимальной пролетной базой $\sim$500 м, выходящие из здания экспериментального комплекса. Эти нейтроноводы снабжены промежуточными павильонами. Нижний замедлитель, толщиной 6 см, предполагается использовать в экспериментах с тепловыми и медленными нейтронами. Соответствующие каналы выходят в экспериментальный зал.

Предусмотрена возможность использования холодного жидководородного замедлителя, легководных замедлителей, отравленных кадмием, отражателей замедлителей. Мишень и система замедлителей импульсного источника нейтронов располагается в вакуумном баке в полости защиты (рис.5).

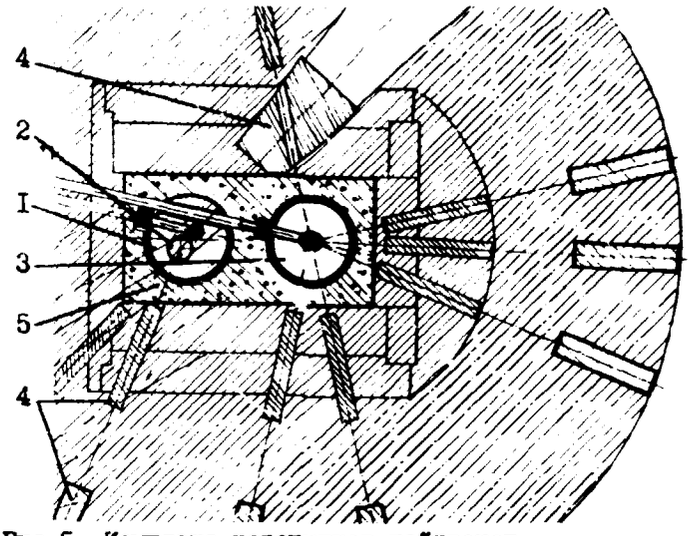


Рис.5. Комплекс источников нейтронов.
I - тяжеловодный бак. 2 - жидкодейтериевый замедлитель. 3 - вакуумный бак. 4 - шибера каналов. 5 - тепловая защита.

Средняя интенсивность нейтронов, испускаемых в $4\pi$ в режиме резонансного селектора (25 нсек, 400 герц) $3.10^{16}$ нейтр/с, что примерно на два порядка превысит среднюю интенсивность наиболее мощных современных импульсных источников нейтронов для резонансной области энергий на основе сильноточных ускорителей электронов (см.например *ORELA*, США).

Пиковая плотность потока тепловых нейтронов, усредненная по светящей поверхности замедлителя площадью 400 см$^2$ составит $\sim 2.10^{15}$ нейтр/см$^2$с при длительности импульса $\sim$50 мкс. Использование отражателя из железа позволит получить пиковые потоки плотностью до $5.10^{15}$ на светящей поверхности $\sim$100 см$^2$.

Средняя интенсивность быстрых нейтронов из мишени (испарительных и каскадных) в режиме быстрого селектора при длительности импульсов $\sim$0,3 нс и частоте повторения 200 гГц $\sim 3.10^{13}$ нейтрон/с в $4\pi$.

Литература


I. В.М.Лобашев, А.Н.Тавхелидзе. Мезонная фабрика - новый мощный инструмент исследований. Вестник АН СССР, т.2, стр.II5, I983.
2. Э.А.Коптелов, В.В.Королев, Ю.Я.Стависский. О возможности исследований по радиационной физике на основе сильноточного ускорителя протонов Московской мезонной фабрики. Препринт ИЯИ АН СССР, П-0288, М., I983.
3. Ю.Я.Стависский. Импульсные источники нейтронов на основе протонных пучков мезонной фабрики. Препринт ФЭИ-389, Обнинск, I973.
4. L.W.Alvarez. Rev.Sc.Instrum., v.22, p.705L, 1951.
5. Г.И.Будкер, Г.И.Димов и др. АЭ, т.I9, стр.507, I965.
6. A.A.Vasiliev et al., USSR, USA Patent 3.860.828, aug.1972-jan.1975.
7. А.С.Ильинов, М.В.Казарновский, В.А.Кузьмин, Е.А.Монич, Ю.Я.Стависский, Б.Е.Штерн. Нейтрон-антинейтронные осцилляции: предложение эксперимента на мезонной фабрике ИЯИ АН СССР. Препринт ИЯИ АН СССР, П-0278, М, I983.
8. Б.С.Думеш, Н.В.Колмычков, Э.А.Коптелов, С.Г.Лебедев, С.Ф.Сидоркин, Ю.Я.Стависский. Импульсный источник нейтронов на основе протонного пучка мезонной фабрики. Препринт ИЯИ АН СССР, П-0232, М., I982.

# KARIN - A SEALED HIGH POWER GENERATOR TUBE OF 14 MEV NEUTRONS FOR RADIOTHERAPY , ACTIVATION ANALYSIS AND NEUTRONIC APPLICATIONS

K.A. Schmidt
Kernforschungszentrum Karlsruhe, Institut für Kernphysik III, FRG,

Abstract:
A 14 MeV neutron generator tube based upon the d-t-fusion reaction from a 150 mA mixed deuterium-tritium ion beam (22 atomic) accelerated onto an internal 200 kV Scandium-tritium-deuterium target has been developed. The tube is constructed as a compact, closed glass-ceramic-metal sealed UHV system. It contains about 500 Ci of Tritium and has a life-expectancy of several hundred hours due to sputtering-through of the target sheath. The source strength is $6.5 \times 10^{12}$ neutrons/sec.

The average flux inside the central hollow target cylinder is nearly isotropic and very homogeneous in a volume of up to 30 $cm^3$. This irradiation site, having a saddle point flux distribution with more than $5 \times 10^{10}$ $N/cm^2$ sec is accessible by a 1" diameter rabbit system. At the GKSS Installation "KORONA" a very fast (120 msec) rabbit-system is in use (since 1980), which allows repeated activation and counting of fast decaying samples.

Clinical radiotherapie with fast Neutrons at a kerma dose rate of 20 rad/min is performed at a distance of 100 cm from the target center, 20 cm outside of a 70 cm long collimator. Optimum collimation is acieved by avoiding self-shielding of the target structure by using a target shaped into a truncated cone with its apex on the collimator axis in the direction of the neutron beam, the apex angle being chosen according to the maximum size of the irradiation field to be used. A movable isocentrically mounted radiator head shield with exchangeable collimator inserts is provided at the radiotherapeutic installations at the DKFZ Heidelberg (1977), Zürich (1980) and Münster (1984).

The Neutron source at the "LOTUS" - Fusion-Fission Hybrid Test Facility (1984) at the ETH Lausanne is provided for by an unshielded version of the medical tube KARIN.

Operational experience with the KARIN-Installations is presented.

# DESIGN OF A $10^{12}$ n/s COMPACT NEUTRON GENERATOR

Sun Biehe
Institute of Nuclear Research, Lanzhou University People's Republic of China

This generator will give a neutron yield of $10^{12}$n/s. It will be used mainly in the experiments of neutron physics and the applications of the nuclear techniques. In the design program of this generator we have adopted the Duoplasmatron ion source, high current accelerating tube, symmetrical Cockcroft-Walton type voltage multiplier circuit, intermediate frequency power supply with the thyristor inverter, rotary target. Meantime, we plan to use oilless vacuum pumping system and tritium purgation facility. A computer control system is used for the generator.

Design parameters of the generator are as follows

| | | |
|---|---|---|
| 1 | Neutron total yield | $(2-1)\times10^{12}$n/s |
| 2 | Deuteron beam energy | 300 keV |
| 3 | Target current (direct) | 20 mA (unanalysed) |
| 4 | T-Ti target diameter | 200 mm |
| 5 | Rotating target speed | 1100 rpm |

It is expected that the generator will come into all-sided operation by the end of 1985.

# THE INTENSE NEUTRON GENERATOR CONCEPT IN DEBRECEN+

T. Sztaricskai

Institute of Experimental Physics, Kossuth University, Debrecen, Hungary

An intensive neutron generator based on a 30 mA duoplasmatron ion source and a 200 kV high voltage power supply is under construction at the Institute of Experimental Physics in Debrecen. The neutron generator shall use a single gap acceleration tube, a quadrupole quartet focusing system, a Wien-filter type beam selector and a rotating disc titanium target. The ion optical system makes it possible the use of the accelerator as a charged particle low energy accelerator up to neon ions. The paper delivers a short survey on the design concepts and the present state of this accelerator.

## Introduction

The intense ($\geq 10^{12} ns^{-1}$ yield) 14 MeV neutron sources are mostly used in the neutron therapy, CTR material program, hybrid reactor studies. Their use in the fast neutron activation analysis, 14 MeV neutron cross section measuring laboratories are not typical, but they have more advantages. These generators as a low energy high current accelerators can be used for the study of nuclear astrophysical reactions, charged particle blistering and low energy heavy ion reactions too 1>.

The intense neutron generator under construction in Debrecen shall be used as a charged particle accelerator for low energy heavy ion reaction, CTR materials blistering studies, nuclear astrophysical reaction cross section measurements and as a neutron source for the measurement of the 14 MeV cross sections and in fast neutron activation analysis too.

The preliminary studies of the neutron generator project 2,3,4> have been shown, the economical and labour situation of our small institute allows only well organised more year design and construction. The construction of the generator has been planned in the next steps:

A/ The duoplasmatron with the einzel lens on the high vacuum system forming an ion source test stand

B/ As in point A with addition of the acceleration tube, high voltage terminal and power supply and a target

C/ As in point B with addition of the ion species selector, quadrupole lenses and the rotating tritium target assembly resulting an 10-20 mA, 200-220 kV charged particle accelerator and an intense neutron generator.

The system in state A can be used as a low energy high current accelerator in the 0-50 keV region for charged particle blistering investigations on CTR construction materials. The state B makes it possible the testing of the designed target assembly construction and to use it as a neutron generator e.g. for health physical measurements on shielding materials and for fast neutron activation analysis. The state C is a complete intensive neutron generator with analysed beam wich can be used not only as a 14 MeV neutron generator but as a low energy high current charged particle accelerator for low energy nuclear astrophysical and heavy ion reactions study too.

+This project is supported by the IAEA

The ion source and the acceleration tube

The ion source used in this design is a commercial DP-30 type duoplasmatron, manufactured be the High Voltage Engineering Co. The DP-30 delivers up to 30 mA of ion current, 60 % monoatomic ions 5 >. The DP-30 with the built in einzel lens gives an emmitance of $6.10^{-3}$ rad $MeV^{0.5}$. The study of the ion optical parameters of the ion source has been done by a personal computer based measuring set-up 6>. The original filament, like the one in the OCTAVIAN project 7>, has a too short life time, so an alteration 8> was needed. The structure of the duoplasmatron with einzel lens is shown in Fig.1.

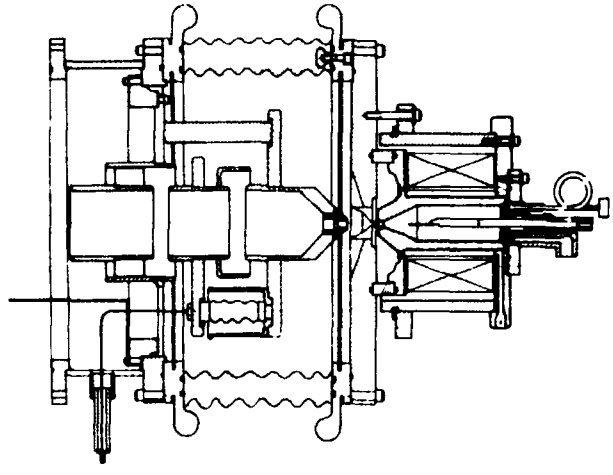

Fig.1.
The DP-30 duoplasmatron with the built in einzel lens

According to the emittance date of the DP-30 duoplasmatron, the working area of the planned accelerator is placed in the vicinity of the border separating the areas in which the emittance and perveance plays a leading role respectively. Consequently, the space charge effects can be considered as a slight perturbation. The designed acceleration tube meets all the basic requirements summarized in 9>. The tube represents a single gap immersion lens placed in a homogeneous acceleration tube, like at the pre-injector of the CERN PS-LINAC 10>.

The construction of the accelerator tube follows the arrangement of the Chalk River generator 11>. The homogeneous field acceleration tube design uses the glass-metal technology and the mechanical construction of the single gap immersion lens enables the change of inner electrode configuration in the case of an eventual trouble which might appear. The inner conical electrodes of the homogeneous tube are easily replacable without unjointing the glass-metal bond. The calculated conductivity of the complete tube for $D_2$ gas amounts to 3100 $l.s^{-1}$. The acceleration tube, the quadrupole focusing unit and the vacuum connection of them is shown in Fig.2.

Beam handling and transport

For compensating the space charge effects in the beam emitted by the duoplasmatron and accelerated by the acceleration tube, a quadrupole focusing system has been designed. The selection of ion species and a mass analysis of the beam is planned by a Wien-type velocity filter.

The electron optical calculation for various electrostatical quadrupole arrangements have been described in 9>. The stigmatic focusing and high optical flexibility the simple power supply (max. 20 kV, twin unit), of the two parameter (symmetrical) quadruplet have been preferred for the construction. The chosen version is

shown in Fig.2.

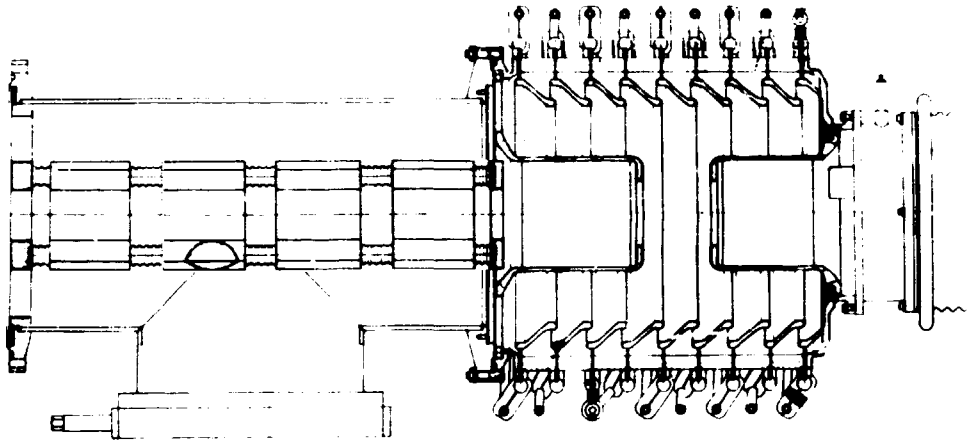

Fig.2. The acceleration tube and the quadrupole lenses

The Wien-type velocity filter has been designed as a beam analyzer to be used up to the ion masses of 20 a.m.u. Three version have been calculated with various characteristics. The final version of the configuration shall be chosen on the basis of experimental determination of ion optical characteristics of the accelerated beam. A schematic representation of the Wien-filter is shown in Fig.3.

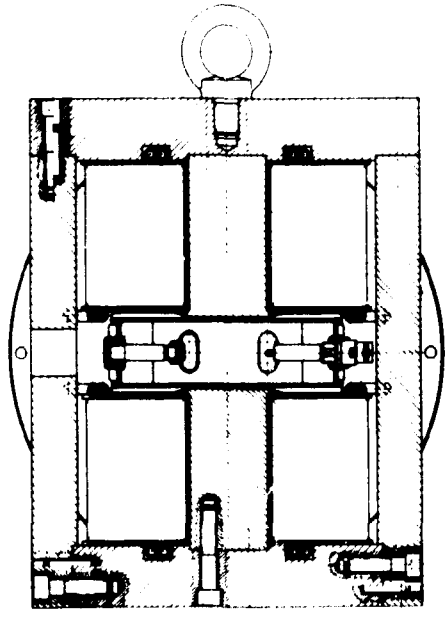

Fig.3. A schematics of the Wien filter planned to use as a beam analyser

The space charge effects has been neglected throughout the calculations on ion optical elements of the accelerator. A rough estimation of beam expension based on the formulae of Green 12> showes the space.charge expansion will not be caused serious troubles above energies of 100-150 keV 9>.

The rotating target

A thick copper disc rotating target, diameter of it about 20 cm, similar to the Multivolt Limited of Crawley series RTH targets is under construction. These targets have a maximal loadibility of 3-8 kW $cm^{-2}$ and the total tritium activity of them are about $(11-19)10^{12}$Bq. The half life of the targets are about 300 hours at a load of 5 kW $cm^{-2}$ load bombarded by analyzed beam 13>. The rotating magnetic ferrofluid seal in it allows a speed up to 30 revolution per second 14>. A schematic view of the planned target is shown in Fig.4.

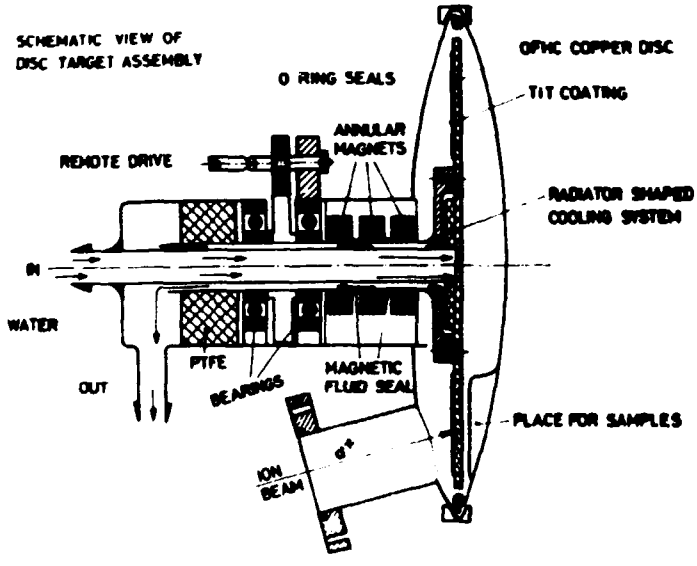


Fig.4. The schematics of the target assembly

The most important problem connected to the target assembly is the lack of the tritiating company for our Amzirk equivalent oxigenfree target backing.

The HV power supply and the cooling system

The acceleration voltage to the generator will be produced by a Heafely 200 kV 40 mA high voltage power supply. The ripple of this power supply is smaler than 1kV at maximum output voltage and current. The high voltage can be regulated by the motor driven variac from zero to 220 kV. The power supply is overcurrent and overvoltage protected and withstands the direct breakdowns and short circuits. The power consumption of the high voltage power supply is about 17 kW at full load.

The duoplasmatron and the target need two closed circuit cooling system. The duoplasmatrons power consumption takes about 1.5 - 2 kW and the target load shall be about 3.5 - 4 kW. The cooling machine is capable for cooling up to 7 kW. The duoplasmatron cooling water should be controlled for a 3-5 Mohmcm conductivity. An ion exchange conductivity control system, similar to the one used at the Heafely sealed tube neutron generators 15> is under design. The separate closed circuit target cooling system will use an adequate on stream detector for neutron yield monitorization.

Vacuum system

The main vacu system of the generator consists of a 2700 $l.s^{-1}$ diffusion pump with water and liquid nitrogen traps and a 40 $m^3$ $h^{-1}$ mechanical pump. An additional vacuum system is planned at the rotating target because the conductivity of the Wien-filter does not allow the appropriate pumping speed. The vacuum system of the target assembly consists of an titanium ion getter pump, a primary pump with the additional valves and vacuum guages to connect and to separate to and from the generator and the exhaust system.

The generator hall and the health physical aspects

The expected source strength of $10^{12}$n $s^{-1}$ of the generator needs a proper shilding. The lack of the places in the institute and the minimum 2 m of thickness of the concrete walls suggested to construct an underground generator hall. The planned generator hall has an area of 8.8x4.8 $m^2$ and its height of 4.5 m. The floor has been built at -7 m, thickness of the ceiling is 0.8 m of concrete and 1 m of soil up to the ground level. The removal cross sections of the all construction materials has been measured during the construction 17>. The horizontal plan of the generator hall and the controlling room connected to it is shown in Fig.5 16>. The construction of the building finished in 1984.

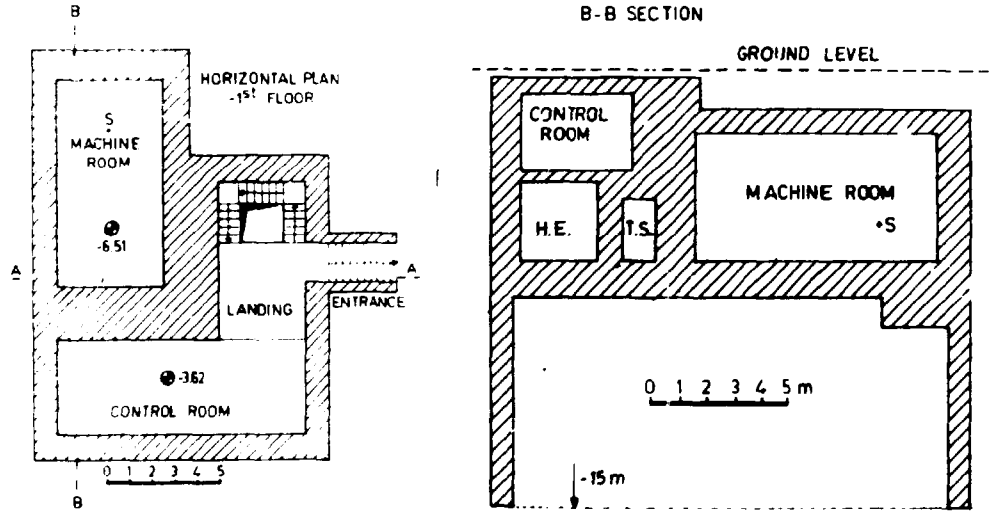


Fig.5. The plan of the underground generator rooms

The machine room is heated by air, the speed of the air exhange is five times per hour. The exhaust of the vacuum systems and the target storage are connected to two ventillated 4" tube. The air outlet and the two 4" tube are led through an underground ventillator room to a 16 m height exhaust tower. The filtering and the sample taking (in the ventillation systems as well as in the water wast-pipe) is possible. The door of the machine room is manufactured of stainless steel. It is water filled and pneumatics operated.

Acknowledgements

The author is very indebted to Prof. Dr.J.Csikai, head of the project, for his

attention and supervision, to Prof. Dr. Koltay, Dr. Szabó, Dr. Berecz, Dr. Bohátka and Dr. Mórik from the Institute of Nuclear Research, Debrecen for their ion optical and partly mechanical design. The colleagues Mr. Berkes, Dr. Dezső, Dr. Raics, Dr. Szegedi and Dr. Daróczy are taking an active part in the project. Mr. Halmi, Mr. Bolyán and Mr. Szegedi are very active in the solution of the technical problems. The author would like to express his gratitude for their co-operation.

References

1 > J.Csikai: Atomic Energy Review 11 (1973)415
2 > T.Sztaricskai: ATOMKI Közl. 22 (1980)47
3 > T.Sztaricskai: ZfK-459 (1981)176
4 > J.Csikai: INDC/NDS/-114/GT (1980)265
5 > High Voltage Engineering Co.: DP-30 Data sheets
6 > T.Sztaricskai, L.Nyitrai, I.Berkes: ZfK-476 (1982)95
7 > K.Sumita, A.Takahashi, et al.: Proc. 12-th Symp. Fusion Technology B-23 (1982)
8 > A.Goede: Private communication
9 > E.Koltay, G.Morik, G.Szabó: ATOMKI Közl. 22 (1980)155
10 > J.Hufuenin, R.Budois: CERN 65-23
11 > J.D.Hepburn, J.H.Omrod, B.C.Chidley: IEEE Trans. NS-22 (1975) No-3 1809
12 > T.S.Green: Rep.Prog.Phys. 37 (1974)1325
13 > M.R.Cleeland, N.Wells: Radiation Dynamics Inc.N.Y. TIS-74-2 (1974)
14 > Ferrofluidics Corp.: Vacuum Seal Grade Ferrofluids Catalouge
15 > E.Freiberg, G Reinhold: Private communication
16 > E.Karvaly: to be published
17 > L.Vasváry et al.: to be published

# INTENSE NEUTRON GENERATOR DEVELOPMENT AT THE INSTITUTE OF PHYSICS

J. Rivarč, S. Hlaváč, P. Obložinský, I. Furzo, V. Matoušek, R. Lorencz and L. Dostál

Institute of Physics, Electro-Physical Research Centre of the Slovak Academy of Sciences, 842 28 Bratislava, Czechoslovakia

Abstract: An intense neutron source based on a 20 mA duoplasmatron ion source and a 300 kV high voltage power supply is under construction at the Institute of Physics in Bratislava. The beam generated in the ion source is separated on a high voltage potential level. A 20° magnet as a beam selector, an electrostatic air insulated acceleration tube, a quadrupole triplet focusing system and a rotating target will be used in the system. The paper gives a short survey on the design concept and the present state of the intense section of the accelerator.

## 1. Introduction

There has been a steadily growing interest in intense neutron sources in the past decade probably mainly stimulated by fusion material research, radiotherapy and also nuclear physics /1/. At the Institute of Physics in Bratislava a step-by-step development of a multipurpose intense 14 MeV neutron source /2/ has been under way.

The intense section of the source should be capable of producing 300 keV/10 mA of a separated $D^+$ ion beam. With such a beam and a fresh target a neutron yield of $10^{12}$ $n.s^{-1}$ for a beam spot of 1 $cm^2$ and a useful target life-time of about 10 h can be expected.

The dc section has been designed to produce a neutron yield of up to $10^{10}$ $n.s^{-1}$ and the fast pulsed section will be capable to generate a compressible $D^+$ ion beam of up to 1 ns on a target sport.

In the present paper the design concept of the source, recent developments and status are reported.

## 2. Neutron source design

The preliminary stage of the design was discussed in ref. /2/. Now the final stage of the design has been reached.

The scheme of the neutron source is in Fig.1. Deuterons are extracted from the plasma of a duoplasmatron ion source. The beam from the duoplasmatron ion

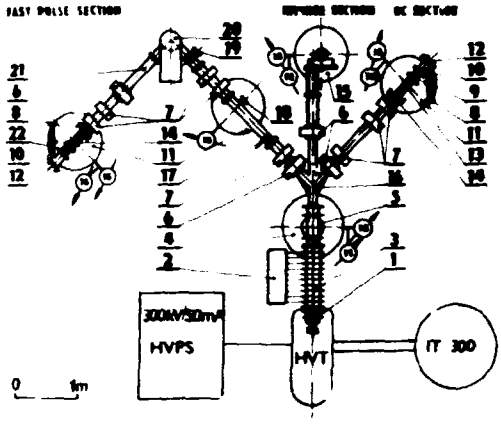


Fig.1. Layout of major components of the neutron source. 1-ion source, 2-column resistors, 3-acceleration tube, 4-main vacuum system, 5- beam corrector, 6-gate valve, 7-quadrupole lens, 8-monitor, 9-static beam monitor, 10-target chamber, 11-auxiliary vacuum system, 12-water-cooled target, 13-water cooled slit, 14-beam profile monitor, 15-rotating target chamber, 16-analysing-switching magnet, 17-chopper, 18-slit, 19-diaphragm, 20-90° magnet, 21-bunching system, 22-pick-up system, TC-thermocouple gauge, IG-ionization gauge, IT 300-isolating transformer, HVT-high voltage terminal and HVPS-high voltage power supply.

source passes through a double focusing magnet placed directly on the high voltage terminal. The magnet is designed for the $D^+$ separation from molecular ions, allowing the acceleration tube and the beam transport system to be optimized for a single species. A sufficient conductance path is provided from the ion source to the acceleration tube and an 80 $l.s^{-1}$ air auxiliary pump is used to pump the ion source simultaneously with the main vacuum pump. An Einzel lens is included to meet desirable focal properties of the acceleration tube. The not necessary molecular ions, the energetic neutral fraction and other unwanted gases produced by the ion source should be removed from the high field region of the accelerator column. The final details have been finished.

After acceleration the beam will be directed either to the rotating target section or to the dc and fast pulse sections.

## 3. Recent developments and status

### 3.1. HIGH VOLTAGE POWER SUPPLY

The major components of the high voltage power supply have been supplied by TUR Dresden (R.E.Transformer and Roentgen Plant). The scheme of the supply together with a cappacitor battery, water resistors and a stabilizer are shown in Fig.2. The supply has been constructed with respect to a long operation at

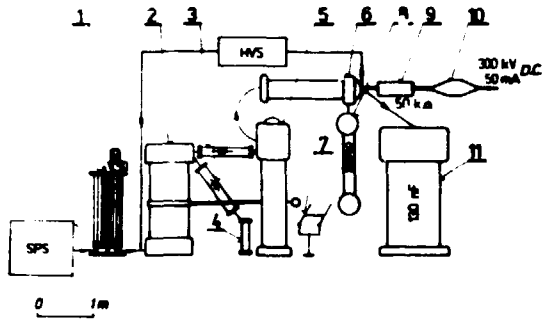


Fig.2. Scheme of the high voltage power supply. 1-regulating transformer REOgs 16/380, 2-high voltage transformer REOI (Z) 25/300/C, 3-Se rectifier, 4-resistor, 5-multiplier capacitors, 6-protective resistor, 7-discharger, 8,9-water resistors, 10-high voltage cable and terminal, 11-capacitor battery, SPS-stabilized power supply and HVS-high voltage stabilizer.

40 mA/ 20° or 30 mA/35°C. The high voltage is regulated by a motor-operated regulating transformer. The ripple factor of the supply is 2.5 %. The capacitor battery consisting of 12 capacitors (1.5 μF/30 kV) is added in order to obtain better parameters of the system. We are able to reduce the ripple factor to 1% by use of such a capacitor bank. Moreover, the whole system will be stabilized. The test of a similar stabilizer /3-4/ showed a long term stability of 0.15% in 6 h caused mainly by thermal fluctuations in the reference voltage system. The high voltage power supply is separated from the neutron source terminal. They are interconnected through a water resistor with a high voltage cable. A suitable water resistor and cable terminals have been constructed to prevent a breakdown between the polyethylene isolation and the lead cable covering.

### 3.2. HIGH VOLTAGE TERMINAL AND ION SOURCE

A high voltage terminal of a 3.4 $m^2$ surface and a 0.90 m height will contain the ion source and the associated equipments. The proposed arrangement of the ion beam optic elements on the high voltage terminal in configuration with the duoplasmatron ion source is shown in Fig. 3. Power will be supplied by the isolating transformer IT 300 /5/. Its development has been completed and the transformer is at present being operated by the old neutron source configuration.

The ion source selected for operation in the intense section of the neutron source is a modification of the duoplasmatron source developed at Vakutronik Dresden (N.E. Vacuum Electronic Plant). The preliminary ion source tests have been performed. It has been shown that one can achieve the expected 20 mA

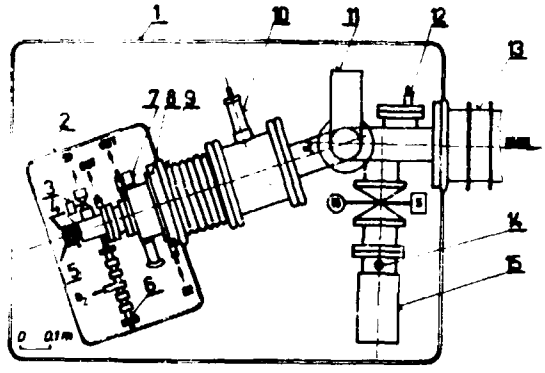

Fig.3. Scheme of the high voltage terminal. 1-300 kV equipment dome, 2-50 kV duoplasmatron dome, 3-solenoid valve, 4-cathode feedthrough, 5-cooler, 6-Pd valve, 7-holder, 8-anode, 9-aluminium oxide ceramic, 10-50 kV feedthrough, 11-analysing-focusing magnet, 12-beam monitor, 13-acceleration tube, 14-feedthrough, 15-ion sorption pump, SP-sorption pump and IG-ionization gauge.

beam at an approximately 40 kV extraction voltage. The tests did not include the 20° double focusing magnet.

The acceleration tube has been supplied by the Institute of Nuclear Research, Warshaw. In addition, the production documentation concerning the multiple series of resistor blocks (10 MΩ/30 kV) built into an oil-filled insulating box, has been given to the workshop of our Institute.

## 3.3. BEAM TRANSPORT

The optical properties of the accelerator components have been calculated taking into account the effect of the beam space charge. The SLAC electron trajectory program was used /6/. The calculations are iterative for beams with self-fields. Using the finite difference method over a regular square mesh with succesive overrelaxation, the electric fields are calculated first from the given configuration of the electrodes and their potentials. Then the rays representing the beam are traced through the calculated fields. The space charge distribution for the next iteration is calculated from the ray trajectories.

Beams of various intensities within 10-20 mA have been traced. The ray tracing through the Einzel lens system is shown in Fig.4. The current density at the end of this system is not constant but depends on the beam radius. An almost laminar beam is obtained when the ratio $U_{foc}/U_{ext} \approx 0.8$, where $U_{foc}$, $U_{ext}$ are the focusing and the extraction voltage, respectively. For the higher $U_{foc}$, the stronger the focusing is the stronger is the ray crossing. The focusing action of the entrance part of the constant gradient acceleration tube is shown in Fig.5. The beam emerging from the acceleration tube is nearly parallel. Its diameter is Ø 1.5-2 cm. The value depends on the focusing and the extraction voltage. Our calculations show that the space charge effects of the accelerated

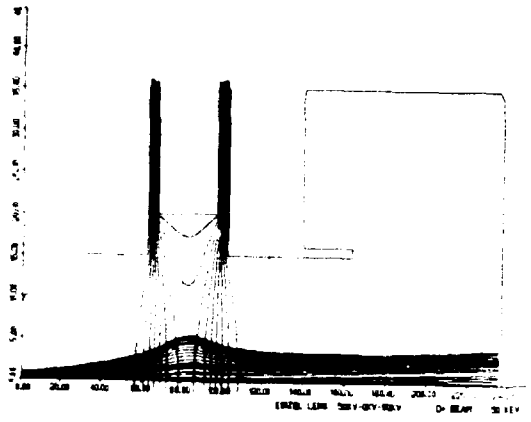

Fig.4. Ray tracing through the Einzel lens system. Beam current, energy of deuterons and focusing voltage are 18 mA, 50 keV and 41 kV, respectively. Equipotential lines are superimposed on ion trajectories. The whole system is axially symmetric around the beam direction (z axis). Description of axes (z,r) is given in mesh units. One mesh unit is 2.0 mm.

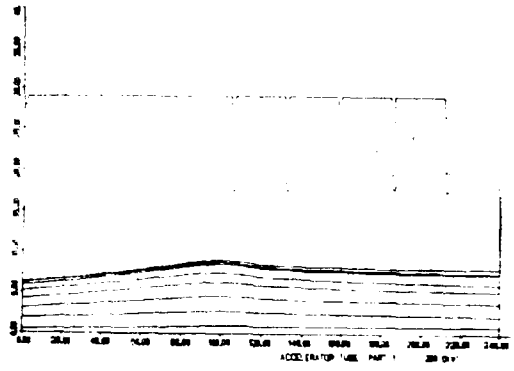

Fig.5. Focusing action of the entrance part of the acceleration tube. Beam current and accelerating voltage are 18 mA and 300 kV, respectively. Whole system is axially symmetric around the z axis. Description of axes (z,r) is given in mesh units. One mesh unit is 2.5 mm.

beam are already small. Then, one can focus such a beam by a magnetic focusing system using either a quadrupole multiplet or a solenoid.

Envelope calculations for the beam transport in the dc and the pulse sections have been given in a previous paper /2/.

### 3.4. ROTATING TARGET SYSTEM

For the intense section of the accelerator a rotating target is being considered. Its preliminary version should use 16 pieces of Ø 4.5 cm TiT targets /7/. A detailed scheme of the rotating target system is shown in Fig.6. The targets elements are located on a rotation disk. The ring shaped target contains a total of 15 TBq tritium. During target operation, the target is cooled by water let into the centre of the rotating target assembly to a cavity wherefrom it is supplied to eight Ø 0.5 cm channels. Two targets are connected to one channel. Our design assumes that water consumption would be lower than 70 $l \cdot min^{-1}$.

The rotor is moved in a vacuum of $10^{-3}$-$10^{-4}$ Pa. It is separated from the high vacuum by special "O" rings sealing. Simmerings separate the vacuum chamber

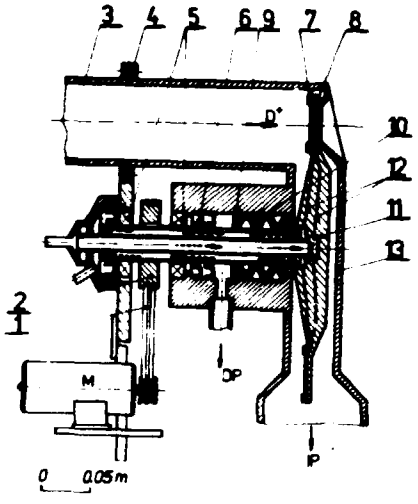


Fig.6. Detailed scheme of the rotating target. 1-"V"belt, 2-pulley, 3-beam tube, 4-isolation support, 5-bearings, 6-simmerings, 7-ring, 8-target, 9-support, 10-sealing "rings", 11-rotor, 12-water channels, 13-stator, IP-ion pump, DP-differential pump and M-electric motor.

from the outside environment. The cavity placed between the rings and the simmerings is pumped by a differential pumping system. The target chamber is pumped by an ion pump. The rotor is supported by two high precision ball bearings which allow only a small free vibration. We expect that the bearings will be suitable for target operations at any speed of up to 1100 rpm although the necessary target revolution rate for the heat dissipation of 1.5 $kW.cm^{-2}$ is about 35 rpm /8/.

At present the documentation concerning the rotating target assembly has been delivered to the workshop of the Institute.

### 3.5. ION SOURCE ELECTRONICS AND CONTROL SYSTEM

Documentation concerning the power supplies for the duoplasmatron ion source have been designed and delivered to the workshop of the Institute. Ion extraction should be performed by the 50 kV potential. For this reason two transformers have been developed. One provides the 50 kV d.c. voltage and the 3.75 kVA power for the extraction source. The other the isolating transformer IT 50 for the 50 kV potential and the 2 kVA power, should transmit the mains for the rest of the duoplasmatron power supplies. The transformers of about 150 kg and 80 kg weight, respectively, are put into insulation cylinders made of laminated paper and filled by inhibited transformer oil.

The electronic control system has been developed. It should maintain the accelerator for the required operation regime. At the first stage, however, it should allow an easy setup of the sources placed on the high voltage terminal.

A block scheme of the system is shown in Fig.7. The hardware was designed according to CAMAC specification. The main control modul is an intelligent crate controller based on a 8080 microprocessor /9/. The system is capable of controlling about 20 analog and 100 digital quantities. This corresponds to a total

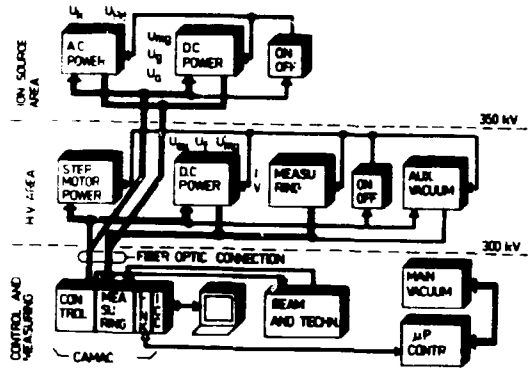


Fig.7. Block scheme of the ion source electronics and control system of the intense source section

information flow of about 250 byt.$s^{-1}$. This fact allows to use the microprocessor with a throughput of about 50 kbyt. $s^{-1}$ in a real time control application.

Sensors and control elements are placed on different potential levels (0,300, 350) kV. They are interconnected by fiber optic cables. In order to eliminate a balance of the analog signals a pulse-duration modulation is used.

The hardware of the intelligent crate controller for the system has been completed and tested at the JINR Dubna. The software will be designed with respect to initiating, to the control algorithm, to operator-aided resetting and control in breakdown situations.

### 3.6. VACUUM SYSTEM

The system is constructed of stainless steel. Conflat flanges and cooper gasket seals are used throughout the high vacuum side. In solenoid valves VITON rings and in the target chamber aluminium wire-rings are used. The high vacuum part is bakeable.

The main vacuum unit has been completed. It is based on a 2000 $l.s^{-1}$ diffusion pump with water and liquid nitrogen traps, two sorption Zeolite pumps, a foreline trap and a mechanical pump. The EGZ 100 and the IZ 90 ion pumps produced by High Vacuum Dresden and Leybold-Heraeus, respectively, will be used as auxiliary vacuum units.

At present the control unit of central vacuum system has been designed and delivered to the workshop of the Institute.

### 3.7. NEUTRON SOURCE CELLS

The original floor plan /2/ for the accelerator has not been changed. Suitable doors for the separation of the accelerator rooms and the operating room have been assembled.

## 4. Conclusion

The next steps in the construction of the accelerator should be as follows: The completion of drawings and the assembling of a high voltage power supply (1984); putting into operation the main vacuum system, the acceleration tube and the new high frequency ion source and to obtain the strength of the source of $10^{10}$ n.s$^{-1}$ (1985); to put into operation the duoplasmatron ion source on a high vacuum level (1986); forming the intense section of the accelerator (1987) and achieving the fully operating level of the intense neutron source (1988).

The authors wish to thank Ing. Ľ. Luby,DrSc. the director of the IF EMRC SAS and Dr.M.Blažek, DrSc. for their support and kind interest in this work. They wish to thank Ing. K.Málek, Ing.B.Bajcsy, P.Rovný, E.Cerva, Ing.L.Pekete and J. Vaňová for technical help.

## References

1) J.Pivarč, Jaderná energie 29 (1983)244-254.
2) J.Pivarč, S.Hlaváč, J.Král, P.Obložinský, I.Ribanský I.Turzo and H.Helfer, Acta Physica Slovaca 30 (1980)119-136, see also Report INDC (CSR)-2/L$^{+}$ Special, IAEA Nuclear Data Section Report, Vienna May 1980.
3) S.Kliszevski, Z.Lewandovski, A simple stabilizer of high voltage supply for a fast neutron generator (Report No.826 /E/ Pl,Krakow 1973).
4) I.Izumi, M.Kukubu, Nucl.Instr. and Meth. 28 (1964)349.
5) J.Pivarč, K.Málek, B.Bajcsy and P.Rovný, Isolating transformer IT 300 for 300 kV and 10 kVA, see Proc. of this Symposium.
6) W.B.Herrmannsfeldt, SLAC Report 226, Stanford Linear Accelerator Center Stanford University, Stanford, California 94305, November 1979.
7) J.Pivarč, J.Král, Rotating target for a 300 keV neutron source: design, Proc. of the 10$^{th}$ Int.Symp.on Sel.Top.of the Inter. of Fast Neutrons and Heavy Ions with Atomic Nuclei-Fission-Heavy Ion Reactions, Gausig, 17-21 November (1980)185.
8) J.Pivarč, Heat diagnostic of a rotating target for a 300 keV neutron generator, Bratislava 1979 (unpublished).
9) T. Nemes, L. Rottelbusch, H.Rapp, Real-Time Application Examples of the Intelligent Crate Controller Type KKI-661 at the JINR Dubna, Proc. of the Real-Time Data Handling and Process Controll, ECSC,EEC,EAEC, North-Holland Publish. Comp., Brussels and Luxemburg 1980, 583.

# DESIGN OF A MULTI-PURPOSE INTENSE NEUTRON GENERATOR

P. Eckstein, F. Gleisberg, H. Helfer, R. Krause, U. Jahn, E. Paffrath,
D. Schmidt, D. Seeliger
Technische Universität Dresden, Sektion Physik, DDR-8027 Dresden

A.I. Glotov, V.A. Romanov
Physics and Power Institute Obninsk, USSR

## 1. Introduction

There are several nuclear reactions for neutron production, the mostly used ones producing intense neutron beams are shown in Table 1. Assuming an incident particle current of 1 mA neutron source strengths between $10^{11}$ and $10^{17}s^{-1}$ could be obtained. The well known DT-reaction is not the best candidate in this sense, but it shows two remarkable advantages: a very narrow spectral distribution near 14 MeV ("monoenergetic neutrons") and the lowest technical requirements and costs for accelerator instrumentation. There are some quite different possibilities for the design of intense DT-neutron sources. The mostly used type is the pumped small accelerator consisting of the main components source, acceleration tube, target, vacuum system. This generator type shows the greatest variability with respect to intensity variation and adaption to specific utilization. Table 2 shows the parameters of some typical pumped intense DT-generators which are under operation with emphasis on high intense machines. The aim of the present work was the conceptual design of an intense DT-neutron generator (ING) within the intensity range $(1...5)10^{12}s^{-1}$ basing on the experience of existing machines of this type (as far as available from the literature), already existing components and technological equipments in both institutes as well as on the posibilities of modern electronical circuits. In the following the main components of the resulting concept are characterized in some details. As far as the project of the Technical University Dresden is concerned the name INGE-1 is used.

## 2. The general scheme of the intense neutron generator INGE-1 proposed

The general arrangement proposed for the generator INGE-1 is similar to that of the RTNS-I neutron source /1/ and other generator projects /2,3/. The main components of the neutron generator are shown in fig. 1 with respect to their location. The high voltage terminal (1) is isolated from ground potential by ceramic insolators (2) up to 350 kV potential difference. Within the high voltage terminal the ion source (3), an ion pump (4), and power supplies (7,10) are located. The main vacuum system (4) is located on ground potential. The ion beam is accelerated by the acceleration tube (5) with anticorona rings and resistors for potential dividing. Power supplies and ion source within the terminal are controlled by opto-electronical circuits in connection with glass fibres (6). The accelerated beam is focussed by the lens (8) on to the rotating target (9), where the neutrons are produced by the DT-reaction. The position of the beam axis over ground floor is about 1,6 m, the overall dimensions of the generator amount to 1,4 x 2,3 x 4,3 $m^3$. Fig. 2 shows the scheme of the generator components in connection with the control elements and cooling and electrical supplies.
The proposed scheme seems to be reasonable for production of a high-quality (mono-energetic) 14 MeV-neutron beam for a broad field of different applications including also physical investigations with definite beam parameters.

## 3. Description of the main components

The ionoptical layout of the intense neutron generator INGE-1 is shown in fig. 3. The diaphragms at the end of the acceleration tube and also in front of the rotating target are water-cooled. The two valves near the target provide the possibility of exchange of

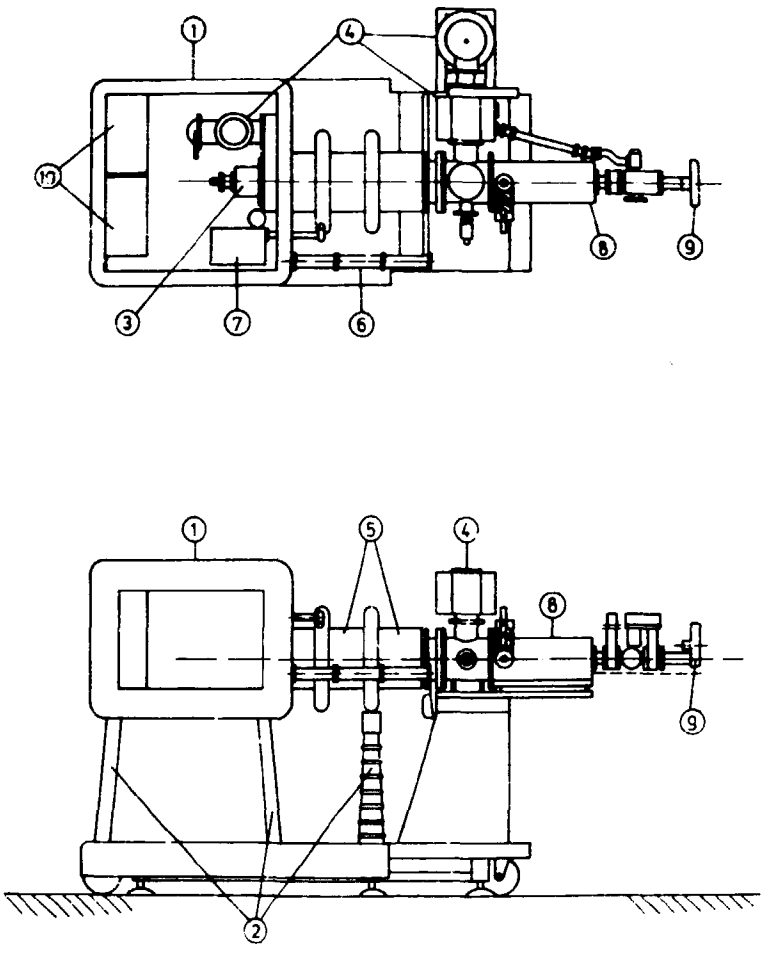


Fig. 1:
Schematic view of the intense neutron generator INGE-1.
1 - high voltage terminal,
2 - insulators,
3 - duoplasmatron ion source,
4 - vacuum pumps,
5 - acceleration tube,
6 - bulk of glass fibres,
7 - 50 kV power supply,
8 - quadrupole lense,
9 - rotating target,
10- power supplies

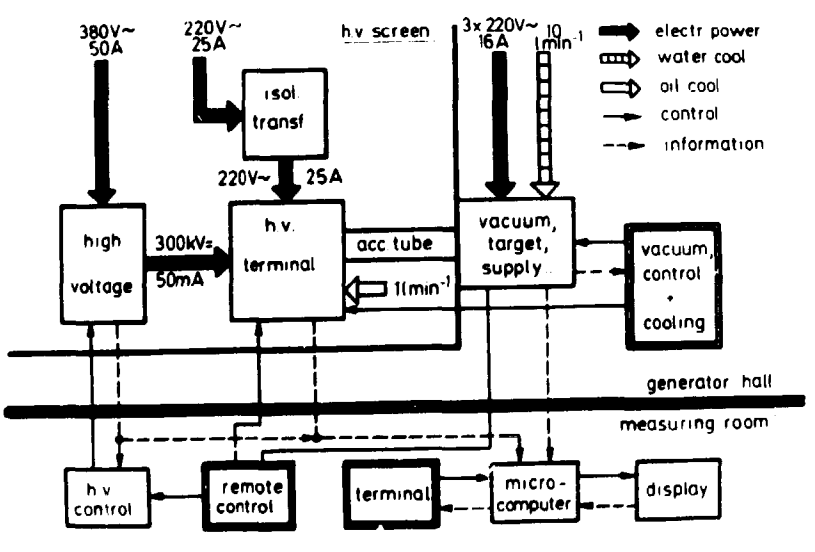


Fig. 2:
General scheme and location of the main components of the generator INGE - 1.

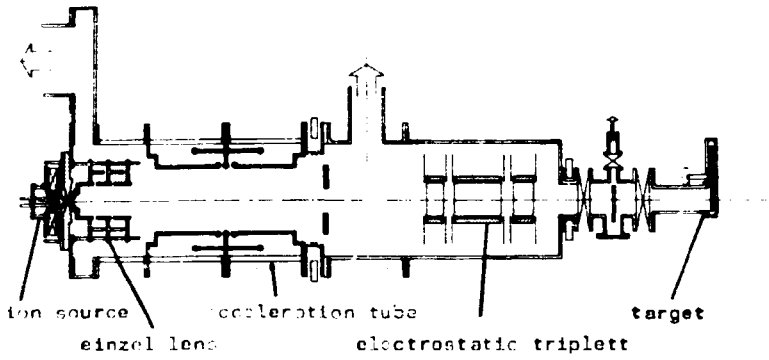


Fig. 3:
Ionoptical system of INGE - 1

the target.
The ion source is of the duoplasmatron type with specified extraction geometry. It is able to provide ion currents in the order of some 10 mA. The cathode consists of a nickel grid with embedded barium, calcium, and strontium. The source is cooled by oil from ground potential /4/.
The einzel lens is directly connected with the extraction electrode. It is constructed as a tube lens with an inner diameter of 78 mm. The maximum voltage of extraction is 50 kV, normally 30 kV are used. The zwischen electrode has also a negative potential with respect to the anode of the ion source, but at maximum 10 kV.
The acceleration tube is a two-acceleration-gap version (see fig. 4).

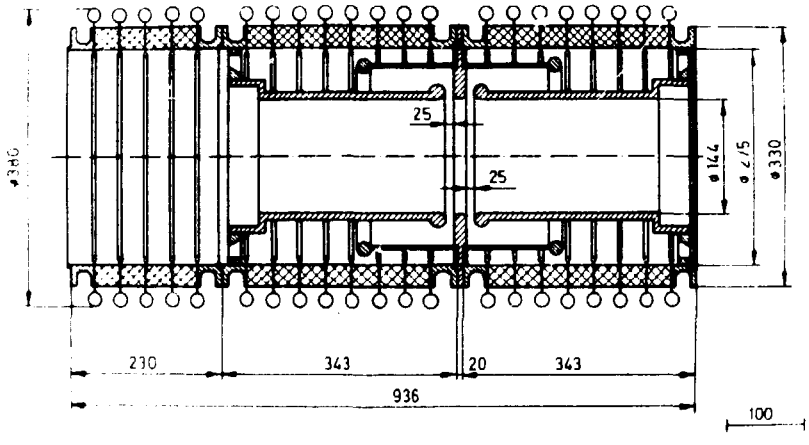


Fig. 4:
Schematic drawing of the acceleration tube (the left hand side section contains the einzel lens)

The electrodes are performed as tubes in order to screen the tube walls against particle striking as well as against soft X-rays. For the same reason, the zwischen electrode of the tube is also connected with a screening ring. The tube wall is built by ceramic rings, separated by stainless steel anticorona rings. For a definite linear potential distribution along the tube a divider is necessary. Despite of the relatively small current through the resistors of the divider ($R_{total}$ = 7 GOhm) no high power resistors are needed because of the effective screening mentioned above.
As shown by ionoptical calculations a focusing lens after acceleration was needed. For

this purpose a magnetic as well as an electrostatic quadrupole lens could be used. The target is of the rotating type with water cooling, see fig. 5. The active layer is 30 mm broad, therefore a water-cooled diaphragm in front of the target is arranged. The effective power per square centimeter is reduced by circulating with a speed of 300 rpm, the integral power may be up to 5 kW.

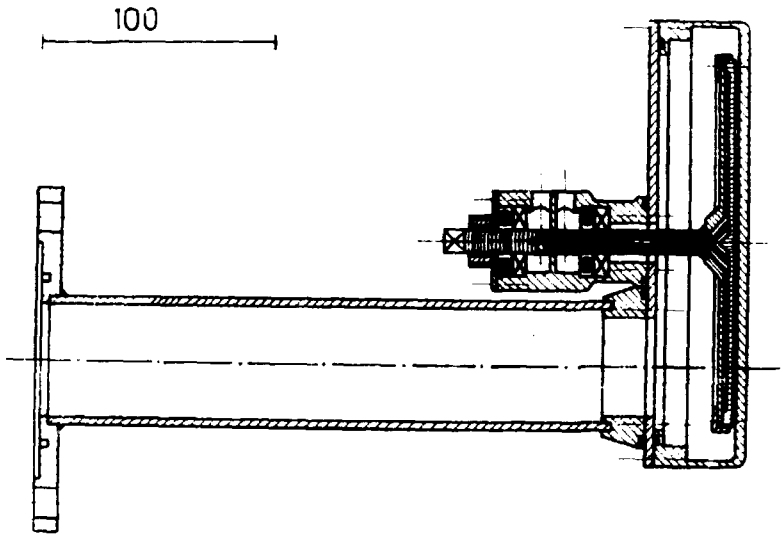


Fig. 5: Schematic drawing of the rotating target

Main components of the vacuum system are the pumps of three different types /5/: the getter pump for holding the vacuum without operation, an oil-free pump for ion source operation only and the oil diffusion pump (together with a $LN_2$-trap) for beam handling. The pumping speed during beam operation must be at least 2000 $ls^{-1}$ or higher. The scheme of the high voltage supply is shown in fig. 6

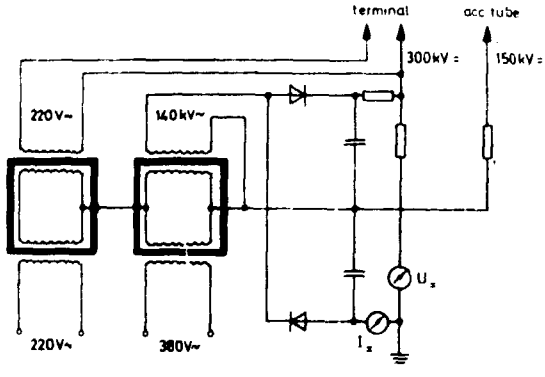


Fig. 6: Scheme of the high voltage power supply and the isolating transformer

It can provide a maximum voltage of 300 kV with a current up to 50 mA. The given version allows to use the half of the momentary voltage value at the zwischen electrode of the acceleration tube. The power flux to the high voltage terminal is realized by an isolating transformer with a maximum power of 12 kVA at 50 Hz frequency. A commercially available power supply GP 50/300 from VEB TuR Dresden is foreseen for this purpose. For operation of the generator INGE-1 a lot of different types of electric power supplies are needed. Supply units with a power below 500 W are realized in a switching mode using frequencies near 20 kHz /6/. This type is known to have a high efficiency, low mass and

small size. For the supply units with higher power a more conventional solution was found. All electric supply units should be controlled remotely and are able to provide reference signals within a standardized level.
The general scheme of control and data acquisition is shown in fig. 2. The connection between the high voltage terminal and ground potential is realized by glass fibres and ground potential is realized by glass fibres and opto-electronical units /7/. All analogue data are standardized within the range 0...+5 V corresponding to the maximum value of the controlled/checked magnitude. The vacuum control desk is located near the generator because no operation during beam handling is needed. It contains also safety-back loops for vacuum and high voltage. The ion source, high voltage power supply and the triplet can be controlled remotely by hand. The data acquisition is handled by a micro-computer in connection with a colour display for all electrical magnitudes and additionally for informations as temperature, pressure, flow rate of cooling circuits and others.

## 4. Conclusions

The project of the intense neutron generator INGE-1 described here seems to be suitable for a machine producing DT-neutron intensities above to $12 s^{-1}$. Some parts of it are realized already and show convenient properties. The concept hopefully allows a compact design as well as reliable operation of this small intense neutron generator.

Table 1: Some reactions for the production of intense neutron beams

| Reaction | $E_i$/MeV/ | n/z | $E_{in}^{z}$/GeV/ | $N_n/s^{-1}$/ | $\Delta E_n$ | accelerator |
|---|---|---|---|---|---|---|
| $T(d,n)^4He$ | 0.2 | $2.10^{-5}$ | 20 | $10^{11}$ | 0.2MeV | small acc. |
| X(d,pn) | 40 | $4.10^{-3}$ | 10 | $2.10^{13}$ | 10MeV | Cycl.,LINAC |
| $e^-$-(γ,n) | 100 | $2.10^{-2}$ | 5 | $10^{14}$ | broad | LINAC |
| Y(p,xn) | 800 | 20 | 0.04 | $10^{17}$ | broad | LINAC,Synch. |

$N_n = N_i(n/z)$; $N_i = 1$ mA/$1.6 \cdot 10^{-19}$As
$E_i$ - incident energy
n/z - neutrons per incident particles
$E_{in}^{z}$ - energy deposition in the target per neutron
$\Delta E_n$ - neutron energy spread

Table 2:

| generator | location | U/kV/ | I/mA/ | $N_n/10^{12}\ s^{-1}$/ | ref. |
|---|---|---|---|---|---|
| RTNS-II | Livermore/USA | 400 | 150 | 40 | /8/ |
| RTNS-I | Livermore/USA | 400 | 22 | 6 | /1/ |
| LANCELOT | Valduc/France | 160 | 160 | 6 | /9/ |
| CHALK RIVER | /Canada | 300 | 25 | 4 | /10/ |
| OKTAVIAN | Osaka/Japan | 300 | 20 | 3 | /11/ |
| JAERI | Tokio/Japan | 400 | 20 | 5 | /12/ |
| DYNAGEN | Hamburg/FRG | 500 | 12 | 3 | /13/ |
| INGE-1 | Dresden/GDR | 300 | 20 | project | |

References

/1/ R. Booth et al., Nucl. Instr. Meth. 145 (1977) 25
/2/ J. Pivarc et al., INDC(CSR)-2/L , IAEA Vienna (1980)
/3/ T. Sztaricskai, ZfK-459, ZfK Rossendorf (1981) 176
/4/ U. Jahn, J. Dietrich, Contribution to this Conference
/5/ U. Jahn et al., Contribution to this Conference
/6/ F. Gleisberg, J.-J. Esche, ZfK-503, ZfK Rossendorf (1983) 135
/7/ P. Eckstein et al., Contribution to this Conference
/8/ D.W. Heikkinen, C.M. Logan, UCRL-86747, Livermore (1982)
/9/ J.B. Hoorst, M. Roche, Acta Physica Slovaca 30 (1980) No. 2
/10/ J.D. Hepburn et al., IEEE Trans. Nucl. Sci. 22 (1975) 1809
/11/ H. Ullmaier et al., Nucl. Instr. Meth. 145 (1977) 1
/12/ T. Nakamura et al., Proc. VII. Symp. on Ion Sources and Ion Assisted Technology, Antwerp (1982)
/13/ M.R. Cleland, B.P. Offermann, Nucl. Instr. Meth. 145 (1975) 41

# ИОННО-ОПТИЧЕСКИЕ СВОЙСТВА УСКОРЯЮЩЕЙ ТРУБКИ НЕЙТРОННОГО ГЕНЕРАТОРА.

С.В.Бажал, В.А.Романов.
Физико-энергетический институт, г.Обнинск, СССР.

На основании расчета огибающей пучка рассмотрены ионно-оптические свойства ускоряющей трубки интенсивного нейтронного генератора.

Важным этапом разработки нейтронного генератора является расчет огибающих пучка заряженных частиц, который позволяет, во-первых, выбирать тип, положение и характеристики элементов фокусирующей системы, и, во-вторых, сформулировать требования к параметрам пучка в момент инжекции. Огибающие, согласно I), могут быть определены численным интегрированием системы дифференциальных уравнений

$$\left.\begin{aligned} \frac{d^2 r_1}{dz^2} &= \frac{I}{2\pi\varepsilon_0\sqrt{2\eta}\,U^{3/2}(r_1+r_2)} - \frac{U'}{2U}r_1' - \frac{U''}{4U}r_1 - \frac{(1-P)}{R_m^2}r_1 - \sqrt{\frac{\eta}{2U}}G_1 r_1 + \frac{U_0 E^2}{U r_1^3} \\ \frac{d^2 r_2}{dz^2} &= -\frac{I}{2\pi\varepsilon_0\sqrt{2\eta}\,U^{3/2}(r_1+r_2)} - \frac{U'}{2U}r_2' - \frac{U''}{4U}r_2 - \frac{P}{R_m^2}r_2 - \sqrt{\frac{\eta}{2U}}G_2 r_2 + \frac{U_0 E^2}{U r_2^3} \end{aligned}\right\} \quad (I)$$

где $r_1$, $r_2$ - поперечные координаты огибающих, $z$ - продольная координата; $U$, $U'$, $U''$ - распределении потенциала по оси системы и его производные, I - ток пучка, E - двумерный эмиттанс, $R_m$ - радиус поворота в магните, P - показатель спада магнитного поля; $G_1$, $G_2$ - градиенты магнитной индукции в квадрупольной линзе.

В вычислительной программе I) предполагаетсяя известным аналитическое выражение для распределения потенциала на оптической оси системы. Однако, для нейтронного генератора Технического университета это распределение получено численно в виде таблицы значений осевого потенциала, что обусловило необходимость его аппроксимации и численного дифференцирования.

Рассмотрим методику вычисления потенциала и его производных. Пусть потенциал известен в точках $x_0, \ldots, x_n$. Воспользуемся для его определения параболической интерполяцией третьего порядка, формула которой имеет вид 2)

$$y(x) = \sum_{i=0}^{3} y_i \frac{\prod_{\substack{s=0\\ s\neq i}}^{3}(x-x_s)}{\prod_{\substack{s=0\\ s\neq i}}^{3}(x_i-x_s)} \quad (2)$$

где x - координата точки, в которой вычисляются значения функции y(x), $x_0, \ldots x_3$ - координаты узлов интерполяции, $y_0, \ldots, y_3$ - значения функции в узлах. Оценка максимальной абсолютной погрешности при этом может быть сделана из соотношения 2)

$$|R(x)| < \frac{M_4}{4!}\prod_{i=0}^{3}|x-x_i| \quad (3)$$

где $M_4$ - верхний предел $/y^{(IV)}(x)/$ в интервале $[x_0, x_3]$.

Для достижения приемлемой точности потенциал должен не слишком быстро изменяться на интервале интерполяции, т.е., по крайней мере, должно выполняться неравентсво

$$/x_3 - x_0/ < Д \quad (4)$$

где Д - характерный размер апертуры фокусирующего элемента.

Вычисление производных выполняется по следующей схеме.

1. Дифференцированием соотношения (2) определяем производные во внутренней точке $x_I$ интервала интерполяции.
2. Сдвигая интервал на шаг интерполяции $h_i = x_i - x_{i-1}$ и повторяя п.I, образуем массив производных в точках $x_I, \ldots, x_{n-2}$.
3. Для вычисления производных в точках $x_0$, $x_{n-1}$, $x_n$ воспользуемся узлами $x_0$, $x_2$, $x_3$ соответствующих интервалов.
4. С помощью интерполяционной формулы (2) по найденным значениям производной определяем производные в любой точке участка интегрирования.

Оценка показывает, что использование внутренней точки повышает точность вычисления в узлах (при равномерном шаге интерполяции) по сравнению с точками границы интервала для первой производной - в 3 раза, для второй - в II раз.

Данная схема вычисления была проверена численными расчетами, проведенными для распределения потенциала, заданного соотношением

$$U = \frac{U_0}{2}\left[1 + th\left(\frac{1,32x}{R}\right)\right] \qquad (5)$$

где $R$ - радиус апертуры.

Расчеты показали, что при интерполяции с переменным шагом, удовлетворяющим соотношению

$$h < 0,15 \qquad (6),$$

относительная погрешность вычисления потенциала не превышает 0,I%, а его второй производной - 3%. Вблизи I-ой и $n$ - ой точек наблюдалось незначительное увеличение относительной погрешности.

Расчет огибающей в ионно- оптической системе нейтронного генератора был выполнен для следующих параметров пучка и фокусирующих элементов (экспериментальное исследование оптических свойств нейтронного генератора предполагается выполнить на протонном пучке), близких к реальным. Ускоряемые частицы - протоны, ток пучка - 7 мА, эмиттанс - $1,2 \cdot 10^{-4}$ м·рад при энергии частиц 25 кэВ. Начало координат совмещено с анодом ионного источника, находящегося под потенциалом 150 кВ (рис.I). Потенциалы электродов электростатической линзы: 125, 145 и 125 кВ, центральный электрод ускоряющей трубки находится под потенциалом 75 кВ. Исходная точка интегрирования, в которой поперечная координата огибающей равна $4,51 \cdot 10^{-3}$м, а ее угол наклона - $7,77 \cdot 10^{-3}$ рад., смещена от начала координат на $5 \cdot 10^{-2}$ м.

Огибающая протонного пучка представлена на рис.Iа. Более полную информацию о транспортировке пучка можно получить, вычисляя предельную огибающую, под которой понимается кривая, ограничивающая собой все пучки с начальными параметрами, изменяющимися в предполагаемых пределах. Условимся, что предельной огибающей в начальный момент на фазовой плоскости соответствует прямой эллипс, внутри которого находятся фазовые множества интересующих нас пучков.

На рис.Iб в качестве примера приведена предельная огибающая, которой соответствует фазовый эллипс со следующими параметрами:

$E = 3,6 \cdot 10^{-4}$ м·рад., $r_0 = 6 \cdot 10^{-3}$ м, где E - эмиттанс, $r_0$ - начальный радиус пучка.

Указанная огибающая охватывает пучки, начальные параметры которых изменяются в довольно широких пределах. Это позволяет сделать вывод о том, что при ускорении протонного пучка до энергии 150 кэВ ионно-оптическая система нейтронного гене-

ратора обеспечивает достаточное формирование пучка на мишень, установленную примерно в 1 м от ускоряющей трубки. При энергиях ~ 300 кэВ кроссовер пучка значительно смещается в сторону трубки. В этом случае для дополнительного формирования пучка целесообразно использовать квадрупольную линзу.

В заключение авторы выражают глубокую благодарность Д.Шмидту и У.Яну за предоставленные данные о параметрах пучка, распределении потенциала в трубке и за плодотворные обсуждения, а также А.И.Глотову - за участие в обсуждениях и полезные замечания.

## СПИСОК ЛИТЕРАТУРЫ

1. Комаров О.Л., Кузнецов В.С., Фидельская Р.П. Программа для расчета прохождения интенсивных ионных пучков через фокусирующие системы ускорителей прямого действия. Препринт НИИЭФА П-К-0512, Л, 1981.
2. Анго А. Математика для электро- и радиоинженеров. М., Наука, 1965.

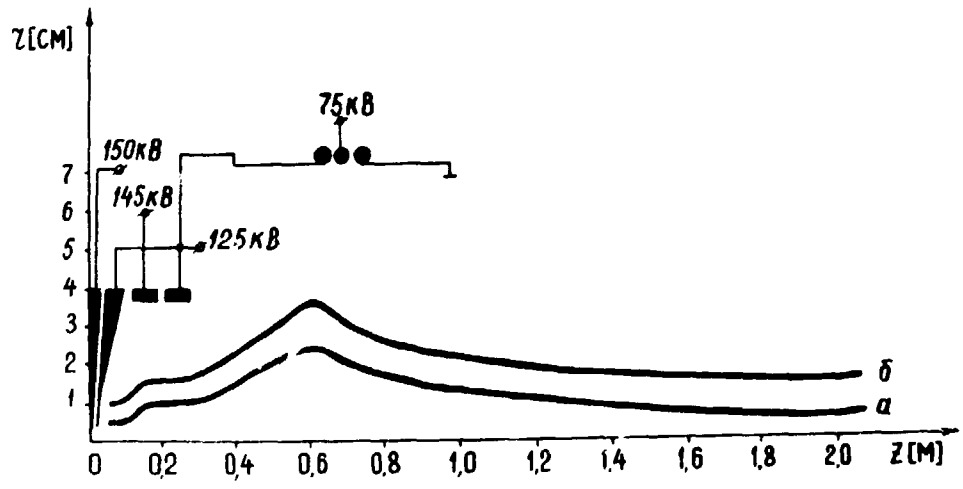


Рис. 1. Огибающие протонного пучка в ионно-оптической системе нейтронного генератора

# A DUOPLASMATRON SOURCE FOR THE PRODUCTION OF INTENSE DC ION CURRENTS

Sun Biehe, Wang Fulin, Chen Qin
Institute of Nuclear Research, Lanzhou University, Lanzhou, China

Abstract. A Duoplasmatron source for the production of intense DC ion currents has been investigated. Constant hydrogen ion currents up to 100mA have been obtained with extracting voltage of 20 kV. The mass ratios of hydrogen ions have been analyzed by 90° deflection magnetic analyzer for currents up to 50mA. In this range, up to 54 per cent of total currents is $H_1^+$. The emittance of ion source has been determined by the methods both multislits-probe and photocopying paper as well. A typically normalized emittance (phase space area x $B\gamma/\pi$) of 0.48 mm · mrad and the brightness of $4.4\times10^6 A/cm^2 \cdot rad^2$ have been obtained for 50mA beams at 16 kV accelerating voltage. The operating characteristics of the source were investigated. In this paper, the experimental results for the production of a variety of heavy ion beam, such as helium, nitrogen, oxygen, mixed neon-helium (78 % Ne + 22 % He) and argon are given as well.

## 1. Introduction

The ion source developed originally by M. von Ardenne and coworkers[1]), called a "Duoplasmatron", has been furthermore investigated by many other authors[2,3]). This Duoplasmatron is used as ion source of the intense neutron generator (This neutron generator has total neutron yield of (2-1) x $10^{12}$n/s.) , which is being setup in Lanzhou University. It is necessary to have high gas efficiency because of the limited pumping speed, and in addition, it would be desirable to have a high ratio of atomic ion to molecular ion in order to increase the specif yield of the neutrons. For a high efficiency of the beam transmission, it is expected to have a small emittance of the beam leaving the source. The Duoplasmatron source seems to fit the requirements of high current and high efficiency and has been adopted as a practical and satisfactory ion source for use in neutron generator of intense flux[4,5]).

## 2. Description of Source

A cross-sectional view of the construction and the component arrangement of the Duoplasmatron source is shown in Fig. 1 and an insert shows an expanded view of the anode region. The intermediate electrode is made of mild steel and cooled by the transformer oil from the bottom to the top. For a better effect of cooling the outer surface of the intermediate electrode is made of cooling frocks. In order to prevent the leakage of cooling oil the frock and intermediate electrode are joined at the end by arc welding. The cooling oil is pressed into the frock by using an oil pump of 15 l/min flow rate, 10 atm/$cm^2$ pressure and the oil flows circularly along the outer edge of intermediate electrode as shown.

The intermediate electrode and the anode are insulated by employing ceramic ring and give an electrode spacing of 5 mm. The entire assembly is aligned mechanically with a plug. Silicium rubber washer is used to make the vacuum seal. The molybdenum anode button with 1 mm aperture is pressed into the anode which is made of mild steel as well, and the anode is cooled by oil as above. This type of construction permits continuous operation with discharge currents up to 10 Amperes.

The magnetic field is produced by a coil wound with approximately 1000 turns. The coil case slips loosely over the intermediate electrode assembly and is fixed entirely outside the vacuum system. The magnetic field produced between intermediate and anode with ~5000 Amp-turns is about 5 kilogauss.

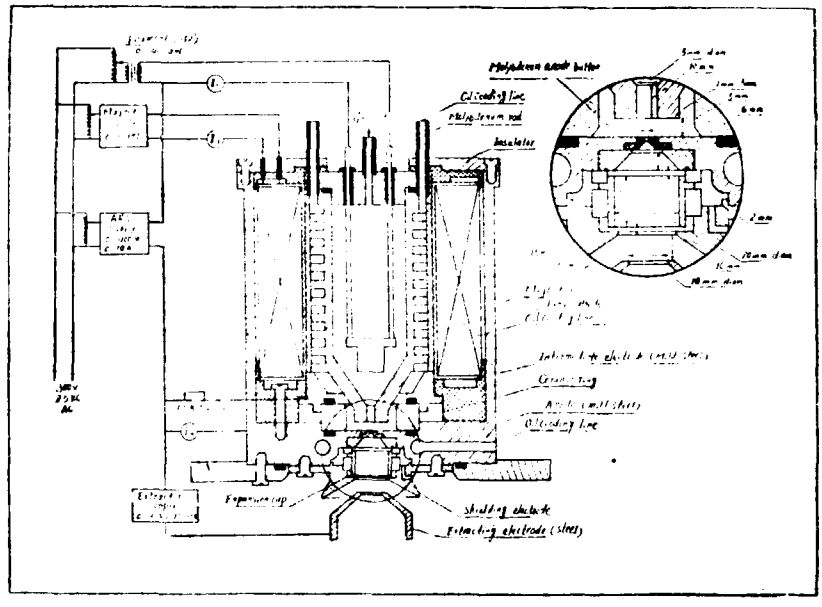

Fig. 1 Cross-sectional view of the construction and the component arrangement of Duoplasmatron ion source. Insert shows an expanded view of the anode region.

The gas inlet is in the cathode assembly as shown, although this position is a matter of convenience. The palladium leaker has been used to insure purity of the incoming hydrogen gas.

For prolongation of lifetime of the cathode a lanthanum hexaboride emitter was adopted. The construction of the cathode is shown in Fig. 2. The emitter is shaped into a disk of 12 mm in diam, 2 mm in thickness and heated indirectly by the tungsten heater. In order to obtain adequate ion beam optics and to increase ion emission area over which the ion is extracted, thus, higher total beam currents can be extracted, a plasma expansion cup has added after the anode aperture. The cup was electrically isolated from the anode by small ceramic insulators. So the expansion cup was assumed at a floating potential during the course of the operation. In order to obtain adequate initial beam diameter and to prevent the effects of disperion field for ion emission surface, a shielding electrode at anode potential has been added to exit hole of the expansion cup.

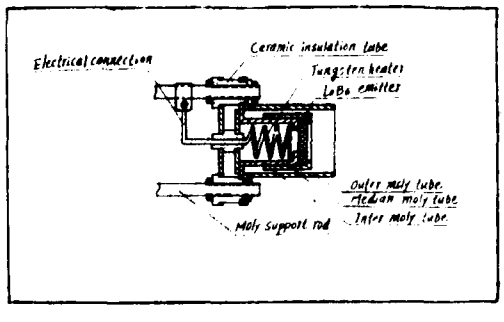


Fig. 2
The construction of the $LaB_6$ cathode

The shielding electrode and extracting electrode are shaped as the quasi-Pierce type geometry. According to Pierce theory, [6]) it is possible to maintain a parallel beam. The beam intensity Ii(A), under these condition is given by[7])

$$Ii = \frac{5.44 \times 10^{-8}}{M^{1/2}} \cdot A \cdot \frac{V_{extr}^{3/2}}{Z^2} \qquad (1)$$

where $V_{extr}$ is the applied potential difference in Volts. M is the ionic mass number. A is the ion emission area and Z is the effective spacing between electrodes.

## 3. Experimental Apparatus and Methods

The arrangement of the test-stand is shown schematically in Fig. 3.

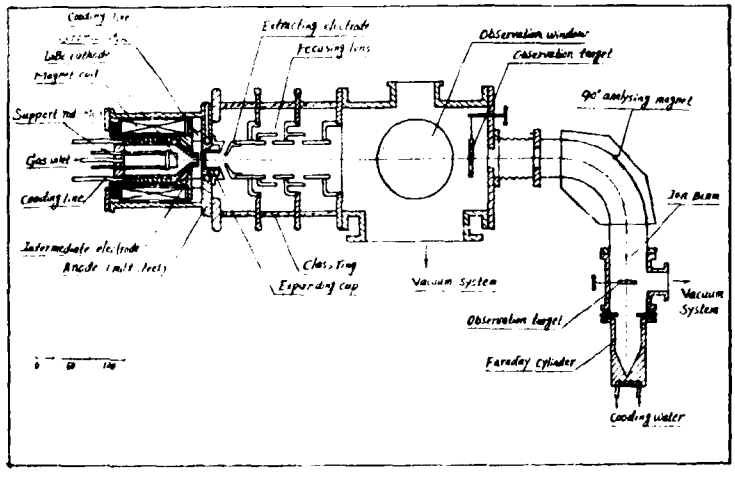


Fig. 3
Schematic drawing of experimental apparatus of Duoplasmatron ion source.

The ion beam extracted from the source was focused by means of the einzel lens. The focused beam flying about 500 mm goes through a 90° deflection magnetic analyzer. Analysed beam was received by Faraday cup with the water cooling. The evacuation system consists of a main pumping system fitted before the analyzer and an auxiliary pumping system fitted behind the analyzer. When gas consumption of the ion source is zero (i.e. palladium leaker hasn't been heated) the vacuum of the vacuum chamber is measured better than $4 \times 10^{-6}$ Torr. During the operation the vacuum has a variation range of $(1 \sim 1.5) \times 10^{-5}$ Torr according to difference of gas consumption of the source.

Unanalysed beams were determined by the use of a Faraday cup located after the einzel lens (this cup isn't drawn in Fig. 3 as an adjunct, may in or taken out). A diaphragm was equipped at the entrance of the Faraday cup. And it was biased at 350 Volts negative potential with respect to cup (grounded).

Both multislits-probe method and photocopying paper method were used to determination of emittance of the ion beams from the source. A schematic drawing of the apparatus for the determination of emittance is shown in Fig. 4. A Faraday cup with a thin-plate metal diaphragm in the bottom was located at the path of ion beam. The diaphragm with seven slits is made of tantalum plate of 0.2 mm in thickness and the slit width is 0.12 mm,

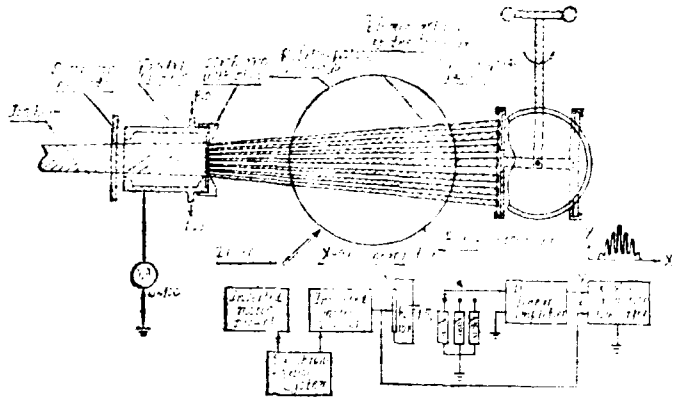

Fig. 4
Schematic drawing of apparatus for the determination of the emittance diagram of ion beams.

the slit distance from one slit center to another is 3 mm. The elementary parts of the ion beam singled out from incident beam by the diaphragm slits were determined by using rotating needle-like electrode or the ZnS coated plate at 170 mm from the diaphragm. The normalized emittance of the ion beam is given by [8])

$$En = 1/\pi \cdot A \cdot \beta \cdot \gamma \quad \text{in mm} \cdot \text{mrad.} \tag{2}$$

and brightness

$$Bn = \frac{2I \times 10^8}{(\pi En)^2} \quad \text{in mA/cm}^2 \cdot \text{rad}^2 \tag{3}$$

where A is the phase space area in mm · mrad, β is the ratio of the ion velocity to light velocity, γ is relativistic factor, I is the intensity of beam current in mA.

## 4. Experimental Results

Unanalysed output currents were determined as the functions of the various source parameters. Some results of these experiments are shown in Fig. 5. The data were taken with a constant gas flow through the source. The pressure in the cathode region was measured by a thermocouple gauge before the discharge started. The pressure values are uncorrected thermocouple gauge reading for hydrogen gas. In order to know the gas flow rate of the source the measurements of gas flow rate were made using a gasflowmeter.

It may be noticed that the beam intensity extracted from the source increases rapidly as the arc current increases, and maximum output current is correspond to adequate magnetic field values. At high magnetic field, the output does not increase.

The experimental results in Fig. 5 show that the output beam intensities are dependent on $V_{extr}^{3/2}$ as given in eq (1). Due to the limitation of the output power of the extracting supply, all data were taken at lower arc current and the extracting voltage below 22 kV.

The mass spectrum of beam have been determined for currents up to 50mA under various operating parameter. Some results are shown in Fig. 6 and Fig. 7. The mass resolving power of the analyzer was sufficient that the three mass species could be clearly separated on the mass spectrum figure. The percentage of $H_1^+$, as shown in Fig. 7 can reach 64 per cent for 6 Ampere arc current and $1.3 \times 10^{-1}$ Torr source pressure. It is worth noting that the mass components are mainly dependent on the source pressure and arc

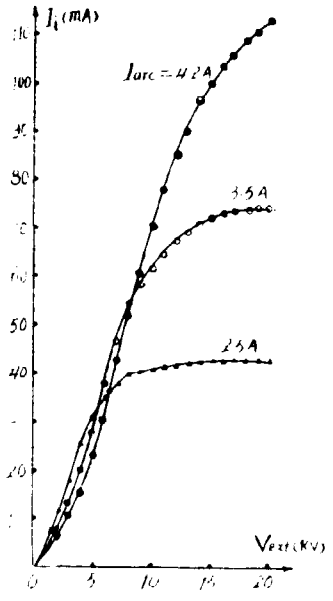


Fig. 5

Dependence of hydrogen ion currents from the source on the extracting voltage.
Parameter: exciting current: Im=3.5A(~3700Gs).
source pressure: $2.4 \times 10^{-1}$ Torr.

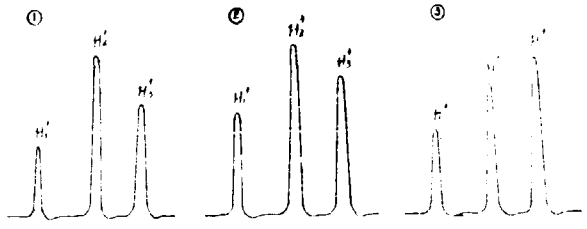


Fig. 6

Dependence of mass spectrum of ion beams from the source on the source pressure. Parameter: Iarc=3A. Im=2A(~2130Gs). Vextr=16kV. source pressure:
1) $1.9 \times 10^{-1}$ Torr. 2) $2.7 \times 10^{-1}$ Torr 3) $3.9 \times 10^{-1}$ Torr

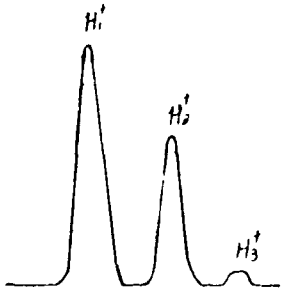


Fig. 7

Mass spectrum of ion beams from the source. Parameter: Iarc=6A Im=2A(~2130Gs). Source pressure: $1.4 \times 10^{-1}$ Torr.

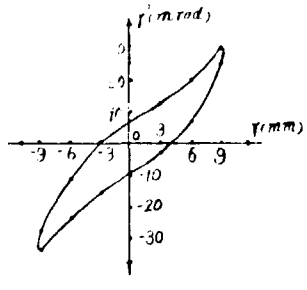


Fig. 8

Emittance diagram of ion beams from the source.
Ii=50mA. Vextr=16kV.

current under the constant distance between the intermediate electrode and anode. When source pressure was increased, as shown in Fig. 6. $H_3^+$ component was rapidly increase.

The emittance diagrams of the beam current were made by using the photocopying paper method, the ZnS coated plate was used. The result is shown in Fig. 8. The phase space area is 83.2 mm · mrad for 50 mA beam currents, at 16 kV extracting voltage. Therefore, a normalised emittance and the normalized brightness of 0.48 mm . mrad and $4.4 \times 10^6$ A/cm$^2$ . rad$^2$, respectively, are given.

When the value of arc current is 5 A and the value of extracting voltage is 20 kV, 59 mA helium, 48 mA nitrogen, 35 mA oxygen, 41 mA mixed neon-helium and 22 mA argon ion currents extracted from the source have been obtained. The results of some experiments are shown in Fig. 9 - Fig. 13.

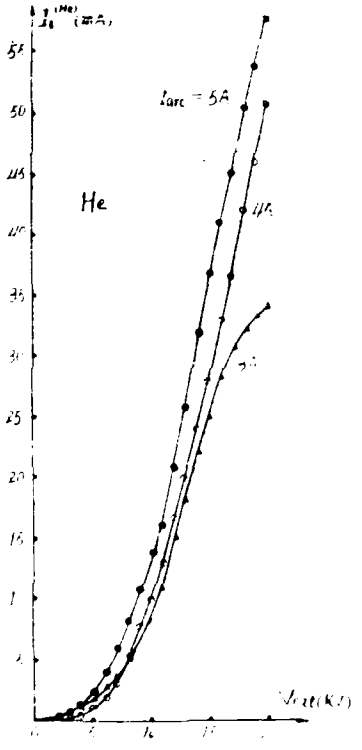


**Fig. 9**

Dependence of helium ion currents from the source on the extracting Voltage. Parameter: Source pressure: $1.2 \times 10^{-1}$ Torr. Gas consumption of the source: 64.5. ml · atm/hr.

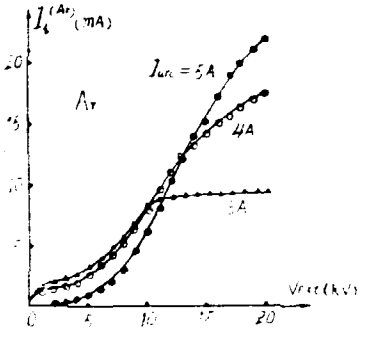


**Fig. 10**

Dependence of argon ion currents from the source on the extracting voltage. Parameter: Source pressure: $1.2 \times 10^{-1}$ Torr. Gas consumption of the source: 20.5. ml · atm/hr.

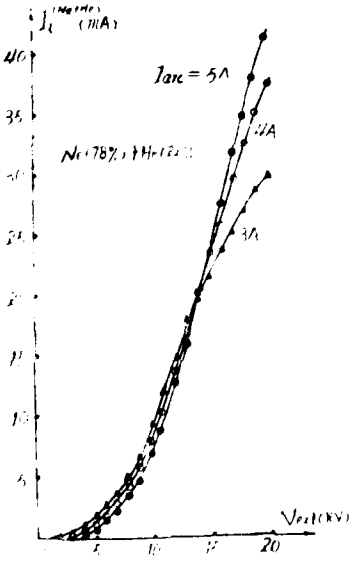


**Fig. 11**

Dependence of the mixed neon-helium ion currents from the source on the extracting voltage. Parameter: Source pressure: $1.2 \times 10^{-1}$ Torr. Gas consumption of the source: 31.8. ml · atm/hr.

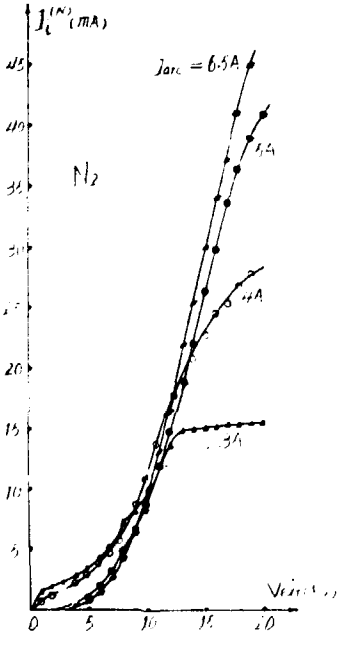


**Fig. 12**

Dependence of nitrogen ion currents from the source on the extracting voltage. Parameter: Source pressure: $1.2 \times 10^{-1}$ Torr. Gas consumption of the source: 36.7. ml · atm/hr.

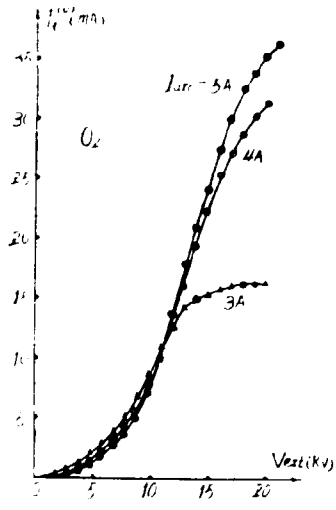


**Fig. 13**

**Dependence of oxygen ion currents from the source on the extracting voltage. Parameter: Source pressure: $1.2 \times 10^{-1}$ Torr. Gas consumption of the source: 33.5. ml · atm/hr.**

**The experimental results show that the operation of indirectly heated lanthanum hexaboride cathode is of good repeatability and stability. The lifetime of a cathode could be 300h approximately. Finally, the cathode was destroied due to tungsten heater become thin and brittle under the environment of high temperature and hydrogen gas, thus, tungsten filament break off.**

## References

/1/ M. von Ardenne, Atomkernenergie, 1, 121(1956).
/2/ Masanori Watanabe, Japan. Jour. Appl. Phys., 6, 9, 1127 (1967).
/3/ F.M. Bacon, Rev. Sci. Instr., 49, 4, 427 (1978).
/4/ H. Ullmaier, Nucl. Instr. Meth., 145, 1 (1977).
/5/ Jinchoon kin, Nucl. Instr. Meth., 145, 9 (1977).
/6/ J.R. Pierce, J. Appl. Phys., 11, 548 (1940).
/7/ O.B. Morgan, G.G. Kelley, and R.C. Davis, Rev. Sci. Instr., 38, 4, 467 (1967)
/8/ J.H. Billen, Rev. Sci. Instr., 46, 33 (1975).

# A 300 KEV COMPACT NEUTRON GENERATOR

Su Tongling, Sun Biehe et al.
Department of Modern Physics, Lanzhou University, Lanzhou, China

This paper describes a neutron generator. Because a neutron yield of $(1-2)\times10^{11}$n/s is required, the accelerator is rated at 300 kV, 1.5 mA. The experiments have given a maximum neutron yield of $5.1\times10^{11}$n/s by bombarding the tritium-titanium target with a deuteron beam of 3.1 mA at 300 keV. The generator worked steadily within the limits of yields $(2-3)\times10^{11}$n/s. For a fresh target with better quality with a 36 mm effective diameter; a neutron yield of $1\times10^{11}$n/s can be kept constant for ten hours.

For ion source we selected high frequency type. An assembly-type acceleration tube with the quartz-epoxide resin insulation rings is adopted. The high voltage DC power supply is a three-section type Cockcroft-Walton voltage multiplier circuit, each section consists of two stages. The HV supply and the power supplies of the whole ion source are fed by two 2.5 kHz frequency thyristor inverters respectively. Besides, a vacuum cold trap with semiconductor thermoelectric cooling, two sets of electrostatic deflection beam scanners and a programme controller for beam impulse modulating are used.

This neutron generator is characterized by its compactness, small dimension, light weight, steady work, easy operation and maintenance.

## 1. Introduction

For certain special applications of this neutron source, the requirements, such as a total yield of $(1-2)\times10^{11}$n/s, an intensity variation less than 5 % within five minutes, an outside diameter of the target holder and drift tube less than 90 mm and so on are needed. For this reason, in order to produce a neutron yield of $(1-2)\times10^{11}$n/s and to prolong target lifetime, the accelerator is rated at 1.5 mA and 300 keV and the beam is scanned over all the effective target area.

## 2. Accelerator description

Fig. 1 shows a general view of the neutron generator. The distance, from the axis of the beam to ground, is 1480 mm; the length, from the high voltage terminal to the front of the scanners, is 2210 mm; the maximum height and width are 1830 mm and 900 mm respectively; the total weight is about one ton. Four small wheels fitted under a bottom plate can make the generator move about in the room.

### 2.1. Ion source

A high frequency ion source was adopted because it has high atomic ion fraction in the beam and can easily produce a deuteron beam of a few milliampere[1,2,3]. Fig. 2 shows the general view of the ion source.

We expect that an ion source not only can give a stabilized beam more than 3 mA, but also has a longer useful lifetime.

Stability of the beam is principally dependent on stability of the power supplies of the ion source, therefore, besides the stabilized 2.5 kHz source, for screen grid bias of the oscillator and the heating power supply of the palladium tube, the stabilised DC power supply has also been used.

Lifetime of a high frequency ion source is mainly dependent on that of extraction electrode. B.A. Dyachkov indicated that for a source of top-extracting type, the lifetime

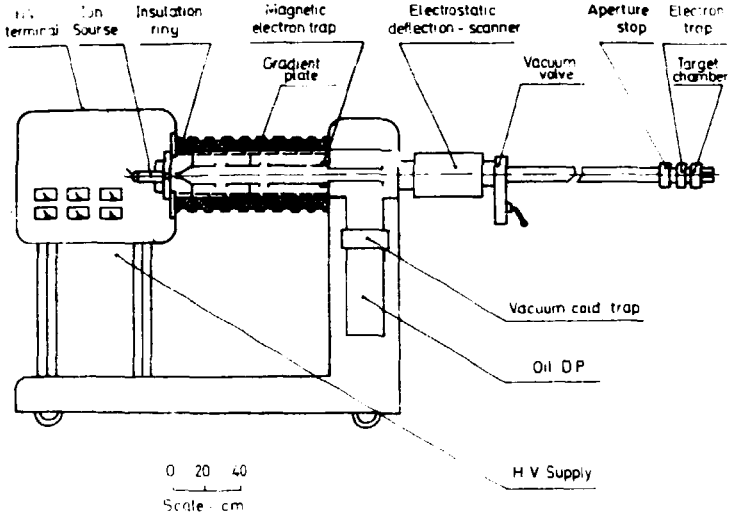


**Fig. 1**
**Diagram of the neutron generator**

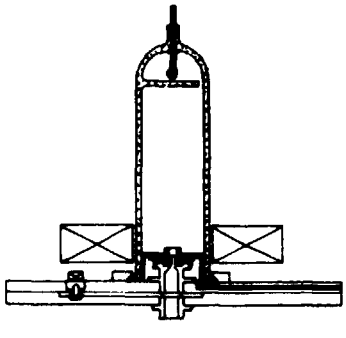

**Fig. 2**
**Assembly drawing of the high frequency ion source**

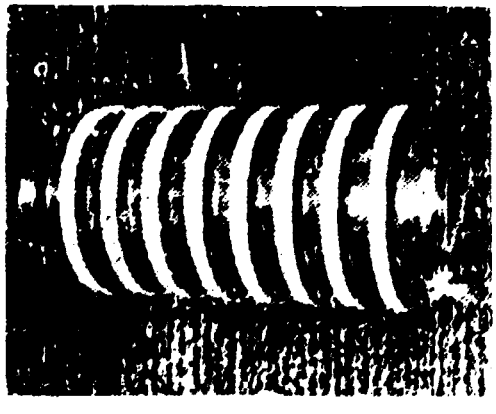

**Fig. 3**
**Assembly-tybe acceleration**

of an extraction electrode is inversely proportional to extracted beam. If the extracted current is 0.1-0.5 mA, it can reach a few hundred hours; but when current is 5-10 mA, only 20-30 hours[4]).

For this reason, the best geometries and electric parameters of the extraction system have been determined through a great deal of experiments. Two types of the beam aperture of the extraction electrode, neck type and cylinder type, have been tested. Both can give a maximum extracted beam of 8 mA on a test stand. But the gas consumption of the former is less than that of the latter, while the beam of the latter is more stable. At 3 mA the maximum variation of top-extracted beam is less than 1.3 % in 8 hours, furthermore, the beam drops to 90 % of its initial value in 120 hours. The atomic ion fraction in the beam is over 80 %.

## 2.2. Acceleration tube

The acceleration tube adopts the assembly-type which is divided into nine stages by nine insulation rings. It is shown in Fig. 3. Between the rings are inserted the alloy aluminium plates. Several 72MΩ resistors are installed between each plate grading the potential along the whole tube. The accelerating and focusing fields are formed in the gaps of three cylindrical electrodes with equal diameters, the prefocusing electrode, the middle electrode and the ground electrode. The total length of the acceleration tube is about 830 mm.

The insulation rings are cast with 30 % epoxide resin and 70 % quartz-powder in vacuum because this material has better machinability, and therefore is suited for assembly.

It is known that the predischarge current density and breakdown voltage on the surface of dielectrics in vacuum are very much dependent on the angle $\theta$ between the surface of the insulator and the cathode, when $\theta=31.5^{\circ}$, the surface current density is zero[5]). The experiments for epoxide resion indicated that its surface breakdown strength in vacuum varies from 20 kV/cm to 300 kV/cm with angle $\theta$; when $\theta=50^{\circ}$, it is a maximum[6]). We selected $\theta=45^{\circ}$. The insulation rings are shielded from the stray ions or secondary electrons by the metal rings fitted on each plate.

The experiments found that some of the secondary electrons produced by the stray ions fallen on a water-cooling aperture stop in front of the electrostatic deflection scanner were accelerated in opposite direction of the beam and fell on some of the electrodes and the plates, therefore, caused an uneven distribution of the potential along the whole tube, temperature rise and gas desorption of some components, and consequently led to the breakdown of the acceleration tube.

The secondary electrons were effectively screened by means of a magnetic electron trap fitted on the ground electrode and a metal tube prolonged the ground electrode to the adjacent water-cooled aperture stop.

## 2.3. HV supply

The high voltage power supply is a Cockcroft-Walton type voltage multiplier circuit which is rated at 300 kV - 6 mA.

A three-section type circuit with two stages per section as shown in Fig. 4 is adopted, in which the voltage drop due to the descharge of the column condensers is 1/8 of that of a 6 stage circuit.

For a small voltage drop, a high operating frequency is desired. However, high-power, high-voltage transformer is limited in frequency; a reference indicated that 2 kHz seems to be reasonable choice. At this frequency, the transformer core can still be built with a normal thickness of iron sheet metal and losses will still be low[7]). We adopted 2.3 kHz.

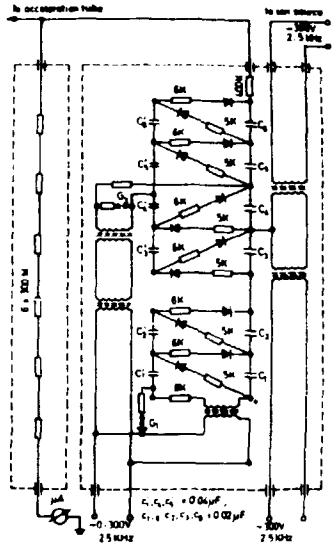

**Fig. 4**
**Three-section type voltage multiplier circuit with two stages per section**

In practice, besides the voltage drop due to the discharge of the column condensers, the voltage drops due to the transformers and the forward resistance of the rectifiers can not be negligible either.

The voltage drop due to the transformers was approximately calculated utilizing the measured parameters of the stray capacitance, leakage inductance and resistance of its equivalent circuit[8]).

The voltage drop due to the forward resistance of the rectifiers was calculated utilizing the measured forward resistance of the rectifiers varied with the direct load current by Baldinger formula[9]).

The calculated curves of the total voltage drop with respect to the direct load current is in agreement with measurements in general. Results show, under small load current, the total average voltage drop is larger and decreases with the load current more quickly than that under large load current mainly because of the non-linear forward resistance of the rectifiers. For example, an input voltage of 100V of the driving transformers being kept constant, for a load current of the first 4mA the average voltage drop of the output voltage is about 3.3kV/mA, while that for a load current from 4mA to 22mA is about 1kV/mA.

The rectifier rack, protective resistor, driving transformers, insulation transformers providing power for the ion source and so on are assembled in an epoxide resin-glass cloth cylinder with a 500 mm inside diameter and a 950 mm height. In the cylinder is filled transformer oil for improving insulation and dissipation.

## 2.4. Frequency generator with the thyristor inverter

The HV supply and ion source are fed by two 2.5 kHz-3kW generators of thyristor inverter, respectively. The output voltage of that for the HV supply can be continuously adjusted from zero t 300 V and is stabilized within range of 200-300 V. The output voltage of that for ion source is 300 V and is stabilized at one point.

Our measurements gave:

| | |
|---|---|
| - frequency stability | better than ± 1 %, |
| - stability of the output voltage | better than ± 1 %, |
| (when the variation of the input voltage is ± 15 %,) | |
| - efficiency | more than 90 %. |

A routine operation over a period of more than four years has shown that these generators are characterized by its continuous adjustment of the output voltage, steady work, reliability of the protection against overcurrent, easy operation and maintenance.

## 2.5. Vacuum system

The high vacuum in acceleration tube is maintained by an oil diffusion pump with a rated speed of 1200 l/s for air. A semiconductor thermoelectric cooling vacuum cold trap capturing pump oil is fitted on the top of the oil diffusion pump. After thermal equilibrium, the measured temperature at a centre shield sheet of the cold trap is about -13 $^{0}$C.

## 3. Result and performance

### 3.1. Accelerator

Experiments have given a maximum beam of about 3 mA at 300 keV. Under 2 mA at 300 keV, the accelerator can be continuously and steadily operated. For a beam of 1.5 mA at 300 keV, the variation of the beam current is less than 4 % in one hour. The minimum beam diameter on the target is about 1 cm.

### 3.2. Neutron yield

The cooling structure of tritium-titanium target is a narrow slit of 0.5 mm. A reference evaluated that under a velocity of 5 m/s of water in the slit this structure can withstand a power of 1000 W (beam diameter 30 mm), 500 W (beam diameter 20 mm) and 200 W (beam diameter 12 mm)[10]).

We used high pressure water with a velocity of 10 m/s to cool the back surface of the target directly and made the beam to scan over area of the target. For a deuteron beam of 3.1 mA at 300 keV, the (d, T) reaction gave a neutron yield of $5.1 \times 10^{11}$n/s. For a fresh target of better quality with a 36 mm effective diameter, the neutron yield decreased from $2.4 \times 10^{11}$n/s to $1.2 \times 10^{11}$n/s in 4.8 hours for a beam of 1.5 mA at 300 keV, and a neutron yield of $1 \times 10^{11}$n/s could be kept constant for 10 hours by means of gradual increasing the target current.

### 3.3. Beam impulse modulation

In some applications an impulse neutron yield is required.

First convert the electric pulses produced by a programme controller into the light pulses through a light emitting diode fitted on the bottom plate, then transmit them into the high voltage terminal. Through a light sensitive transistor and a control circuit convert the light pulses back into the electric pulses, whose amplitudes are from -150 V to + 300 V, and finally use them to modulate the screen grids of the oscillator of the ion source, and then we can get an impulse neutron yield.

Our experiments gave:

- impulse width 10 ms - 10 s,
- rise time of the neutron pulses less than 1 ms,
- fall time of the neutron pulses less than 2 ms,
- switching ratio of neutron impulse is greater than $10^{6}$.

A routine operation over a period of more than three years have shown that this neutron generator has realized all desired characteristics.

## References


1) L.C.W. Hoblis, J. Nucl. Energy, Part C, Plasma Phys. I (1960) 130.
2) V.I. Petrov, At. Energiya 2 (1960) 163.
3) G. J. Witteween, Nucl. Instr. and Meth. 158 (1977) 51.

[4]) B.A. Dyachkov, Prib. Techn. Exp. 4 (1966) 32.

[5]) H. Boeysch, et al, Z. angew. Phys. 15 (1963) 518.

[6]) R. Hawley, et al, Vacuum, 18 (1964) No7. 393.

[7]) O. Reinhold, et al, IEEE Trans. Nucl. Sci. NS-14, No3 (1975) 1289.

[8]) G.S. Tsaidjin, Project of a low frequency transformer

[9]) E. Baldinger, Handbuch der Physik, Band XLIV, Springer-Verlag, Berlin, Göttingen, Heidelberg (1959).

[10]) J. Kas, D. Novak, Nucl. Instr. and Meth. 99 (1972) 359.

# IONOPTICAL CALCULATIONS OF THE INTENSE NEUTRON GENERATOR INGE-1

U. Jahn
Technical University Dresden, Section of Physics, GDR

J. Dietrich
Central Institute of Nuclear Research Rossendorf, GDR

## 1. Introduction

A main component for accelerator designing is how to solve the ionoptical arrangement in order to get optimal ion beam parameters at the target position. In the last years the development of an intense neutron generator has been started for nuclear research at the Technical University Dresden.
For this purpose the deuterons must be accelerated up to several hundred kV with a beam current in the region of 30 mA. This report gives an overview about the ionoptical calculations connected with this project, denoted as INGE-1 /1/.

## 2. General considerations

At first it must be made a remark concerning the influence of space charge on the ion beam transport and the degree of neutralization under realistic vacuum conditions. An order of magnitude of the beam expansion can be obtained using the formula given by Hutter /2/ for the case of zero emittance in a drift region and in an absolute vacuum. In fig. 1 the expanded radii r of deuteron beams with given energies (initial radius $r_0$ = 5 mm and current 30 mA) are shown versus axial distance.

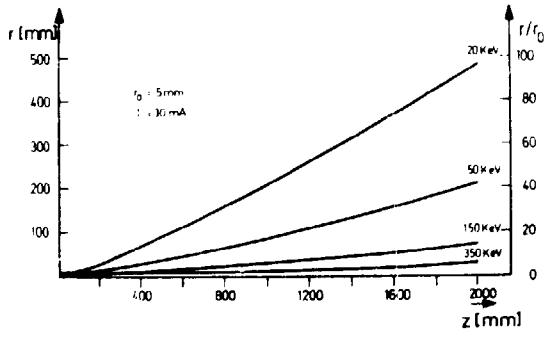


Fig. 1:
Space charge expansion of a parallel deuteron beam in field-free space for different ion kinetic energies between 20 keV and 350 keV

The rough model includes the real vacuum conditions, and so the space charge neutralization by rest gas molecules is considered. That means this effect depends on the influence of real gas pressure on relation to the ion beam diameter. Fig. 2 represents this. From the figures one has to derive the following conclusions:

- in the region of low ion energy the space charge expansion can not be neglected for ionoptical calculations,
- for real beam transport two tendencies are important: low pressure gives good high voltage resistance, but minimum space charge neutralization and opposite.

The basic requirements for the design of ionoptical components can be summerized in the following points:

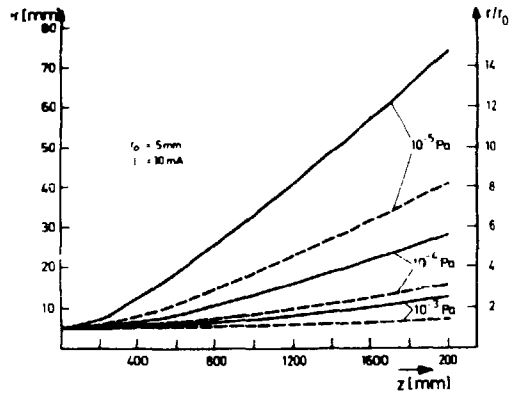


**Fig. 2:**
**Influence of real vacuum conditions on ion beam space charge expansion**
—— 50 keV $D^+$ ---- 350 keV $D^+$

- shielding of all insulating surfaces against particle impacts,
- wide apertures for all individual ionoptical components to provide hig pumping speed,
- minimum drift length to decrease space charge effects especially in low ion energy region,
- high flexibility of the mechanical construction, for providing the possibility of changing parameters during test runs

It is not so easy to fulfil all these requirements simultaneously, but in practice it is possible to obtain a good compromise.

## 3. Ionoptical calculations

As shown, the ionoptical calculations for intense ion beams must include space charge expansion especially in the low energy region. For that reason it was used the computer code ELENS written by Hornsby /3/. This program solves the Laplace-equation in case of rotational-symmetry for a given electrostatic arrangement and calculates the ion pathes. The consideration of space charge expansion will be calculated with the assumptions of quasi-laminar flight pathes of the ions and a constant ion current density over the beam cross section. After passing the acceleration tube the beam envelope was determined with the programm SYSFIT /4/. It solves ion beam transport problems by means of the matrix theory and neglects the influence of space charge expansion. The determination of the initial conditions of the ion beam is a general difficulty for calculations of this type, therefore we assumed two differently shaped plasma emitter surfaces /5/ (plane and curved). Several beam transport calculations were carried out with variation of the electrode potentials and positions. Here are presented two cases with maximum particle energy of 350 keV. At INGE-1 the beam line goes from the duoplasmatron ion source expansion cup through the einzel lens, acceleration tube and quadrupole triplet to the target.
In figures 3 and 4 the shapes of the different electrodes from the ionoptical components are schematically represented. The upper part shows the deuteron beam envelopes up to the end of the acceleration tube, where from left to right are composed the anode of the ion source, the extraction electrode in connection with the einzel lens (3 electrodes) and the three electrodes of the acceleration tube, with the middle electrode lying on the half potential from the left one (300 kV) and the right electrode being connected with ground potential. The base line represents the axis of rotational symmetry and also the optical axis. The lower part demonstrates the action of the quadrupole triplet in the two rectangular planes on the ion beam up to the target position. Fig. 3 shows the beam envelopes with plane plasma emitter for different ion currents. The case of curved plasma surface is illustrated in fig. 4. The extraction electrode has a -50 kV and the

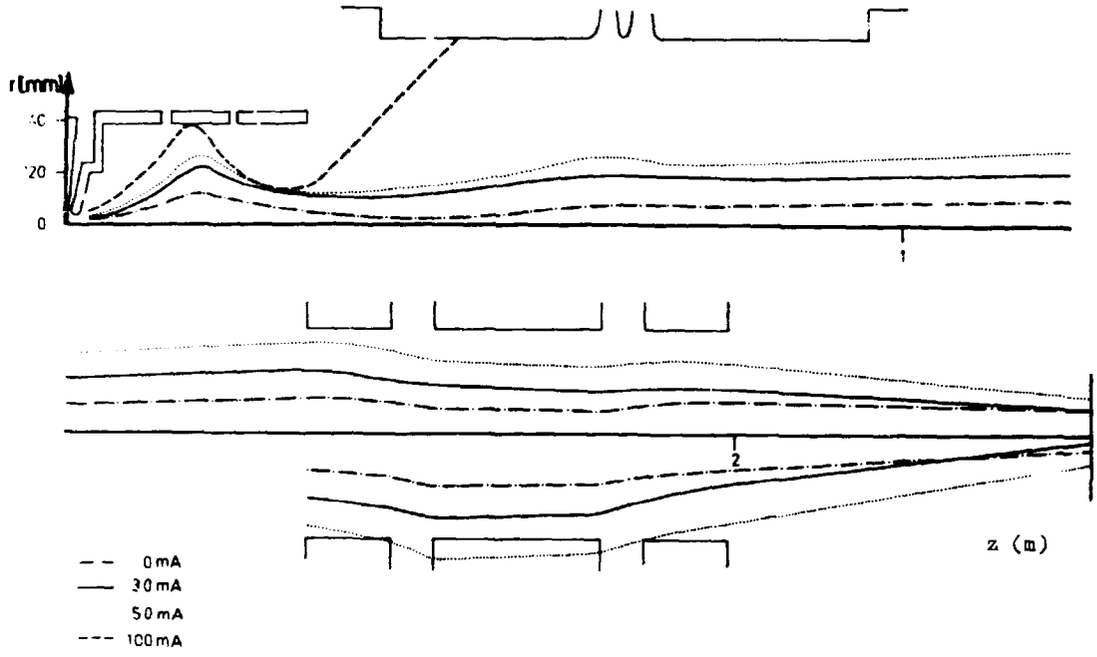


Fig. 3: Deuteron beam envelopes for a plane plasma emitter surface and for different values of ion current up to 100 mA

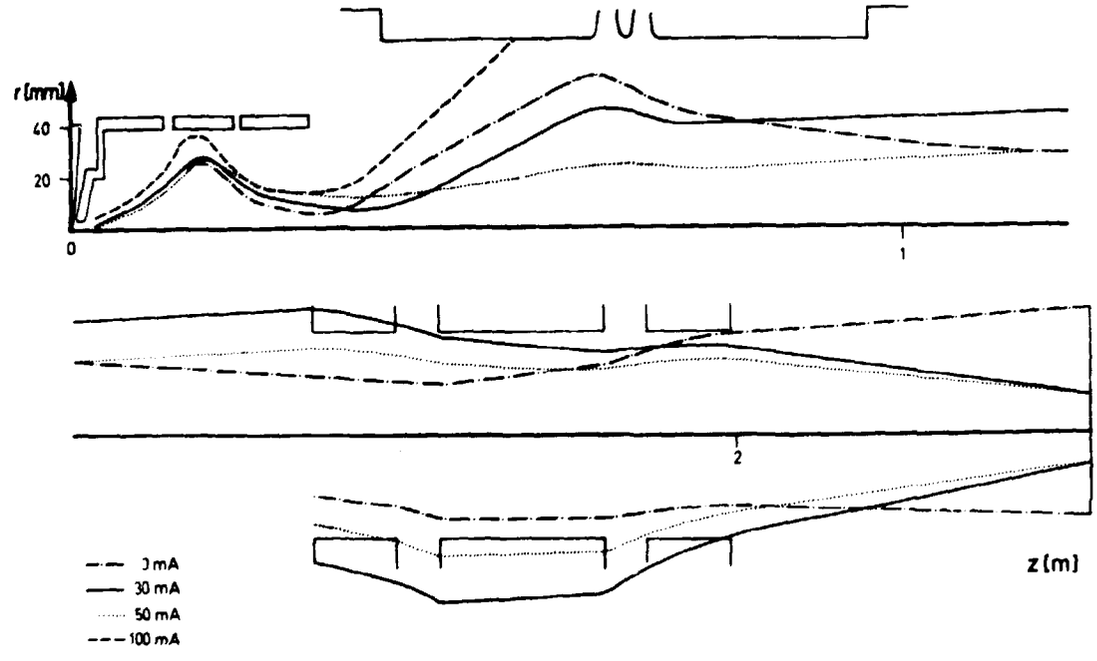


Fig. 4: Deuteron beam envelopes for a curved plasma emitter surface for different values of ion current up to 100 mA

middle electrode from the einzel lens has a -5 kV potential with respect to the anode. At first, it can be seen that the use of the quadrupole lens after acceleration is necessary. For ion currents up to 30 mA only small beam losses occur and the desired beam diameter at the target can be obtained. An opposite situation represents the ion current at 100 mA, already after the einzel lens the beam strikes the first electrode of the acceleration tube. The difference between the two general cases are visible at 0 mA (identical with total space charge neutralization).
For the curved plasma emitter the beam diameter at the target is larger than for plane plasma surface, for equal potential distributions on the electrodes.

## 4. Conclusions

The calculations show the results, that a deuteron beam at 350 keV up to 30 mA for the described ionoptical arrangement can be transported with small beam losses. In this case the ion beam diameter has also the desired value, approximately 20 mm, on the target position. The performed calculations have not taken into consideration the partial space charge neutralization by rest gas molecules which generally should improve the situation. Secondary electron suppression needed for operation also was not investigated. Therefore, the calculated results represent the approximate ion-optical behaviour of the accelerator only. Nevertheless, the authors trust, that this calculations are very successful for the understanding and optimization of the ion transport in the INGE-1 accelerator.

References:

/1/ D. Schmidt et al., Proc. of this Conf.
/2/ R. Hutter, in A. Septier Focusing of charged particles, 1967
/3/ I.S. Hornsby, CERN 6600 Computer Program Library, 1965
/4/ M. Friedrich, to be published
/5/ J. Dietrich, U. Jahn, Proc. of this Conf.

# EXTRACTION-PROCESS CALCULATION FOR A DUOPLASMATRON ION SOURCE

J. Dietrich
Zentralinstitut für Kernforschung, Rossendorf
U. Jahn
Technische Universität Dresden

Ion-beam optics for a two-electrode extraction system of a duoplasmatron ion source is studied by two approaches: (i) a linear optics analytic solution and (ii) numerical solution using the computer program ELENS.

The extraction-process calculation of a duoplasmatron ion source is performed by means of a linear optics model [1] and using the computer program ELENS [2].

The linear optics model is based on the paraxial equation which accounts for lens effects, beam space charge and finite source ion temperature. We assume that the temperature contribution adds vectorially to the sum of the lens and space-charge contributions. The variation of beam divergence $\theta$ with relative perveance $P/P_0$ for a deuterium beam in a two-electrode extraction system is shown in fig. 1. $P_0$ is the Child-Langmuir perveance for a plane diode. The calculation with the linear model suggests an optimum perveance, i.e. perveance for minimum beam divergence $P_{OPT} \approx 0{,}15\ P_0$. With an aspect ratio $S = 0{,}4$ and an extraction voltage of 35 kV we obtain $P_{OPT} \approx 3 \cdot 10^{-9}\ A/V^{3/2}$, i.e. an ion current of 19 mA.

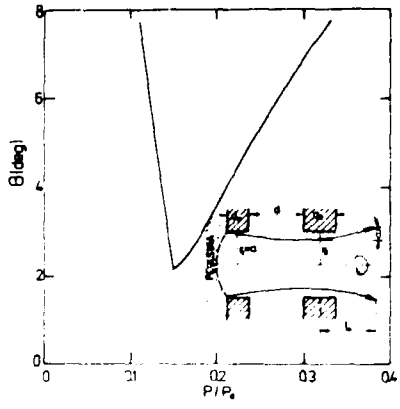


Fig. 1

Beam divergence angle $\theta$ as a function of relative perveance $P/P_0$. Parameters: $d_0$=1 mm, $d_1$ = 3 mm, d = 5 mm, $r_1$ = 2 mm, $r_2$ = 3 mm, L = 32 mm, ion temperature $T_1$ = 2 eV, energy 35 keV

The main problem for numerical calculation of the extraction process is the determination of the initial conditions (radial position and divergence) for the ions. It is known that by extraction of ions from a plasma a curved emitting surface is formed. The curvature of this surface is determined by the relative perveance of the extraction system.

We obtain for a given ion current and extraction voltage from linear optics solution the curvature of the plasma emitting surface and following the initial divergence for the ions. In order to obtain an emittance area we define an initial angle spread. For comparison we use plane and curved plasma emitting surfaces. The calculation is based on the assumption of a fixed emitting surface.

The computer program ELENS includes space charge effects in quasihydrodynamical approximation. Laplace's equation is solved by a finite difference method on a mesh and the method of successive overrelaxation.

The ion trajectories are calculated by integration of the orbit equation for rotationally symmetrical systems:

$$\frac{d^2r}{dz^2} = \frac{1 + \left(\frac{dr}{dz}\right)^2}{2\,\phi(r,z)} \left[ \frac{\partial\phi(r,z)}{\partial r} - \frac{dr}{dz}\,\frac{\partial\phi(r,z)}{\partial z} + \frac{1}{2\,\pi\varepsilon_0}\sqrt{\frac{m}{2Q}}\,\frac{I_0 \cdot r}{\varrho^2\sqrt{\phi(r,z)}} \right]$$

where $I_0$ is the total current in the beam, $\phi(r,z)$ the electric potential, m the ion mass, Q the ion charge, $\varrho$ the radius of beam envelope and $\varepsilon_0$ the dielectric constant of free space.

Fig. 2 shows the a priori initial emittance diagram. The emittance of a deuterium ion beam after the two-electrode extraction system is displayed in fig. 3 for plane and curved plasma emitting surfaces.

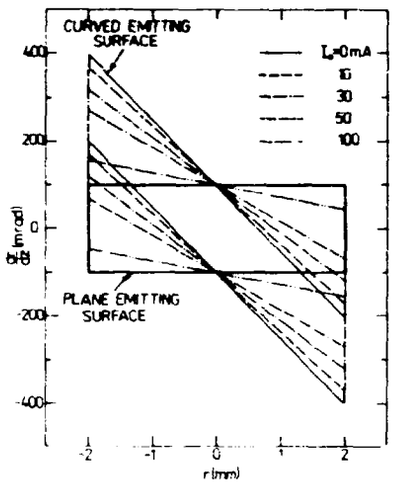


**Fig. 2**
**Initial emittance diagram**

The extraction voltage amounts in these cases 35 kV. The total ion beam current varies between 0 and 100 mA. For a deuterium beam of 10 mA an emittance of about $10 \cdot \pi \cdot$ mm $\cdot$ mrad $\cdot \sqrt{\text{MeV}}$ is calculated. This value agrees with the measured emittance of Tunis [3].
The obtained emittance is used for beam transport calculation of the neutron generator INGE-1 up to the target.

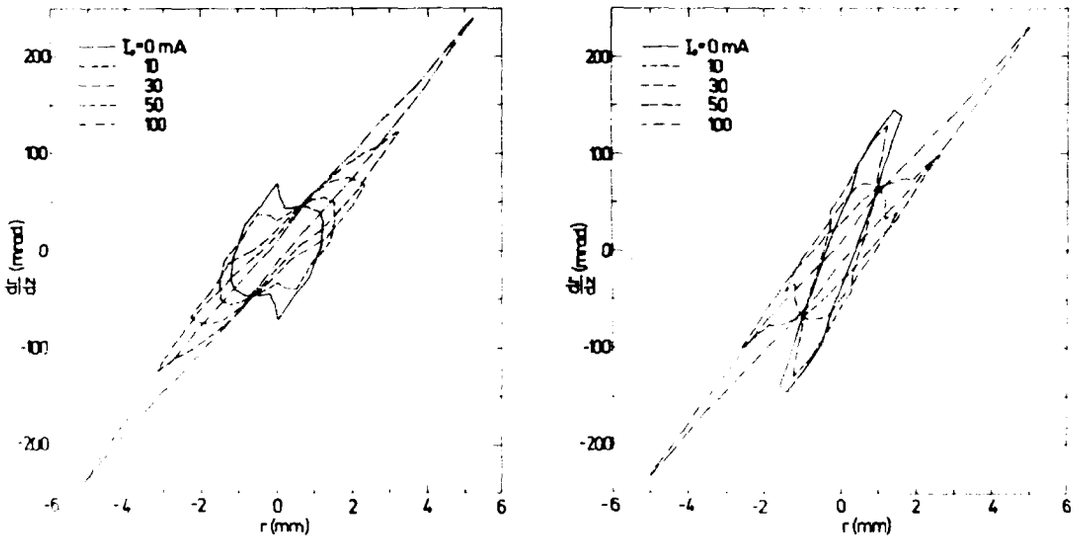


**Fig. 3**
**Emittance diagram for plane (a) and curved (b) emitting surfaces**

**References**

[1] J. Dietrich and Z.A. Kozlowski, JINR 9-82-608, Dubna (1982)
[2] J.S. Hornsby, CERN Program Library (1965)
[3] A. Tunis (this proceedings)

# EXPERIMENTAL INVESTIGATIONS OF DUOPLASMATRON ION SOURCE

A. Tunia, U. Jahn, E. Paffrath
Technical University Dresden, Section of Physics, GDR

## 1. Introduction

There are requirements, imposed nowadays on ion sources, to provide the powerful accelerators with a stable ion beam up to several hundred mA, with convenient optical properties. The duoplasmatron ion source /1/ seems to be one of the most useful devices for such a purpose. Its advantage is not only the obtainable intensity of output ion current but also the ability to generate multiple-charged ions as well /2/. In this report some duoplasmatron ion source investigations are presented.

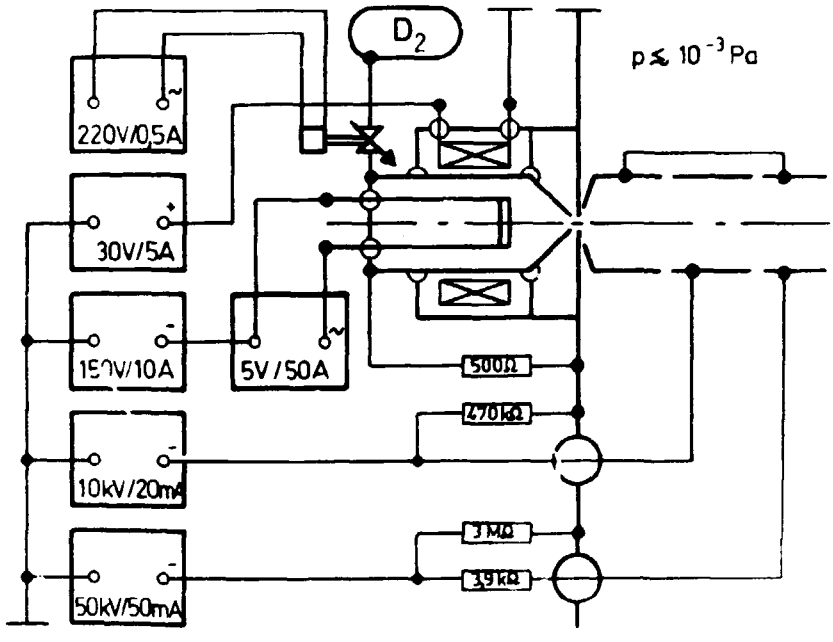


Fig. 1: Electric power supplies for the duoplasmatron ion source

## 2. The experimental arrangement and program of measurements

A test stand was developed and built to realize the experimental investigations. The main components are the vacuum system, the high voltage supply, the high voltage terminal and the measuring system. A 2000 l/s oil diffusion pump with a trap cooled by machine in connection with the rotational pump produce the needed vacuum in order of $10^{-6}$ Torr. The high voltage transformer with a Greatz-rectification generates the 50 kV/50 mA dc high voltage. The high voltage terminal, supplied by an insulating transformer, contains the electronic and control circu-

its for the ion source operation, as shown in fig. 1. The measuring arrangement is presented in fig. 2 in principle. It concists of the duoplasmatron ion source, the extraction system and the arrangements for emittance and ion current measurements.

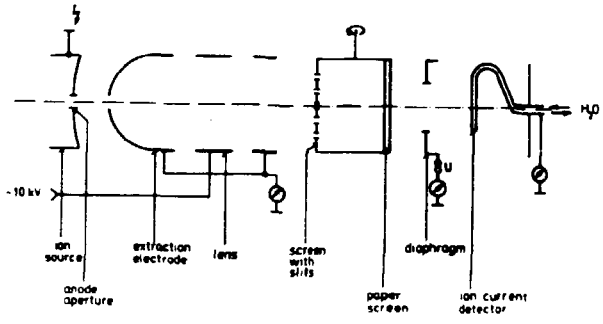


Fig. 2:

Experimental arrangement for emittance measurement

Three items of research program has been realized:

a) the investigation of dependence of ion current on various ion source parameters, as arc current, magnet current, gas pressure, extraction and lens voltage, to obtain a set of optimal operation conditions;
b) the investigation of the influence of the foregoing set of parameters on the emittance, because it is an important quantity for ionoptical computations and for the ion source quality;
c) the mass spectrum analysis of the ion beam is planed.

## 3. Results

This section deals with the realization of the program mentioned above. It is not possible to present the final results, because the investigations are in progress just now. At first it will be illustrated the different ion source operation conditions. As the operating gas, hydrogen has been used. Fig. 3 represents the output ion current versus arc current $I_i(I_A)$. The curve shows a linear behaviour on the left, than a maximum and a sharp decreasing on the right. The experimental errors are mainly caused by instabilities during operation. As an example of other conditions, we can take following set of parameters: $U_{extr}$= 20 kV, $I_A$= 6 A, $I_{magnet}$= 4 A, $U_{lens}$= 5 kV and the resulted ion current $I_{target}$= 17 mA. The fig. 4 shows the influence of the lens. There are four curves for different values of arc current, which represent the dependence of lens voltage on ion current. They show a certain maximum point for $U_{lens}$= 5 kV.

An intention now is the presentation and illustration of a method used for emittance measurement. It is well known, that the emittance is a magnitude which characterizes the phase space area, occupied with the beam particles. One can determine its experimental value as follows:

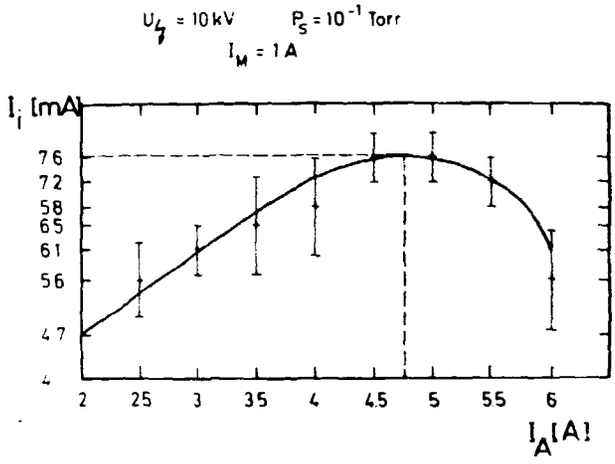


Fig. 3:

Dependence of the output ion current $I_i$ on arc current $I_A$

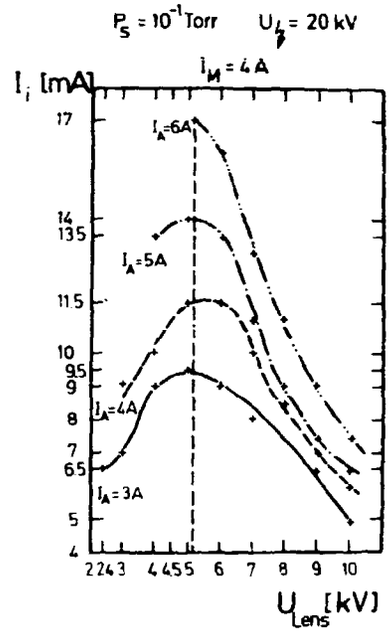


Fig. 4:

Influence of the lens voltage $U_{lens}$ for different arc currents $I_A$ on ion current $I_i$

- by means of measurement one finds the maximum and minimum slopes of trajectories originating in the same point for several, arbitrarily choosed points, located on the diameter of any beam cross section;
- next one constructs a diagram, which represents the dependence of maximum and minimum slopes on position of origin point;
- the surface closed with the so obtained curves gives the information about the emittance.

To obtain the values of slopes, the method with parallel slits and copy-paper is used /3/. The thin slits represent the origin points for elementary beams and the copy-paper screen registrates the shape of their cross sections as dark stripes. The position of upper and lower edges of each stripe determine the slopes. Fig. 5 gives an example of an emittance diagram and shows the corresponding screen with stripes.

The emittance area was determined to 15 cm.mrad. This value corresponds to a normalized emittance of $3 \cdot 10^{-2}$ cm.mrad. The use of paper screen for emittance measurement has the disadvantage that the heated screen leads to gas production. In this way breakdowns occur. Other measuring methods avoid this disadvantage:

- application of a quartz plate instead of the copy-paper;
- use of a movable electrical probe.

The aim of further investigations should be the ion beam analysis as cited above as well as the production of dc ion beams up to 100 mA.

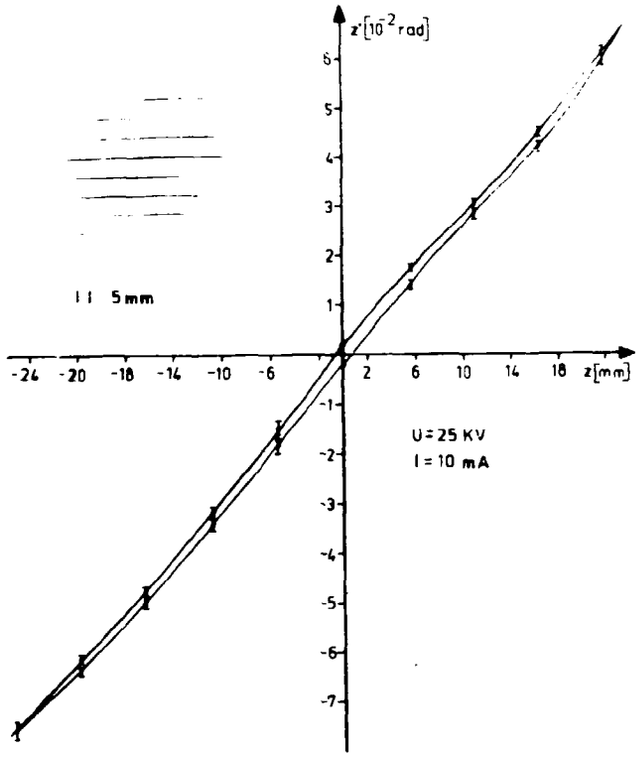


Fig. 5: Emittance diagram with the corresponding screen picture

References:

/1/ M. v.Ardenne, Exp. Technik d. Physik 1 (1961) 227
/2/ C. Leyjeune, Nucl. Instr. Meth. 116 (1974) 417
/3/ H. Wroe, Nucl. Instr. Meth. 52 (1967) 67

# BEAM MONITOR DEVELOPMENTS AT THE ROSSENDORF CYCLOTRON

H. Böttig
Zentralinstitut für Kernforschung, Rossendorf, GDR

Beam monitors, based on three different operating principles, were developed and tested by using the Rossendorf cyclotron beam.

## 1. Beam monitor based on the application of infrared thermography

The operating principle of the beam profile monitor based on the application of infrared thermography is a contactless videofrequency scanning of the infrared radiation emitted by the surface of a target. In view of the application, the target may be designed thick (beamstopper), thin (absorbing a part of the cinetic beam energy) or as a harp. It is imaginable to use a gas jet for observing high density beams. The thermogram obtained provides a visual representation of the particle density distribution over the beam cross section. Fig. 1 shows a block diagram of the monitor. The videoanalyzer digitalizes the signal to six channels represented by six colours (fig. 2). The monitor was tested with the Rossendorf cyclotron beam at a power density of $\approx$ 20 W $cm^{-2}$ [1]. Measurements of an implanter beam were carried out at a power density of $\approx$ 3 W $cm^{-2}$ [2]. The monitor has been used succesfully for optimizing the ion beam of the intense neutron generator "INGE-1" of the Technical University.

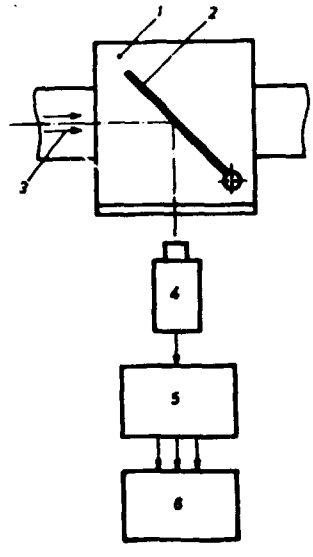


Fig. 1
Block diagram of the beam profile monitor
(1) beam line, (2) target,
(3) beam, (4) infrared camera,
(5) videoanalyzer, (6) monitor

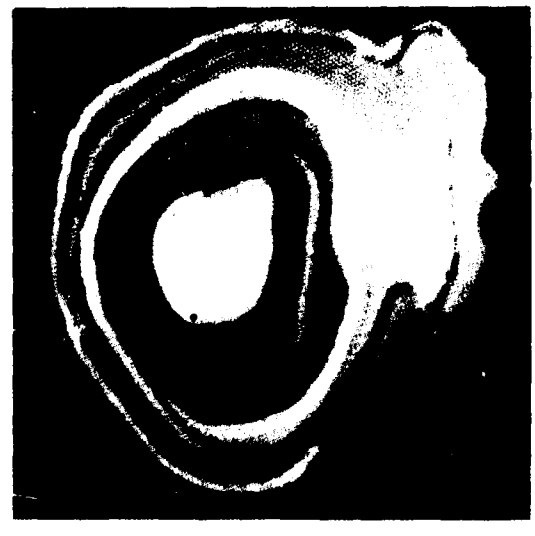

Fig. 2
Beam spot, deuterons, E = 13,5 MeV, $P_3$ = 20 W $cm^{-2}$, area $\approx$ 4 $cm^2$

Technical data:

Detection limit: Surface temperature = 550 K
(vidicon: F 2,5 M3UR, VEB Werk für Fernsehelektronik Berlin, GDR)

Videoanalyzer: "THERMOTRON" (ZfK Rossendorf)
Input: 1 V/50 Ohm, videosignal
Output: 1 V/50 Ohm, 3 channels
Mode: grey values
six isotherms
six colours

.2. Harp monitor [3]

The harp mon tor displays the intensity distribution of a beam in the two transverse directions (x,y). A harp (fig. 3) consists of two orthogonal planes of 15 tungsten wires stopping a part of the particles (heavy ions) or decreasing their cinetic energy (light ions). After converting into voltages the along the wires collected charges represent the beam profile. A multiplexer, driven by a computer fitted control unit, connects the harp wires cyclically to an oszilloscope (fig. 4). In order to suppress secondary electrons a diaphragma (potential -100 V) is placed in front of the harp. Depending on the beam line design the harp may be turned or driven by a linear vacuum-feedthrough into the measuring position. The block diagram of the harp electronics shows fig. 5.

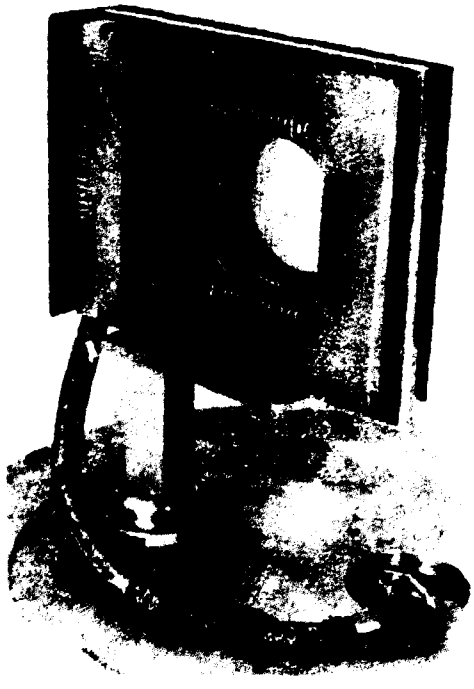

Fig. 3
Harp for beam diameter of 40 mm

Technical data:

| | |
|---|---|
| Wires: | 2 x 15, W or Ta, |
| Diameter: | 0,1 mm (0,05 mm) |
| Wire space: | 2,5 mm |
| Lenght: | 50 mm (100 mm) |
| Insulation: | epoxy glass |
| Detection limit: | $10^{-9}$ A per wire |
| Beam interception: | 8 - 12 % |

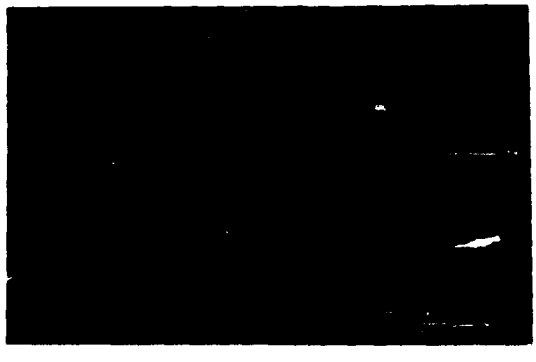

Fig. 4
Beam profile display on an oszilloscope (upper part: x, lower part: y)

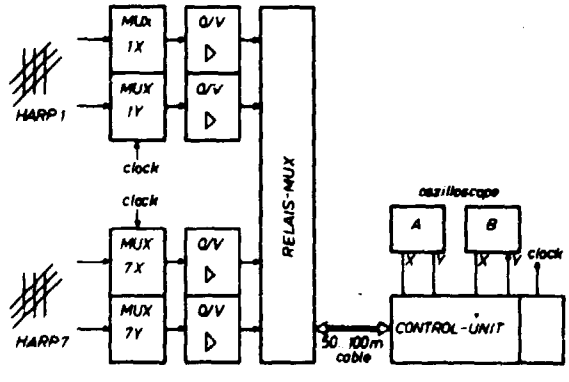


Fig. 5
Block diagram of harp electronics (Mux: Multiplexer, Q/V: Charge to voltage convertar)

## 3. Beam transformer

The beam transformer described here take advantage of the micro-pulsing of the beam in the repetition time of the cyclotron radio frequency. Fig. 6 shows a block diagram. The beam represents one winding of the broadband rf-transformer. The rf-voltage (output of the transformer) is amplified and measured selectively on the cyclotron frequency. The application of the beam transformer at several frequencies requires a retuning. To avoid this we are going to substitute the selective microvoltmeter by a cyclotron frequency controlled device, using a PLL-oscillator.

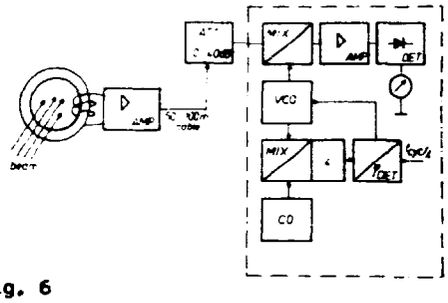


Fig. 6

Block diagram of beam transformer electonics
(AMP: Amplifier, ATT: Attenuator, MIX: Mixer, DET: Phase-detector, CO: Cristaloszillator, VCO: Voltage controlled oszillator)

Technical data (preliminary):

| | |
|---|---|
| Ferrite core: | "Manifer 150" |
| | size 80 x 60 x 20 $mm^3$ |
| | 1 winding for calibration |
| | 5 windings for measurement |
| Detectible ion beam: | ≈ 300 nA |

### References

[1] H. Büttig, NIM 203 (1982) 69
[2] H. Büttig and K. Wollschläger, Bild und Ton 3 (1982) 69
[3] W. Adam and H. Büttig, ZfK-443 (1981) 155

# THE VACUUM SYSTEM OF THE INTENSE NEUTRON GENERATOR INGE-1

E. Paffrath, U. Jahn, D. Schmidt
Technical University Dresden, Section of Physics, GDR

## 1. Introduction

Basic requirements for successful accelerator use are stable conditions during operation, long live time and high safety of all units. Especially during operation with an intense ion beam it is important to get sufficient high vacuum to realize the high voltage reliability of the accelerator components. Some special solutions connected with the intense neutron generator INGE-1 /1/ are represented in this report.

## 2. Vacuum System

Main requirements at the vacuum system during ion beam operation are to obtain pressures lower than $10^{-3}$Pa and a minimum rate of high molecular hydrogen carbon compounds. Then it is possible to extract and accelerate an intense ion beam by electrostatic fields of high gradients (more than 40 $kVcm^{-1}$; in the case of INGE-1 the gradients are 30...60 $kVcm^{-1}$). These high gradient regions are located at the beam extraction, at the first focusing lens and within the acceleration tube. The effective pumping speed needed, should be higher than 1000 $ls^{-1}$. The values of the gas conductivity amount 300...1000 $ls^{-1}$, determined by the system of the ion beam transport. In order, to realize a minimum loss of pumping speed, the accelerator tube had to be evacuated at both high voltage and ground potential side. For this purpose at the high voltage terminal a special developed ionisation-sublimation pump (so-called orbitron pump, /2/) was applied. Most of the gas production in the region of the accelerator located at high voltage is caused by electron stimulated desorption and by the thermal desorption /3/. These gas rates can exceed the normal wall desorption in some orders of dimensions. For that reason both vacuum system and ion beam transport system were optimized to improve the supression of secondary electrons and to reduce the ion beam losses. The necessary pumping speed is attained by using an oil diffusion pump in connection with a liquid nitrogen trap, an orbitron pump and a further getter pump. Their parameters are shown in table 1. The arrangement of the vacuum system, shown in fig. 1, allows some different operation modes under consideration of the outgassing rate. Possible regimes are evacuation of the acceleration recipient or parts of the recipient, maintaining the high vacuum, start or initial regimes, ion beam operation and preparation for opening the vacuum system. Because of the dependence of the use of the main vacuum pumps from the gas consumption, 3 operation modes can be distinguished (fig. 2):

1. Up to a maximum gas rate of 0.4 $Pals^{-1}$ (corresponding to a pressure of $10^{-3}$Pa) the getter pump only is sufficient for maintaining a permanent high vacuum.
2. Up to a maximum gas rate of 4.0 $Pals^{-1}$ (corresponding to a pressure of $10^{-2}$Pa) the orbitron pump must be added, that is in the case of low beam power operation and evacuation of higher desorption amounts after opening the vacuum system.
3. At higher gas rates, that means at high beam power operation, the orbitron and the diffusion pump give the vacuum conditions needed.

In order to evaluate the expected pressures it were carried out some calculations under consideration of the gas production, gas conductivity of the vacuum chamber and application of the high vacuum pumps (see fig.3; curves are calculated using /4/, /5/; points are measured values). A more detailled description of the operation principle of the orbitron pump is given in /2/. The advantages of this type of high vacuum pumps are the low weight and small dimensions, but stable operation especially at high gas rates. The scheme of this pump and its supply units can be seen in fig. 4. The operation time per

sublimator is about 300...500 hours. The other main pumps are commercially available /6/ and used on ground potential. An overview of the cooling system of the vacuum components is given in fig. 5. The devices within the high voltage terminal (ion source, orbitron pump and Pd-valve) are cooled by an oil circulation, where the heat exchanger, the refrigerator and the oil pump are located on ground potential. A first water circulation is used for cooling the diffusion pumps, a second one is used for cooling the target and all diaphragms. The control units of the vacuum system and the cooling system are logically combined. Main parameters of both systems and the target supply are controlled by a monitor. The construction of the target chamber was selected with respect of a frequent target exchange. In order to reduce the hazard of contamination by tritium it is possible to transport the target chamber together with the first valve as a closed container. The second valve closes the accelerator recipient against air. Thus it is possible to evacuate the target chamber separatly up to a high vacuum and also to prepare the target chamber opening.

## 3. Conclusions

In order to realize a stable beam operation we have outlined the necessary conditions for the beam handling in the accelerator recipient. The main condition is the sufficient high vacuum, especially in the regions of high field gradients. Because of the interaction between the ion beam and the vacuum conditions a solution of this problem is only possible by consideration of further factors as for instant a complete supression of secondary electrons, extensive cooling and the use of methods of the UHV-technology. The vacuum system of the intense neutron generator INGE-1 was optimized and can guarantee the high beam power operation.

References:


/1/ D. Schmidt et al., Proc. of this Conf.
/2/ D.G. Bills, Journ. of Vac. Sci. Technol. 4 (1967) 149
/3/ M.D. Malev, Vacuum 23 (1973) 2, 43
/4/ W. Wutz, Theorie u. Praxis d. Vakuumtechnik, Braunschweig, Vieweg u. Sohn, 1965
/5/ M.v.Ardenne, Tab. d. angew. Physik, Bd. II, 3. Aufl., Berlin, DVW, 1975
/6/ HVD-Katalog, Tl. 1, 2, VEB Hochvakuum Dresden


Table 1: Parameters of the high vacuum pumps

| pumping type | $S$ / $ls^{-1}$ | $p^{min}$ / Pa | $p^{max}$ / Pa | $Q^{max}$ / $Pals^{-1}$ | $m$ / kg | dimension / mm |
|---|---|---|---|---|---|---|
| getter pump | 300 | $10^{-9}$ | $10^{-3}$ | 0.4 | 80 | 330 x 410 x 420 |
| orbitron pump | 400 | $10^{-5}$ | $10^{-1}$ | 4 | 20 | Ø 240 x 500 |
| diffusion pump | 800+ | $10^{-4}$ | 10 | 10 | 30 | Ø 400 x 700 |

+with liquid nitrogen trap

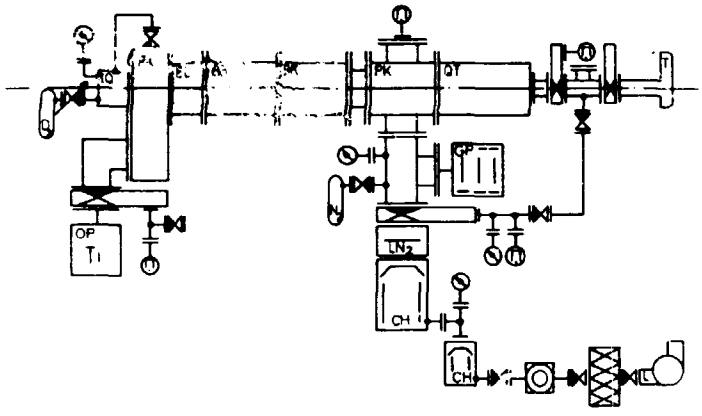


Fig. 1:
Vacuum system of INGE-1
(IQ-ion source, El-einzel lens, BR-acceleration tube, PK-pumping chamber, QT-quadrupole lens OP-orbitron pump, GP-getter pump, CH-diffusion pump, T-rotating target)

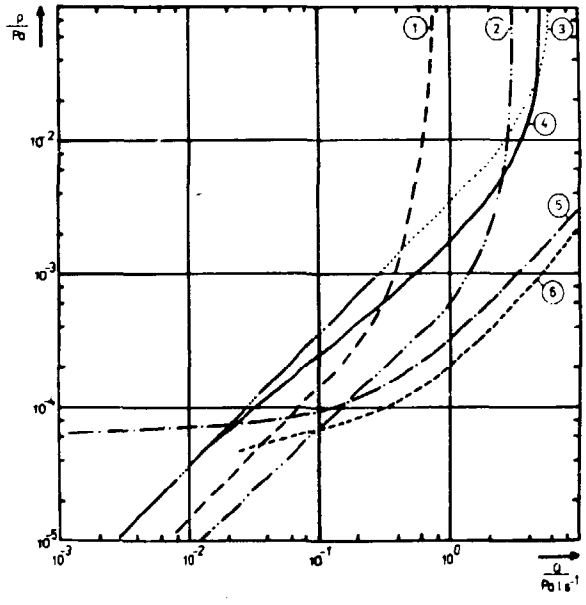


Fig. 2:
Pumping characteristics, minimum pressure as function of maximum gas consumption (1 orbitron and getter pump, 2 orbitron pump /2/, 3 getter pump, 4 orbitron pump (TUD), 5 diffusion pump, 6 orbitron and diffusion pump)

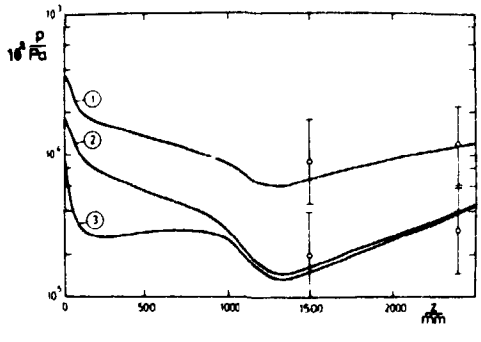


Fig. 3:
Pressure along the beam line
1 orbitron and diffusion pump without secondary electron suppression,
2 only diffusion pump,
3 orbitron and diffusion pump.

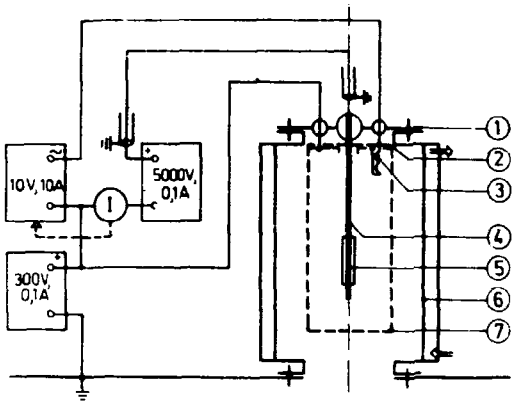


Fig. 4: Orbitron pump and supply
(1 flange, 2 screen, 3 cathode,
4 anode, 5 sublimator,
6 cooled wall, 7 grid)

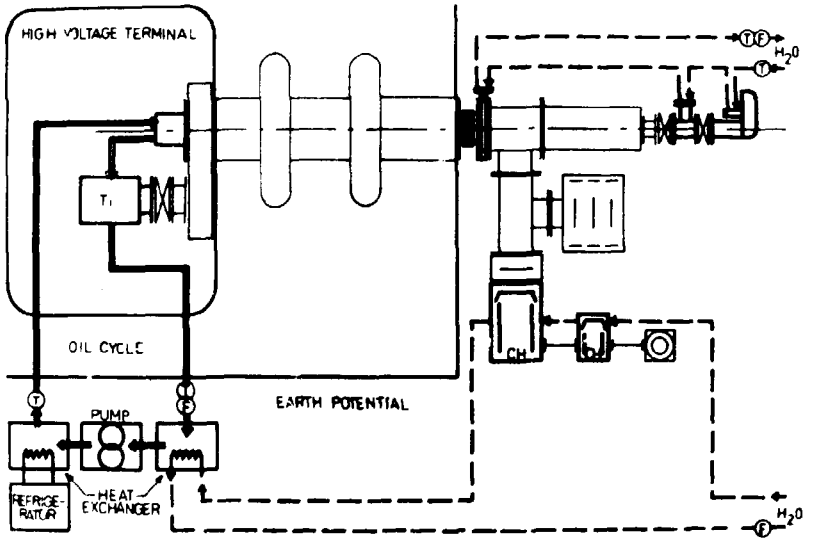


Fig. 5: Cooling systems of INGE-1
T - temperatur control
F - flux control

# COMPUTER CONTROL OF THE NEUTRON GENERATOR INGE-1

P. Eckstein, F. Gleisberg, R. Krause, R. Schwierz, D. Schmidt, D. Seeliger
Technical University Dresden, Section of Physics, GDR

## Introduction

The widespread application of microcomputer techniques promoted the development of control systems for processes or equipment in nuclear physics. An up to date computer control system for such purposes represents an on-line closed loop system consisting of one central computer and additional microcomputers for special tasks. With such a system it is possible to reduce the operating expense necessary for starting and checking the functioning of automation processes. The development of such an automation system for the intense neutron generator INGE-I requires the solution of problems, which are directly connected with the working regimes and the construction of a cascade accelerator.
The first step in developing such a system is based on the open loop system itself, because that can be done in parallel with the development of the intense neutron generator. In order to improve the system while further developing the components of the generator, a modular expandable hard- and software system was designed and developed.

## Hardware

The main part of the hardware system of the neutron generator consists of three microcomputers, a CAMAC-microcomputer AMCA 80 /1/ and two microcomputers in K1520 standard /2/. It allows the on-line closed loop control and on-line open loop control of the generator. Manual control of all or selected parameters during simultaneous on-line process data acquisition in special situations is also possible. During the development of the generator, these two operating modes were used. They are also being used for process identification, the analysis of the behaviour of the generator under various test conditions.
The CAMAC-microcomputer AMCA-80, which together with the Auxiliary Cratecontroller Adapter works as an Autonomus Cratecontroller, represents the master in the multimicrocomputer system. The two others operate as a graphic computer terminal /3/ and as a computer for communication with the operater and for I/O standard peripherals, as shown in figure 1

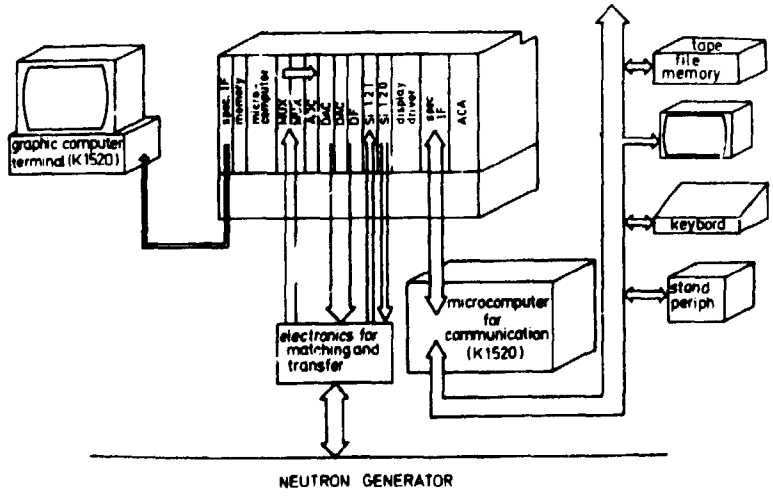


Fig. 1: multi-microcomputer configuration

Because the open loop process data aquisition and process control in the first step of the development of the generator was not so critical with respect to the reaction time, the master computer organized the communication too, as shown in the block diagram in figure 2.

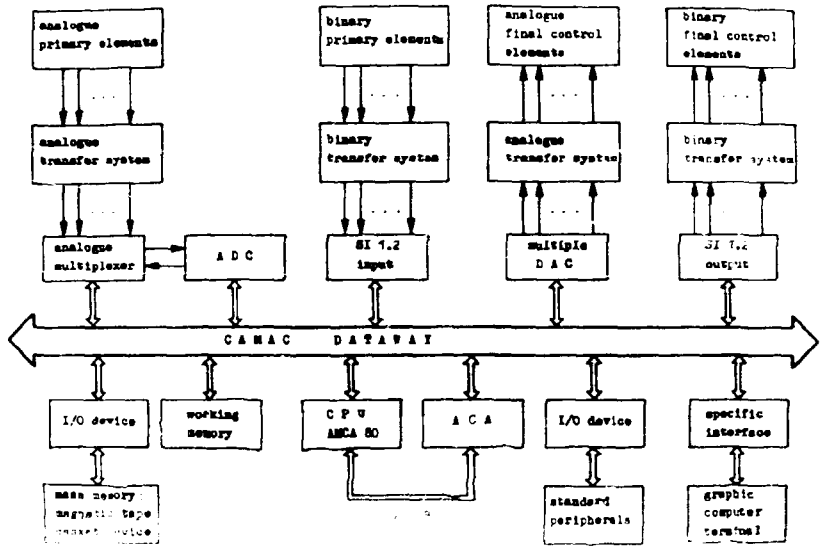


Fig. 2: block diagram of the hardware system for control of the neutron generator

The lower part of this diagram shows once more the computer configuration. The input of measured values and the output of control values take place through the CAMAC-dataway for any number of binary values by means of parallel registers. The input of analogue measured values takes place by multiplexing by means of an Analog-Digital-Converter. The output of analogue control values is realized by a system of Digital-Analog-Convorters.

Transmission techniques and techniques of primary elements and final control elements were designed and developed taking into consideration noise imunity and safety against sparking-over and corona discharges.

It is necessary to distinguish between two kinds of primary informations.

The first type comes from electrical values such as ion beam current at the diaphragms or on the target but also current and voltage of power supply units, whereas the second type is connected with nonelectrical values in connection with pertinent electronic units for temperature and rates of circulation in the cooling system of the ion source and the target as well as inspection of the vacuum valve functioning. The electronic units of primary elements contain limit comparators. So it is possible to use both output signals, the analogue and the binary, as input data for the computer or a hardware control loop.

Operating at the high voltage terminal of the neutron generator, the power supply units must be small and highly efficient. These properties hav been reached using the switching principle /4/, which allows built-in primary elements and final control elements to be realized easily.

The main parameter of the developed power supply units are shown in table 1.

The insulation of the high voltage terminal forced the development of an optical transmission line system for measured values and control values illustrated in the

figures 3 and 4.

| Type | $U_{out}$ | $I_{out}$ | Stability | Ripple | Eff. | Size/mm³ | Remarks |
|---|---|---|---|---|---|---|---|
| [illegible] 10/20 | 0...10 kV | 0...20 mA | $<5\cdot10^{-3}$ | $<10^{-3}$ | > 80 % | 120 x 215 x 220 | $U_{out}$ positive or negative |
| [illegible] 5/100 a | 0...5 kV | 0...100 mA | $<10^{-3}$ | $<5\cdot10^{-3}$ | > 80 % | 160 x 215 x 220 | floating output additional output: 300 V; 10 mA |
| [illegible] 40/7,5 | 0...40 V | 0...7,5 A | $<10^{-4}$ | $<5\cdot10^{-3}$ | > [illegible] % | 80 x 215 x 220 | |
| [illegible] 5/50 | 0...5 V | 0...50 A | $<5\cdot10^{-3}$ | - | > 75 % | 120 x 215 x 220 | floating output $I_{out}$ - sinusoidal current (20 kHz) |
| [illegible] 10/10 | 0...10 V | 0...10 A | $<5\cdot10^{-3}$ | - | > 75 % | 80 x 215 x 220 | floating output $I_{out}$ - sinusoidal current (20 kHz) |

Table 1: voltage-controlled switching power supplies
input voltage AC 220 V $^{+10\,\%}_{-15\,\%}$ (50 Hz)

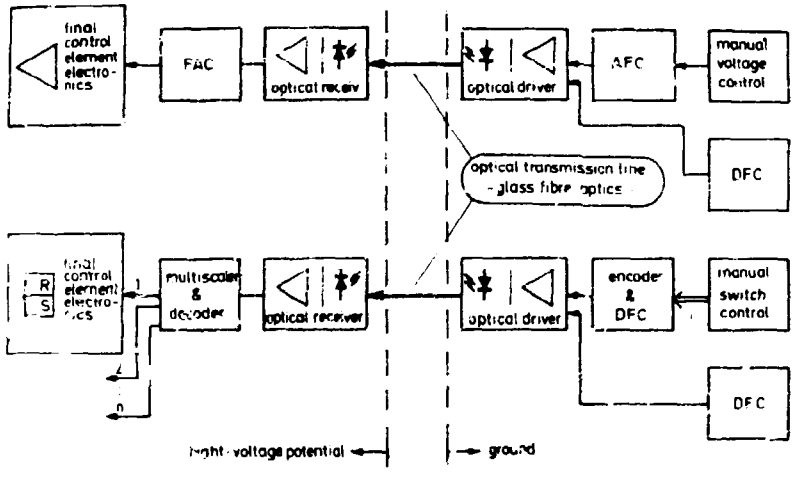


Fig. 3:
block diagram of the optical transmission line system transmission direction: high voltage terminal

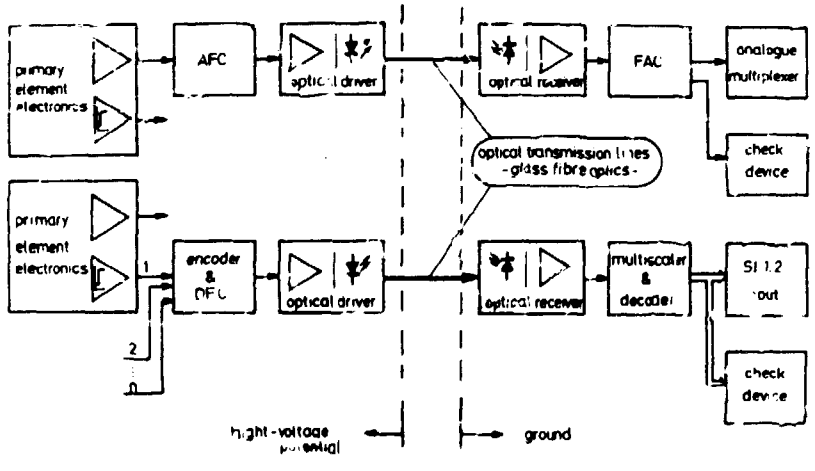


Fig. 4:
block diagram of the optical transmission line system transmission direction: ground (computer or check devices)

The very high noise imunity and the security against influences caused by sparking-over is caused by the pulse distance modulated transmission of analogue and binary values. Analog-Frequency-Converters (AFC) and Frequency-Analog-Converters (FAC) operate as modulators and demodulators Digital-Frequency-Converters (DFC) and gated scalers are applied for binary values.
Especially at the neutron generator itself the optical signals must be transmitted over a distance of about thirty meters, however the power of optical drivers and sensibility of the receivers allow a transmission distance of about one kilometer.
Asymmetric drivers, twisted pair lines and differential input receivers for the transmission of analogue value and push-pull drivers and receivers for the transmission of binary values give the noise imunity necessary also for ground potential transmission.

## Software

The software system of the computer control is based on a modular expandable system of subroutines called by a handling program.
The communication between the components makes use of standardized input/output vectors. In this form the system allows to control any parameter of the intense neutron generator by demands over the keyboard. The on-line process data acquisition demands the cyclic request of all registers and of the analogue measurement complex multiplexer-ADC.
One subroutine control the data transfer to the graphic computer terminal, where are implemented for diagrams with concentrated information of several parts of the generator and one table, showing a complete view. For example, the first diagram, shown in figure 5, contains the most important parameters.

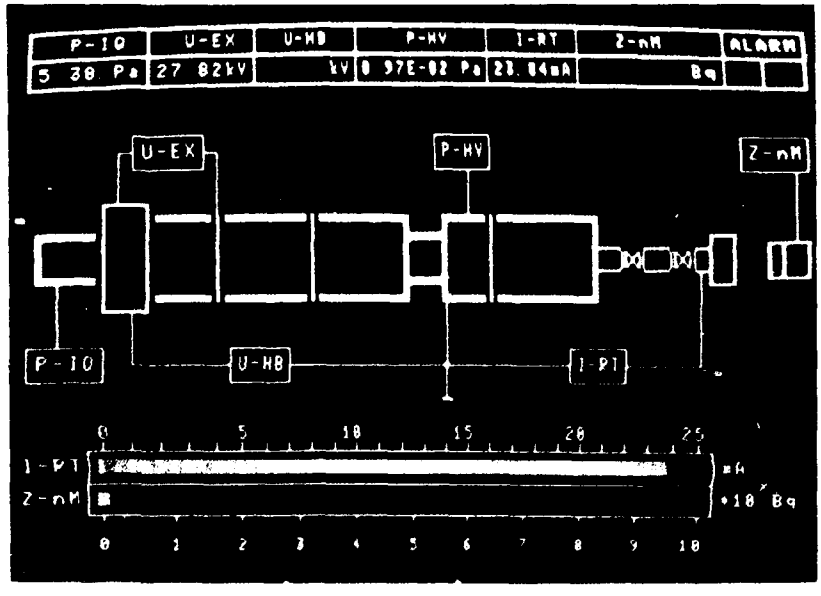


Fig. 5: information on the graphic display;
the main diagram

These are also placed in a table in the upper part of the diagram. The right field of this table signals alarm information, that is to say, the number of the parameter and the number of the diagram, showing that parameter. The other diagrams show the syste of ion optics, the vacuum system and the cooling system, completed by the same table, li the first diagram.
With the help of the keyboard and the alpha numeric display the maximum value, lower and upper limit of the parameters may be given.

References

/1/ Beuchel, T., Starepravo, A., CAMAC-Mikrorechner ZIE-Preprint 82-8, 1982
/2/ Mikrorechner K1520, Betriebsdokumentation VEB Robotron-Elektronik Zella-Mehlis
/3/ Käster, Mensel, Farbdisplay (techn. Dokumentation) TU Dresden, Sektion Informationstechnik
/4/ Gleisberg, F., Esche, H.-J., Jahresbericht ZfK 503, 135 (1982)

# RADIATION PROTECTION PROBLEMS WITH TRITIUM IN HIGH FLUX NEUTRON GENERATORS (HNG)

B. Lorenz, SAAS

Besides shielding against external radiation and protection against induced radioactivity handling of tritium is one of the major radiation protection problems with HNGs. Even with conventional NGs it has been difficult to strike a balance of the tritium inventory, to cope with contamination and to determine environmental release. The problems aggravate due to the 1-2 orders of magnitude higher quantity of tritium in the targets of HNGs.
An evaluation of tritium health hazard was made on the basis of own experience with conventional NGs, literature analysis and calculations according to the ICRP general dosimetric model of incorporation.

To evaluate the associated health hazard it is necessary to determine how much of the tritium target activity can be released, in which form the tritium may occur and during what processes tritium will be released. These data have to be considered in relation to the dosimetric incorporation model and the corresponding protection limits.

## 1. Tritium release and contamination levels

Tritium can be released during manufacture, transport, storage, target change, operation of the generator, maintenance and repair, dismantling and waste disposal.
Targets will be manufactured in a special isotope laboratory, which handles tritium for other purposes too. So protection requirements in this case are not necessarily the same as for HNG operation. It is advisable to transfer as much work with tritium targets as possible to the manufacturer, because adequate tritium handling technology is already established there.
For the release rate of tritium during storage and transport an average value of 10 Bq/h per MBq target activity was determined from literature data. The reported values differ due to the dependence on target preparation conditions, age and use. Very clean conditions during manufacture (ultra high vaccum, inert atmosphere during transport) diminish the release rate as well as increase the target lifetime and decrease the contamination by sputtering. The demands for careful target preparation, inert storage and transport to achieve long targetlife time and high neutron output /1/ completely coincide with radiation protection demands.
Adequate measures against fire during transport, although not included in current transport regulations for sources smaller than 37 TBq, are advisable due to the tritide compound break-off at higher temperatures /2/.
The most significant quantity of tritium will be released during operation. This is to a certain degree due to the thermal burden the ion beam converts on the target (dissipation energy of some kW). The major process, however, is the displacement of tritium by impinging deuterons. As a rough approximation one triton is replaced by a deuteron per 10 impinging deuterons. The release rate from the target is about 6 GBq/h mA after measurement of Booth and Barschall /3/. Many accelerators work with a closed vacuum system, so the released activity remains within the accelerator at first. Therefore, as long as the vacuum is maintained, there is no immediate health hazard. However, all inner surfaces of the vacuum system will be covered with tritium. Any procedure that requires an opening of the vacuum system will cause a release of tritium, which is much higher than a release from the target during storage, because the tritium is bound only superficially. Inadequately stored contaminated accelerator parts can cause enhanced tritium air concentration and unnecessary exposure /4/.
A significant quantity of tritium is released via fore pump during reevacuation. An upper limit of gaseous release can be calculated, using the above-mentioned release rate value.

If getter pumps are used, it is obvious that significant activity is trapped in the getter elements. They should be handled in the same way as targets.
Whereas the getter elements are loaded by gaseous tritium, the inner surfaces of the accelerator get contaminated also by tritide particles.
Data about contamination levels around NGs according to our own inspection results and literature are summarized in Table 1.
As regards the form of tritium it can be
- elemental tritium gas released directly from the target,
- tritiated water or water vapor, i.e. transformed gas, decontamination fluid or cooling water esp. when breaking into the vacuum system, and
- metal tritide aerosols or particles sputtered from the target.

Information about the form of tritium release is important, because there are differences in the radiological effects.

## 2. Dosimetric data

Dosimetric data about tritium water or water vapor (HTO) and gas can be obtained from ICRP Publication 30 /5/. The ALI corresponding to a dose of 50 mSv/a is 3 GBq for HTO. (The term "dose" stands for "effective dose equivalent".)
The equivalent air concentration of working places DAC is 0.8 $MBq/m^3$(HTO) and 20$GBq/m^3$(T-gas). This difference between HTO and T-gas, which is due to the different mode of intake, is substantial. Normally, this difference is not taken into account and conservatively any released tritium is thought to be in the form of HTO. However, this is not the case with respec to tritium targets /6/ and radiation protection measures could be revised, taking advantage of the difference in limits.
The third possible radiation exposure is connected with incorporation of tritide aerosoles. ICRP 30 does not refer to this special form and therefore we have adapted the ICRP dosimetric model for the lung and the gastrointestinal tract to calculate the corresponding dose. The calculated lung dose depends strongly on the aerosol diameter. With an AMAD of 1 $\mu$m the lung dose per Bq intake is $10^{-8}$Sv, whereas an AMAD of 20 $\mu$m results in 9 x $10^{-10}$Sv/Bq. The AMAD was determined to be larger than 20 $\mu$m /7/. The corresponding DAC-value for 20 $\mu$m AMAD would be 0.1 $MBq/m^3$ further increasing with growing aerosol diameter. The major dose results from small particles, which reach the inner part of the lung. With growing particle diameter aerosols will go directly from the nasopharyngal tract into the gastrointestinal tract, causing only small doses.
So inhalation of particles does not present a significant hazard. The same is true for the ingestion of particles. Only trifling doses can be calculated due to the short time of passage, the small rate of release of tritium into the organism and the substantial absorption by the intestine contents and selfabsorption.
With respect to surface contamination limits ($l_s$) we checked the validity of current limits.
Derivation in case of tritium takes into account only inhalation and ingestion. For inhalation the resuspension factor r was taken to be 4 x $10^{-5}m^{-1}$. Then $l_s$= DAC/r is 20 $GBq/m^2$. For ingestion it was assumed, that daily the activity of an area of 10 $cm^2$ is ingested. It follows $l_s$= 10 $GBq/m^2$. Therefore current limits could be relaxed by several orders of magnitude from 50 $kBq/m^2$ to 10 $GBq/m^2$. If particle contamination and only gaseous release is assumed, even higher relaxation factors would result. For several reasons such a tremendous change will not be introduced, but a relaxation factor of 100, as already proposed by ICRP /8/ would be justified.
Despite the deficiencies of the model, it seems that radiation hazard from surface contamination has been overestimated somewhat up to now, and operational contamination levels can be kept well below the relaxed limits (table 1).
The evaluation of tritium release into the environment is important with respect to cost-effectiveness. Without any doubt tritium absorption facilities reduce tritium release

substantially. The question is, whether the corresponding dose reduction is substantial as well. We intend to investigate this problem in the near future.

## 3. Incorporation analysis

According to the metabolic data /9/ tritium uptake can easily be detected by urine analysis. This method is very sensitive and detects activity concentrations which correspond to doses less than 1/10 % of the limit. So the effect of radiation protection measures and working behaviour can be demonstrated by urine analysis. The derived limit is 1 $GBq/m^3$. Our results of monitoring NG personnel give an average of 1 $MBq/m^3$, if samples are taken routinely, and 10 $MBq/m^3$ in case of event related sampling.
A similar value was reported about HNG personnel /10/.
In any case the corresponding dose is low, which is an indication that measures taken are appropriate, although not necesearily an optimum.

## 4. Conclusions

HNG operational tritium health hazard is smaller than expected from the quantity of tritium inventory.
Evaluation of the dosimetric data on the basis of ICRP 30 and monitoring results reveal a possible general relaxation in protection measures to achieve better cost-effectiveness. More detailed investigations in this direction are planned.

## Literature


/ 1/ H.L. Adair, CONF-77 1075-1, 1978
/ 2/ H.M. Butler, F.F. Haywood, CEX-65.05, 1970
/ 3/ R. Booth, H.H. Barschall, Nucl. Instr. Methods, 99, 1972
/ 4/ J. Biro, C. Pongracz, Izotoptechnika, 20, 1977
/ 5/ ICRP Publication 30, 1979
/ 6/ J.A.B. Gibson, AERE-M 1169, 1963
/ 7/ E.M.M. de Ras et al. 5th IRPA Congress, Jerusalem, 1980
/ 8/ ICRP Publication 25, 1976
/ 9/ E.A. Pinson, W.H. Langham, J. Appl. Physiol., 10, 1958
/10/ C.M. Logan et al., UCRL 83405 (Rev. 1), 1980
/11/ B. Glöbel et al., STH 12/80, 1980


Table 1: Contaminations around NG

| | | |
|---|---|---|
| working areas | 50-500 | $kBq/m^2$ |
| target vicinity | 500 | $MBq/m^2$ |
| transport package (inside) more than | 500 | $MBq/m^2$ |
| fore pump oil | | |
| low target activity | 5 | $GBq/m^3$ |
| normal target activity | 50-500 | $BGq/m^3$ |
| high target activity (HNG) | 50 | $TBq/m^3$ |
| cooling water | | |
| normal target activity | 50 | $MBq/m^3$ |
| high target activity (HNG) | 50 | $GBq/m^3$ |

# AN EVALUATION OF NEUTRON YIELDS FROM THICK TITANIUM-TRITIUM-TARGETS UNDER DEUTERON BOMBARDMENT

H. Helfer, B. Hildebrandt, A. Seifert
Technical University Dresden, Section of Physics, GDR

Intention of the present paper is the calculation of differential neutron yields $dQ_n(\delta_n)/d\Omega$ from thick titanium-tritium-targets under deuteron bombardment with simplified assumptions about the structure of the target and about the deuteron trajectories in the target. New data taken from literature are used in the numerical calculations.

A layer of thickness dx located at a depth x of the target with a concentration of $N_T(x)$ tritium atoms per $cm^3$ under bombardment with a current $I_d(x)=N_d(x)$/sec of deuterons yields the following quantity of neutrons per unit of time and solid angle:

$$\frac{d^3N_n(x,\delta_n)}{dt\,d\Omega} = I_d(x)\cdot N_T(x)\cdot\frac{d\sigma(\delta_n,E_d(x))}{d\Omega}\cdot dx. \qquad (1)$$

The target surface turned towards the incident current of deuterons corresponds to x=0; the thickness of the target is appropriately set to $x_{target} \gtrsim R_d$ ($R_d$.. range of deuterons in the target material), i.e. in a thick target the accelerated particles can be slowed down to zero energy. Using $dx=dE:(dE/dx)$ and, if the current of deuterons and the number of tritium atoms per volume along the deuteron trajectory are assumed to be constant, $I_d(x)=I_d$ and $N_T(x)=N_T$, by integration one gets the total quantity of neutrons per unit of time and solid angle, i.e. the differential neutron yield:

$$\frac{dQ_n(\delta_n)}{d\Omega} = \frac{d^2N_n(\delta_n)}{dt\,d\Omega} = I_d\cdot N_T\cdot\int_{E_d=0}^{E_d}\frac{d\sigma(\delta_n,E_d)/d\Omega}{-dE/dx}\,dE. \qquad (2)$$

The simplifying assumptions mentioned above about target structure and deuteron trajectories in the target material refer to the following facts:

- all tritium atoms are bound in the same kind of titan-hydride-moleculs; their distribution is uniform in the whole target;
- the angular spread of the deuteron beam caused by Coulomb-scattering on the target nuclei has no essential influence on the value of the differential neutron yield /1;2/.

For the numerical calculations of the neutron yields cross sections $d\sigma(\delta_n,E_d)/d\Omega$ of the reaction $T(d,n)^4He$ in the laboratory system from /3/ are used; values of $dE_d/dx$ are taken from /4/. Energy loss per length unit of the deuterons is assumed to follow the Bragg law of additivity; it is the sum of the energy losses of deuterons in titanium Ti and in the target material:

$$\left(\frac{dE_d}{dx}\right)_{T_nTi} = \left(\frac{dE_d}{dx}\right)_{T_n} + \left(\frac{dE_d}{dx}\right)_{Ti}, \qquad (3)$$

where $n=N_T/N_{Ti}$ is called "atomic ratio" - the average number of tritium nuclei per one titanium nucleus. This consideration is based on the experimental fact that the ionization energy losses of ions per atom/$cm^2$ are equal in isotopes:

$$\left(\frac{1}{N}\cdot\frac{dE}{dx}\right)_H = \left(\frac{1}{N}\cdot\frac{dE}{dx}\right)_D = \left(\frac{1}{N}\cdot\frac{dE}{dx}\right)_T. \qquad (4)$$

With $N_T = n \cdot N_{Ti}$ and

$$\left(\frac{dE_d}{dx}\right)_{T_nTi} = N_{Ti}\left\{n \cdot \left(\frac{1}{N} \cdot \frac{dE_d}{dx}\right)_H + \left(\frac{1}{N} \cdot \frac{dE_d}{dx}\right)_{Ti}\right\}, \qquad (5$$

the differential neutron yield related to $I_d = 1$ mA current of deuterons is given by

$$\frac{d^2N_n(\delta_n)}{I_d \cdot dt \cdot d\Omega} = n \cdot 6{,}24 \cdot 10^{15} \cdot \int_{E_d=0}^{E_d} \frac{d\sigma(\delta_n, E_d)/d\Omega}{-\left\{n \cdot \left(\frac{1}{N}\frac{dE_d}{dx}\right)_H + \left(\frac{1}{N}\frac{dE_d}{dx}\right)_{Ti}\right\}} \, dE. \qquad (6)$$

Numerical calculations according to (6) were carried out in the energy range from 0 to 350 keV and for atomic ratios n=0,5...2,0. Following /5/ titanium-hydride layers with $n > 2$ are instable.

The results are shown in fig. 1. Clearly the rise of the differential yield of 14 MeV neutrons with the accele-rating voltage in the range of 100...250 kV can be seen. In this range the calculation of the <u>total</u> yield gives values of about $Q_n = n \cdot 5 \cdot 10^{11}$ neutrons/sec for every 1 kW of beam power.

Designing the target thickness $x_T \gtrsim R_d$ one can assume that the range $R_d$ of deuterons in pure titanium in every case is an upper limit for the range in the target material, because the stopping power of 1mg/cm$^2$ of Ti is much smaller than that of T. Fig. 2 shows this fact (R' in mg/cm$^2$ is the calculated range of deuterons in the target material). At deuteron energies of 200...350 keV and at n=0,5 (1,0; 1,5; 2,0 respectively) the mass part of 3 % tritium (5,9 %; 8,5 %; 11 %) causes a possible reduction of the titanium layer thickness to 87 % (77 %; 68 %; 62 %) of the thickness at n=0; on the other hand, thick targets have the advantage, that tritium can diffuse from deeper layers during the irradiation.
Together with the inevitable sputtering of the surface this process increases the target life time.

<u>Literature</u>


/1/ A. Meister u.a., TU-Information 05-12-80

/2/ K. Seidel u.a., TU-Information 05-09-82

/3/ H. Liskien u.a., NUCLEAR DATA TABLES, Vol. 11 (1973), Nr. 7

/4/ J. Ziegler, Handbook of Stopping Cross Sections for Energetic Ions in All Elements; New York, Frankfurt - Pergamon Press 1980 (Volume 3)

/5/ L. Shope, SC-TM-66-247, Sandia Lab., Albuquerque (1966)

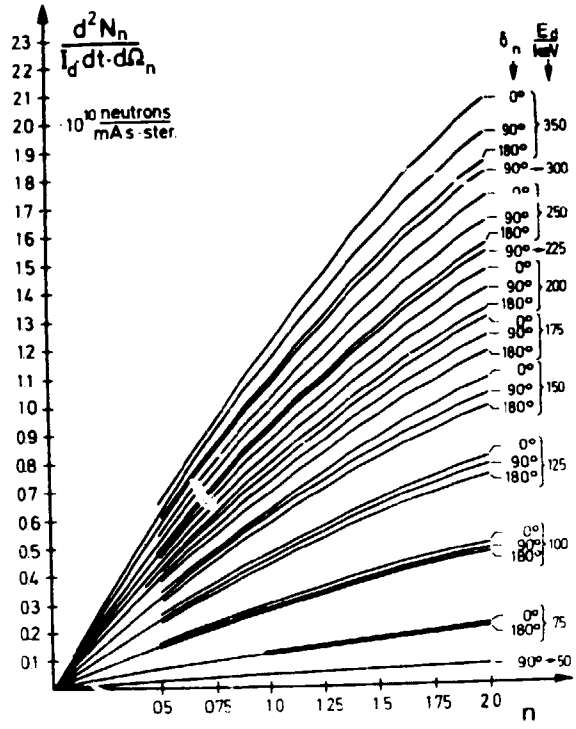


**Fig. 1:**

Differential neutron yields of the $T(d,n)^4He$-reaction as a function of the atomic ratio n ($E_d$=50...350 keV; $\delta_n$=0°...180°).

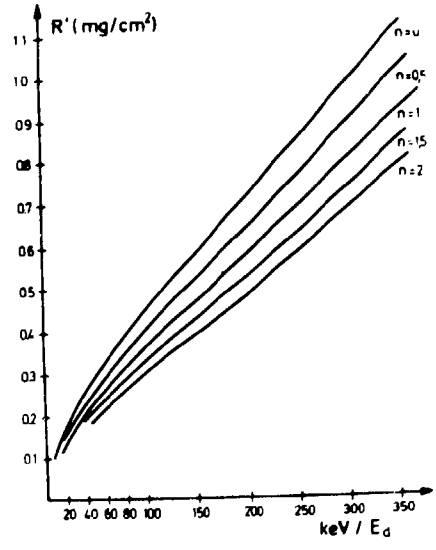


**Fig. 2:**

Range of deuterons in $T_nTi$-materials at different atomic ratios n.

# ISOLATING TRANSFORMER IT 300 FOR 300 kV AND 10 kVA

J. Pivarč, K. Málek[+], B. Bajcsy[x] and P. Rovný[x]

Institute of Physics, Electro-Physical Research Centre of the Slovak Academy of Sciences, 842 28 Bratislava, Czechoslovakia

Abstract: We describe an isolating transformer developed to supply a high voltage terminal of a 300 keV electrostatic air insulated accelerator with the a.c. voltage 220 V and the power 10 kVA. The transformer of an about 1000 kg weight is built into an oil-filled insulating cylinder Ø 0.83 m x 1.5 m. The structure of the transformer is simple.

## 1. Introduction

One usually considers two kinds of power supply for equipments placed on a high voltage potential. One is based on a motor generator and the other uses an isolating transformer. This latter solution is preferred in the majority of small accelerators due to lack of undesirable noise and vibrations.

In the paper presented the isolating transformer IT 300 developed for the 300 kV potential and the power 10 kVA is discussed. The design of the transformer was stimulated by the structure of an intense 14 MeV neutron source /1/. A pertinent equipment was not available in the COMECON countries market at that time.

## 2. Description and technical specifications

The isolating transformer IT 300 should feed systems placed on the 300 kV d.c. potential with the a.c. voltage 220 V. Its scheme is shown in Fig. 1. The transformer is put into an insulating cylinder of laminated paper filled by inhibited transformer oil. Primary and secondary windings are specially protected against overvoltages between the windings. The insulation is designed for the d.c. voltage 350 kV. The ratio of transformation is 1. The parameters are summarized in Tab. 1.

---

+ Permanent adress: ČKD T.C., Electrical Engineering Plant, 150 00 Prague, Czechoslovakia.

x Permanent adress: BEZ C.C., Electrical Technology Plant, 831 07 Bratislava, Czechoslovakia

| | |
|---|---|
| Isolating d.c. voltage | 300 kV |
| Primary voltage | 220 V/50 Hz |
| Secondary voltage | 220 V/50 Hz |
| Rated power | 10 kVA |
| Short circuit voltage | 10 % |
| Gross weight | aprox. 1000 kg |
| Dimensions | Ø 0.83 m x 1.5 m |

Tab.1. Technical parameters of the isolating transformer IT 300.

## 3. Magnetic circuit and windings

The scheme of the magnetic circuit is shown in Fig.2. The circuit consists of transformer-core laminations continuously tightend by insulating tape.

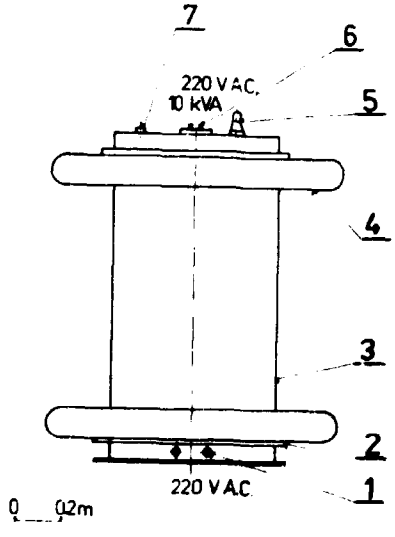


Fig.1. Isolating transformer IT 300. 1-primary winding, 2-frame of the transformer, 3-vessel, 4-equipotential rings, 5-air desiccator, 6-secondary winding and 7-oil gauge.

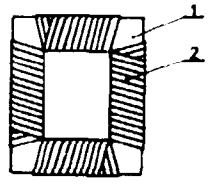


Fig.2. Magnetic circuit of the transformer. 1-transformer-core lamination and 2-insulating tape.

No furher clamping structural elements are placed between the tape and the magnetic circuit. The circuit is tightend without special joints and countershafts. This simplicity is the main advantage of the circuit setup. The actual setup of the magnetic circuit is patent pending /2/.

The magnetic circuit is palced and fixed into the insultating cylinder by a stand. The stand is also simple and inexpensive, see Fig. 3.

The primary winding is coiled on a cylinder and fixed by a devided annular ring /4/. The secondary winding is fitted with another annular ring of a drop's

form with a cut for the location of the winding and the conducting surface. Insulating covering cylinders and insulating cups are used to increase the spark-over distance. The scheme of the windings is shown in Fig. 4.

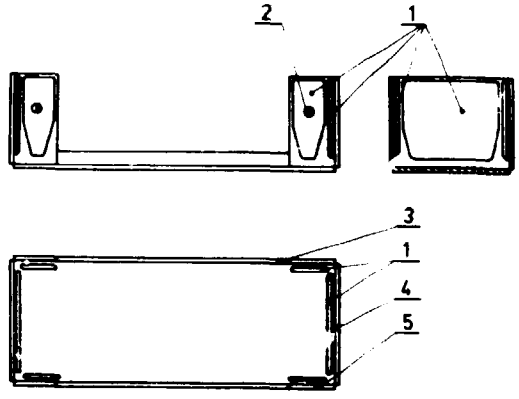


Fig.3. Scheme of the transformer stand. 1-fixing wedges, 2-screw and 3,4,5-walls of the stand.

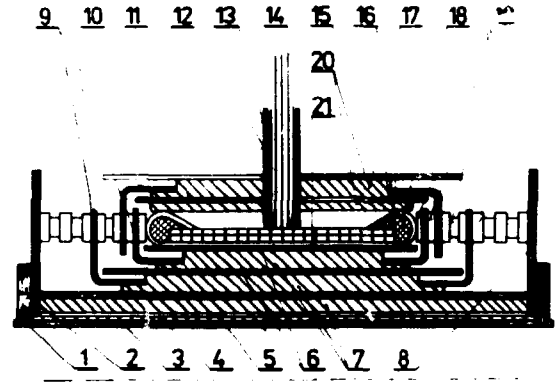


Fig.4. Layout of the primary and secondary windings. 1-pin, 2,18-annular rings, 3-cylinder, 4-primary winding, 5,13, 21-coverings, 6-insulated cylinders, 7,20-slats, 8-distance plate, 9-cups, 10,15-covering cylinders, 11,16-cuts, 12-tube, 14-output of the secondary winding, 17-secondary winding and 19-foots.

The transformer has four inside and four outside insulating cylinders. The distance between cylinders is 1.5 cm and the distance between primary and secondary windings is 9 cm. The structure of the windings is patent pending as well /3/.

The whole structure of the isolating transformer IT 300 is simple compared with others. For exemple, its windings are joined by a relatively simple structure without a complicated system of joints, the insulating cups are glued not pressed and the annular rings are fixed at the end of the front face of the windings. They are not components of the coils. Further, the isolating cylinders have symmetric slots and the outlet conductor is covered by insulating material and an equipotential tube.

## 4. Conclusion

The isolating transformer of the above parameters has been made in Czechoslovakia for the first time. Its insulating properties and ionization were tested in the state test stand installed in the Institute of Heavy-Current Engineering (IHCE) and the Institute of Power Engineering (IPE), Běchovice near

Prague . The test confirmed all designed values /4-5/.

The authors wish to thank Ing. Š. Luby, DrSc. the director of the IP EPRC SAS and Dr. M. Blažek, DrSc. for their support and kind interest in this work. They are grateful to L. Dosoál for technical help. Useful discussions with Dr. P. Obložinský and Dr. S. Plaváč are acknowledged.

References

1) J. Pivarč, S. Hlaváč, L.Král, P Obložinský, I.Ribanský, I.Turzo and H.Helfer, Acta Physica Slovica 30 (1980) 119-125, see also Report INDC (CSR) - 2/L+ Special, IAEA Nuclear Data Section Report, Vienna, May 1980.

2) K.Máliek, J.Pivarč, B.Bajcsy, ČS Patent Pending - PV 751-84

3) K.Máliek, J.Pivarč, B.Bajcsy, ČS Patent Pending - PV 752-84.

4) L.Kočiš, Ionization test, IHCE Běchovice, private communication (letter of December 1982).

5) A.Zajíc, IHCE State Certificate No. 82-141, Běchovice 1982.

# THE CURRENT STABILIZER FOR ANALYZING MAGNETS IN SMALL ACCELERATORS.

A.Bieńkowski
Institute for Nuclear Studies, Warsaw, Poland.

Abstract

The design, construction and performance of the current stabilizer for analyzing magnets of small accelerators is described. The stabilizer is designed to provide a stabilized DC current output in the range of 0 - 30 amps at a voltage varying from 0 to 200 volts. The long-term current stability is better than $10^{-4}$ in the range of 1 - 30 amps. This relatively simple and inexrensive device is designed on the basis of the typical integrated circuits.

## 1. Introduction

The separation of accelerated ions by mass and energy is usually made by means of the analyzing magnets. In the typical case stability of magnetic field should be at least $10^{-4}$. Variations in magnetic field strength are caused by fluctuations of the exciting current and changes of a magnet temperature. Since magnets have a large heat capacity the field variations due to temperature changes are very slow. Besides they are very small. Therefore the above requirement of the magnetic field stability can be obtained by the stabilization of the exciting current.

## 2. The current stabilizer

The simplified block diagram of the current stabilizer is shown in Fig.1.

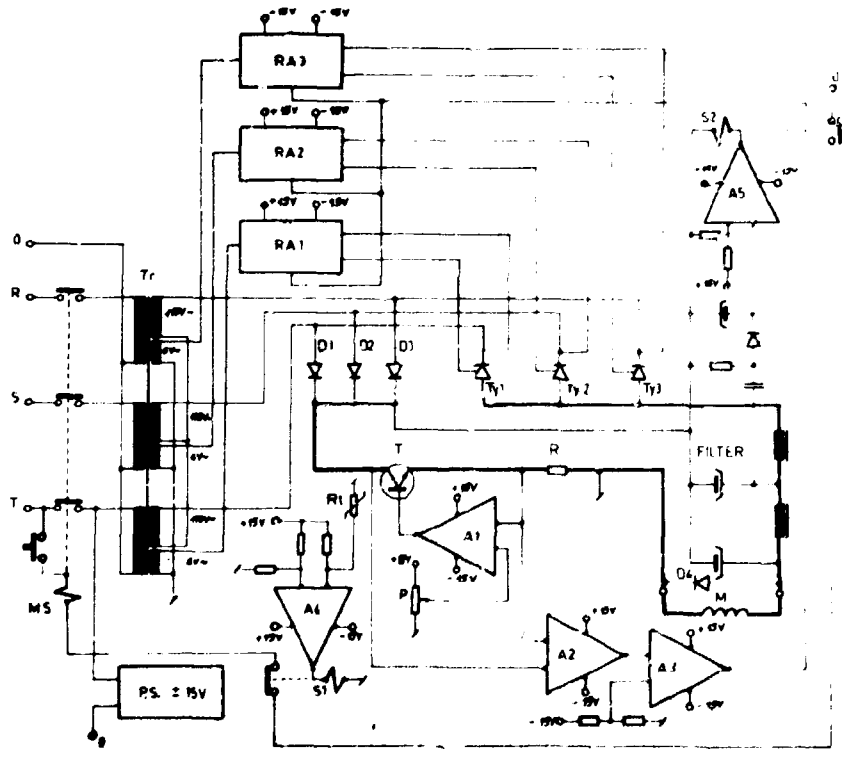


Fig.1. Simplified block diagram of the current stabilizer.

A power supply is composed of a transformer Tr and a conventional 3-phase rectifier made of 3 diodes /D1, D2, D3/ and 3 thyristors /Ty1, Ty2, Ty3/. A filter is connected to the rectifier output for reducing the output ripple.

As can be seen in Fig.1 the stabilizer is provided with two feedback loops: a main loop and an additional loop. In the main loop /or fine regulator/ the voltage drop across a sensing resistor R /0.1Ω/ in series with the magnet M is compared with a reference voltage from the ten-turn potentiometer P by a differential amplifier A1. The difference voltage is then amplified and fed into a series controller T /a bank of twelve parallel connected power transistors 2N3055/. In order to obtain high stability of the resistor R it was made of a water-cooling manganin wire. The voltage for the potentiometer P is supplied from an 8 volts Zener diode. Cooling-water tubes are brazed on to the two thick copper plates. On the first plate the diodes and power transistors were mounted, on the second one the thyristors. An additional feedback loop /or coarse regulator/ including amplifiers A2 and A3 controlls the voltage drop across the series controller T. The output voltage of the amplifier A2 is proportional to the voltage between emitters and collectors of the transistors T. This voltage is compared to the fraction of the supply voltage. The voltage difference is minimized by means of regulators RA1, RA2 and RA3 which controll the cut-off angle of thyristors Ty1, Ty2, Ty3 and therefore the output voltage of the rectifier. The response of the coarse loop is very slow as compared to the response of the fine regulator.

The following protective devices have been provided:

1. Main supply cut-off which becomes active if the transistors T exceeds the preset nominal temperature /amplifier A4/. This can occur when the pressure of cooling water is too low.
2. Main supply cut-off which becomes active if the ripple voltage of the filters condenser exceeds the preset nominal ripple, for example when the one of phase voltages is lacking /amplifier A5/.
3. The fast acting fuses in series with each of diodes D1, D2, D3 and thyristors Ty1, Ty2, Ty3.
4. The voltage limiter located inside of the amplifier A1 which limits the emitter-collector voltage of transistors T. This voltage cannot exceeds the preset nominal value of 12 volts.
5. The diode D4 provides some protection for the output circuit against voltages induced in the magnetic coils by rapid changes of the magnetic field.

## 3. Conclusions

The precission of the regulator was even better than expected. During a 24 hours tests using a proton resonance field meter at a different field strength the precision of the field proved to be better than 1 part in $10^4$. During three years work the current stabilizer have shown a full efficiency, high reliability and convenience of operation.

# Transmission of 14 MeV neutrons by shielding slabs

O.Pentchev, J.Jordanova, K.Ilieva, G. Voykov, S. Antonov

Institute for Nuclear Research and Nuclear Energy, Bulgarian Academy of Sciences, Sofia 1184, Bulgaria

The transmission of collimated 14 MeV neutrons through 1-3 mfp iron, copper and lead slab shielding is experimentally and numerically investigated.

The exsperimental set-up is shown in Figure 1. Neutrons of 14,9 MeV energy of about $10^{10}$ n/s intensity ( 1,5 mA deuteron ions current ) are produced from the $T(d,n)^4He$ reaction using a SAMES type D150 KV accelerator. A cylindrical iron collimator forms the collimated neutron beam. The different shielding slabs whose neutron attenuation has been measured are located just behind the collimator. The cylindrically shaped long counter ( 37,5 cm diameter and 42 cm length ) is placed at 82 cm distance from the collimator edge.

The calculations have been carried out by means of the onedimentional discrete ordinate code ANISN /1/ taking into account that the neutrons are comming to the detector only in angles up to $14^{o}$.

For estimating the attenuation through lead slabs ( Table 2 ) the three-dimentional Monte-Carlo code MORSE /2/ has been applied too. The calculations have been performed in geometry corresponding to the experimental conditions /3/.

All calculations have been done on the basis of our multigroup constant library L26P3S34 /4/.

The results of the calculations and the experiment are given in Tables 1,2. The comparision of the data shows that the calculations are in fairly well agreement with measurements.

Moreover, considering the results in Tables 1, 2 it could be realized that the one-dimentional code ANISN gives satisfactory estimations of the transmission of 14 MeV neutrons, passed forward through the 1-3 mfp barrier shielding slabs.

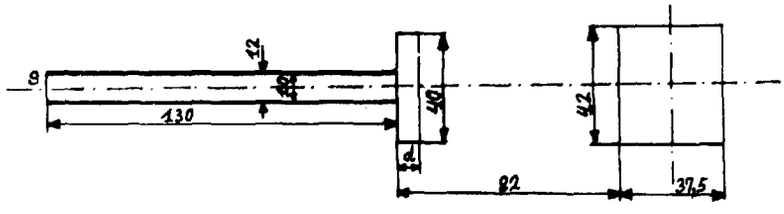


Fig.1

Table 1

Attenuation of 14 MeV neutron flux by shielding slabs

| | Copper | | Iron | |
|---|---|---|---|---|
| d /cm/ | Experiment | ANISN | Experiment | ANISN |
| 4 | 0,478±0,008 | 0,456 | 0,509±0,007 | 0,494 |
| 6 | 0,372±0,007 | 0,303 | 0,362±0,006 | 0,342 |
| 8 | 0,204±0,005 | 0,203 | 0,281±0,005 | 0,238 |
| 10 | 0,123±0,003 | 0,137 | 0,162±0,003 | 0,167 |
| 12 | ——— | —— | 0,123±0,003 | 0,118 |

Table 2

Attenuation of 14 MeV neutron flux by shielding lead slabs

| d /cm/ | Experiment | MORSE | ANISN |
|---|---|---|---|
| 2,5 | 0,765±0,009 | 0,700±0,011 | 0,726 |
| 5,0 | 0,684±0,004 | 0,542±0,021 | 0,536 |
| 7,5 | 0,447±0,007 | 0,394±0,020 | 0,404 |
| 10,0 | 0,340±0,006 | 0,367±0,023 | 0,316 |
| 12,5 | 0,204±0,004 | 0,211±0,024 | 0,256 |

References


1. ANISN - Code. One-Dimentional Discrete Ordinate Transport Technique. WANL-PR-(LL)-034, v.IV,1970.
2. Emmet M.B., The MORSE Monte - Carlo Transport Code System, ORNL, 4972, Feb. 1975.
3. S.Antonov, G.Voykov, K.Ilieva, J.Jordanova, Integral benchmark on the attenuation of 14 MeV neutrons by lead slabs, Yadrena Energia, Bulg. Acad. Sci., Sofia, 24, 1984 (in print, in Russian).
4. Voykov G., V.Gadjokov, S.Minchev, L26P3S34, INDC (BUL)-007/GV, Vienna, March, 1982.

# ТРАНСПОРТ НЕЙТРОНОВ НИКЕЛЕМ СРАВНЕНИЕ ЭКСПЕРИМЕНТАЛЬНОГО И РАСЧЕТНОГО РЕШЕНИЯ

И. Буриан, Институт ядерных исследований Ржеж, Чехословакия

Аннотация

Описывается расчетное и экспериментальное решение для транспорта нейтронов чистым никелем. Спектр нейтронов выходящих из поверхности никелевой сферы диаметром 50 см с нейтронным источником калифорний 252 был измерен сцинтилляционным спектрометром и пропорциональным водородным счетчиком. Для расчетов использована программа ANISN и библиотеки данных EURLIB-4 и VITAMIN C. Сравнение дает рекомендации для выбора данных при решении конкретных проблем транспорта нейтронов.

## Введение

Решение конкретных проблем ядерных реакторов (радиационное повреждение, тепловыделение, активация, доза) вызывают требования на уточнение пространственно-энергетического распределения потока нейтронов в исследуемых средах.

Когда были в ЦЯИ проведены тестовые расчеты спектров при прохождении нейтронов вариантами железа и стали, для объяснения влияния расчетных методик и разных систем данных, диапазон полученных результатов был очень широкий. При этом были использованы разные методы решения транспортного уравнения и разные библиотеки данных. Из этого очевидно, что для развития и проверки точности расчетных методов необходимо проведение реперных экспериментальных исследований. Такие эксперименты, которые дадут широкую информацию о характеристиках излучения, входящего в среду и выходящего из нее могут стать опорными и в сравнении с их результатами можно провести проверку как самых расчетных методик, так и ядерных данных используемых в расчете. Роль таких реперных экспериментов могут сыграть эксперименты в сферической геометрии с точечным источником в центре - на практике с малогабаритным радионуклидным источником нейтронов на основе калифорния 252 или с 14 МэВ нейтронным генератором.

Самыми важными составными стали являются железо, никель и хром. Чистым железом мы занимались в предыдущих этапах (напр. /1/, /2/). Измерения для хрома были осуществлены в Обнинске и будут публикованы в отчете ФЭИ. Результаты первого етапа для чистого никеля приведены в настоящем докладе.

## Экспериментальные работы

Исследования для чистого никеля были проведены с шаром диаметром 50 см, конфигурация эксперимента показана на рис. 1. С помощью защитного конуса была сделана поправка на фон рассеянных нейтронов. Для измерений спектров использован набор спектрометров, именно:

1. Однокрыстальный сцинтилляционный спектрометр (область 0,2 - 15 МэВ)
2. Спектрометр с пропорциональным водородным счетчиком (область 10 кэВ - 0,7 МэВ)
3. Спектрометр нейтронов типа Боннера (область от тепловых до МэВ).

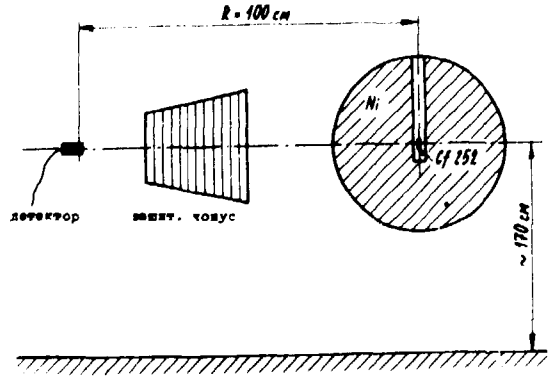


Рис. 1. Конфигурация одномерных экспериментов

Расчетные работы

Одномерные расчеты спектров нейтронов, утекающих с поверхности шаров, были проведены методом дискретных ординат программой ANISN /3/ (модификация на ЕС 1040). Геометрия источника - шар радиуса 8 мм, спектр аппроксимирован распределением Максвелла. Измеренный спектр самого источника находится в полном соответствии с этим распределением. Предварительные расчеты показали, что $S_{12}$ является подходящим приближением для расчетов такого типа, анисотропия рассеяния достаточно описана приближением $P_3$. Количество интервалов по радиусу - до 85, потоки рассчитаны до места измерения, между детектором и сферой предполагается вакуум.

Для расчетов были использованы следующие библиотеки данных: 100 - групповая EURLIB-4 /4/, и 171 - групповая VITAMIN C /5/.

Полученные результаты, выводы

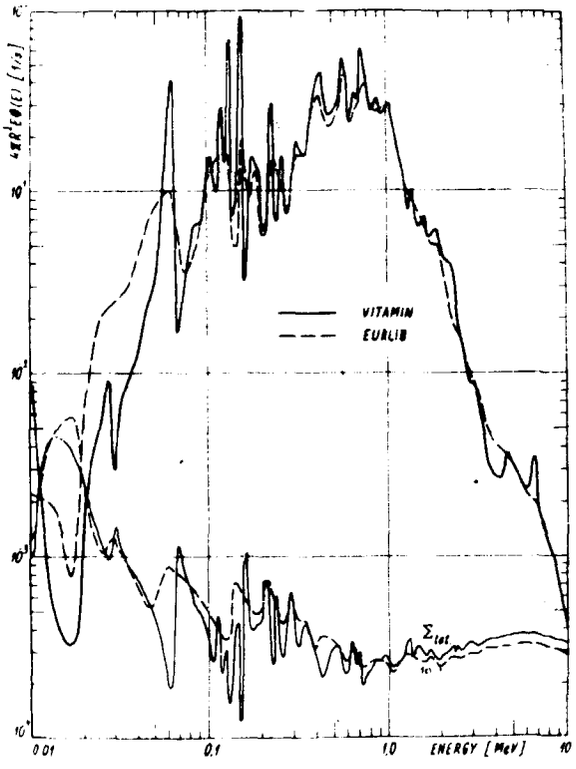


Рис. 2. Сравнение спектров нейтронов для никеля расчитанных с приведенными библиотеками.

На рис. 2 показаны результаты расчетов проведенных обеими библиотеками данных. VITAMIN C позволяет точнее определить спектр нейтронов особенно в области резонансов. Большие отклонения прежде всего в области 20 кэВ - 100 кэВ. Это вытекает уже из хода для иллюстрации приведенных $\Sigma_{tot}$ . В области 4 МэВ - 7 МэВ у EURLIB-4 тоже не появились никакие резонансы.

На рис. 3 сравнение результатов эксперимента с расчетом с данными EURLIB-4 В области 150 кэВ - 350 кэВ расчет ниже эксперимента до фактора два, ниже 100 кэВ наоборот. Дифференции тоже в области выше 4 МэВ.

Рис. 4 сравнивает эксперимент с расчетными результатами полученными библиотекой VITAMIN C. По форме и величине результаты совпадают кроме области выше 4 МэВ, где эксперимент недооценивает потоки нейтронов. В области 150 - 350 кэВ экспериментальные результаты завышены.

Из приведенного вытекает: при следующем этапе измерений сосредоточить внимание на область выше 4 МэВ. Для этого удобнее использовать 14 МэВ нейтронный генератор. Дальше проверить область 150 - 350 кэВ, расширить результаты до 10 кэВ.

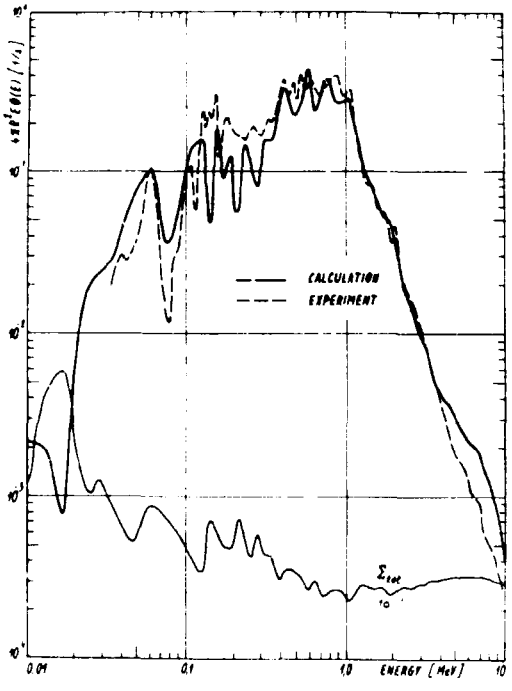


Рис. 3. Сравнение эксперимента для никеля с расчетом проведенным библиотекой EURLIB-4.

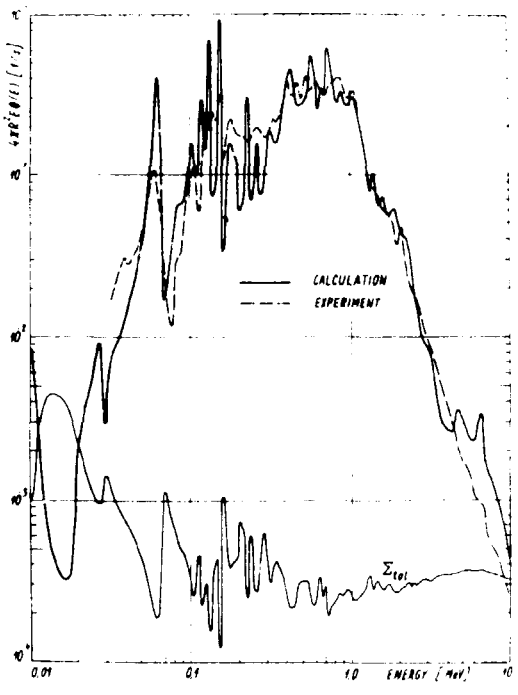


Рис. 4. Сравнение эксперимента для никеля с расчетом проведенным библиотекой VITAMIN-C.

## Литература


/I/ И. Буриан и кол (ИЯИ), Я. Трыков и кол. (ФЭИ):
Исследование спектров нейтронов и гамма излучения в сферах из железа.
ФЭИ-943, 1979

/2/ B. Jansky, M. Marek, J. Rataj, M. Holman:
The neutron leakage spectra from iron spheres
Jaderna energie 4, (30), 1984

/3/ Engle W.W.: A user manual for ANISN
K-1963, 1967

/4/ EURLIB-4 - The 120 group coupled neutron and gamma data library.
NEA Data Bank, 1978

/5/ VITAMIN C - The CTR processed Multigroup cross section library for neutronic studies
ORNL/RSIC-37, 1980

# MEASUREMENT OF NEUTRON LEAKAGE SPECTRA FROM A LEAD SPHERE FED WITH 14 MEV NEUTRONS

D. Albert, W. Hansen, Ch. Reiche, W. Vogel
Zentralinstitut für Kernforschung, Rossendorf, DDR-8051 Dresden

T. Elfruth, D. Seeliger, K. Seidel, G. Streubel, S. Unholzer
Technische Universität, Sektion Physik, DDR-8027 Dresden

In blanket conceptions for D-T-fusion reactors, neutron multipliers are used for enlarging the tritium-breeding coefficients. Multiplier materials must have large (n,xn) cross sections, small neutron-absorption cross sections and appropriate technological properties.
At present Pb is the prefered candidate [1]. It is located direct behind the wall of the plasma torus. Therefore secondary neutron spectra from Pb bombarded with 14 MeV neutrons are of immediate interest, and evaluated differential cross sections are tested with one-dimensional integral arrangements fed with 14 MeV neutrons and measuring neutron leakage spectra and reaction rates (tab. 1)

Table 1: Benchmarks with Pb spheres

| Group | Shell thickness [cm] | Measured quantity and method |
|---|---|---|
| Lawrence Livermore Laboratory [2] | 9 | neutron spectrum time-of-flight |
| IAE Moscow [3] | 2.5, 5, 7.5 | reaction rates activation probes |
| Osaka University [4] | 3, 6, 9, 12 | neutron spectrum time-of-flight |

In these benchmarks, the measured spectra are found to be remarkably harder than the calculated.

We use in our experiment a thicker sphere to have more sensitivity for discrepancies of the evaluated differential emission cross sections in the high-energy region. The outer radius of 25 cm and the inner of 2.5 cm correspond to a shell thickness of 4.1 mean-free-paths for 14 MeV neutrons. Several independent methods are used for measuring energy distributions as well as flux-integrated reaction rates from the same sample for improving the experimental reliability.

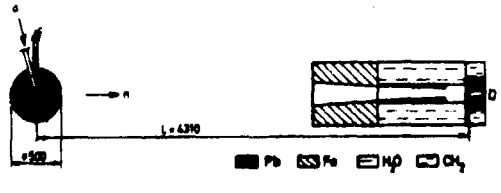

Fig. 1:
Geometrical relations of the arrangement (horizontal cut showing the equator of the sphere)

- The neutron current is measured at detector position D (fig. 1) with time-of-flight spectroscopy and with recoil-proton spectroscopy.
- The neutron flux is determined on the north pole of the sphere with recoil-proton spectroscopy, and reaction rates are taken at the indicated positions of the measuring channel (fig. 1) inclusively at the surface with activation- and fission-threshold detectors.

The D-T-neutron generator produces a few of $10^{10}$ n/s. The source strength is monitored by counting the α-particles using a Si-SB detector [5]; two additional neutron detectors act merely as relative monitors because they are influenced by the sample.

Time-of-flight spectroscopy

The neutron generator working in the pulsed mode [6] has pulse widths of about 2 ns and repetition rates of 5 MHz and 2.5 MHz respectively. The overall time resolution is about 2.5 ns corresponding to energy resolutions of 6 % at 14 MeV and 1.6 % at 1 MeV. The detector scintillator is NE-213 (36 mm in diameter); a neutron-gamma discrimination is used [7]. The detector efficiency is calculated with Monte-Carlo method [8] as well as experimentally determined by measuring time-of-flight spectra of neutrons from a Cf-252 chamber [9] and from the generator without sample. The time spectra are transformed to the energy scale taking into account the anisotropy of the neutron source and thick tritium targets [10].

Fig. 2 shows the result compared with the current calculated with the ANISN-code and ENDF-B/III data. The most apparent discrepancies are at medium and high neutron energies where interaction mechanisms are dominating which are faster than compound-nucleus evaporations.

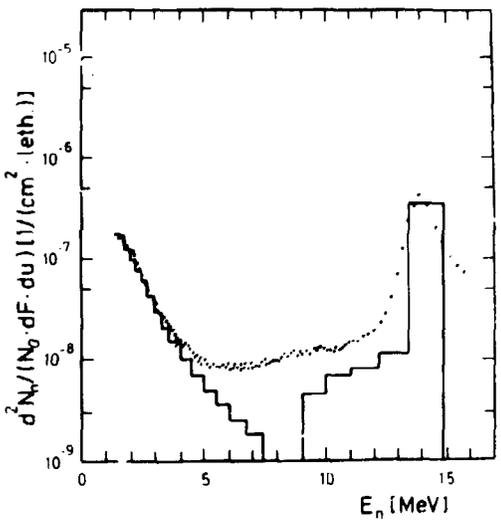


Fig. 2:
Neutron current density per source neutron and lethargy unit (measurement: ••••; P5S16-ANISN calculation: ⎍)

Recoil-proton spectroscopy

The pulse-height spectroscopy used with hydrogen-filled spherical proportional chambers (diameters: 3...4 cm, pressures: 100 kPa...1MPa) [11] and with stilbene scintillators (diameter/length: 10/10 and 30/25 mm) [12] covers neutron-energy regions from 5 keV to 1 MeV and from 0.75 MeV to 14 MeV respectively. The spectral distributions are differentiated in both cases. The chamber spectra are corrected for down-scattering of high-energy recoils and for wall effects [13].

Alpha events in the stilbene spectra created by interactions of 14 MeV neutrons with carbon nuclei as well as end effects are taken into account by a measurement with the source-neutron current.

The uncertainties of both the spectral distribution and the energy resolution are 5...10 %, with exception of the energy region 0.75...2 MeV, where uncertainties of the scintillation-light efficiency enlarge the uncertainties to ± 20 %, and of the energy region near the 14 MeV neutron peak, where the uncertainty of the spectrum is about ± 30 % determined by the subtraction procedure with the 14 MeV neutron spectrum mentioned above.
The neutron-flux spectrum measured on the north pole of the sphere is shown in fig. 3.

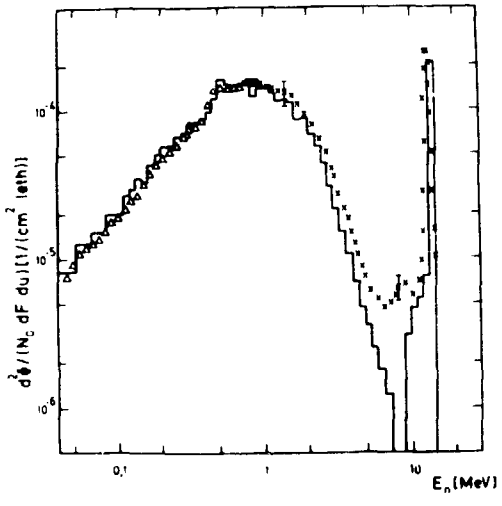


Fig. 3:

Neutron scalar flux per source neutron and lethargy unit. Measurements with hydrogen chamber (Δ) and stilbene scintillator $^{10}/_{10}$ (x) compared with a ANISN-P5S16 calculation with ENDF-B/III data (⌐)

The part determined with hydrogen chambers is normalized to the part from stilbene in the energy region from 800 to 950 keV.
The measurement shows in the energy region from 5 to 14 MeV remarkably more neutrons than the calculation. Also in the low-energy region from 1 to 5 MeV slightly more neutrons are observed in the measurement, a question at present discussed in some papers [4, 14].

## Activation and fission rates

The threshold reaction used are shown in table 2.
The activation probes [15] have a diameter of 20 mm and a thickness of 5 mm. The induced activities are measured with a Ge (Li)-detector. Since it is not a low-background arrangement the uncertainties of the saturation activities determined are about 5 %.
The fission probes [16] consist of a thin layer (20...100 μg) of the fissile material prepared by electrodeposition on a stainless-steel backing, and of polyester foils as track detectors. After etching, the number of holes is determined in a spark counter. The statistical uncertainties of the counts are about 3...5 % caused by limitations of the acceptable hole density.
Calculations of reaction rates are carried out with the ANISN-code using activation cross sections of the Riga dosimetry file [17] and fission cross sections of the ENDL-78 library.
The measured radial distributions normalized with the counts in the surface position agree with calculated within 10...20 %.

Table 2

| Nuclide | Reaction | Threshold [MeV] |
|---|---|---|
| Rh-103 | (n,n') | 0.7 |
| In-115 | (n,n') | 1.2 |
| Ni- 58 | (n,p) | 2.3 |
| Zn-64 | (n,p) | 3.0 |
| P-31 | (n,p) | 3.5 |
| Mg-24 | (n,p) | 7.0 |
| Al-27 | (n,α) | 7.2 |
| Tl-203 | (n,2n) | 7.9 |
| Cu-65 | (n,2n) | 12.4 |
| U-235 | (n,f) | - |
| Np-237 | (n,f) | 0.6 |
| Th-232 | (n,f) | 1.4 |
| U-238 | (n,f) | 1.5 |

If relations of reaction rates are formed for comparisons with the calculation, the uncertainties are smaller because systematical errors are eliminated to some degree. Table 3 shows results where rates from probes with threshold around 1 MeV are used as nominator. They are compared with the rates from the Mg-probe (threshold 7 MeV) as well as from the U-235 probe (no threshold). The calculated relations are 10...20 % lower than the measured. This could be understood as underestimate of the neutron flux in the energy region from about the threshold of the nominator material to ≈7 MeV.

Table 3: $(N_A/N_B)$ calculated / $(N_A/N_B)$ measured at the surface of the lead sphere with probes A/B

| In / Mg | Ni / Mg | Zn / Mg | U-8/U-5 | Th-2/U-5 |
|---|---|---|---|---|
| 0.82±0.06 | 0.89±0.06 | 0.81±0.06 | 0.85±0.06 | 0.79±0.6 |

In principle, the discrepancies observed in the presented work show similar tendencies as reported from the benchmarks mentioned above. As the next step we shall repeat the calculations using a new file of evaluated Pb data [18] where collective excitations, pre-equilibrium emissions, their influence on multiple neutron emissions as well as anisotropic angular distributions are taken into account.

References

[1] International Tokamak Reactor, Phase one, IAEA STI/PUB/619, Vienna 1982, p. 450-476. D. Albert, Kernenergie 26 (1983) 181.

[2] C. Wong et al., California University, Livermore, UCRL-51 144, 1972.

[3] V.D. Aleksandrov et al., Atomnaya Ehnergiya 52 (1982) 427.

[4] A. Takahashi et al., Proc. 12th Symp. Fusion Technology, Jülich, Sept. 1982, p. 687.

[5] W. Kaißen et al., Nucl. Instr. Methods 88 (1970) 251.

[6] H. Helfer et al., 13th Int. Symp. on Nuclear Physics - Fast Neutron Reactions, Gaußig, Nov. 1983.

[7] R. Arlt et al., ZfK-408 (1979) p. 154.

[8] D. Hermsdorf, ZfK-315 (1976) p. 192.

[9] M. Adel-Fawzy, ZfK-408 (1979) p. 150.

[10] K. Seidel, S. Unholzer, Informationen TU Dresden 05-09-82 (1982).

[11] D. Albert et al., Kernenergie 21 (1978) 82.

[12] D. Albert et al., Nucl. Instr. Meth. 200 (1982) 397.

[13] D. Albert, W. Hansen, Kernenergie 20 (1977) 95.

[14] M. Segev, Ann.Nucl. Energy 11 (1984) 177.

[15] G. Streubel, B. Dörschel, Kernenergie 20 (1977) 49.

[16] W. Hansen, W. Vogel, ZfK-523, Rossendorf 1984.

[17] A.A. Lapenas, Izmerenie spektrov nejtronov aktivatsionnym metodom, Zinatne, Riga, 1975.

[18] D. Hermsdorf et al., SOKRATOR-library, FILE-MAT-1502, 1984.

# LEAD SLOWING DOWN NEUTRON SPECTROMETER

A.Górski, H.Małecki, Yu.P.Popov*, M.Przytuła and M.Stępiński.
Institute of Physics, Lodz University, Lodz, Poland
*Joint Institute for Nuclear Research, Dubna

Abstract: A slow neutron spectrometer based on the measurement of the slowing-down time of neutrons in lead has been built at Lodz University. The characteristics of the spectrometer and the time-space distribution of neutron density in the lead pile have been determined experimentally and are discussed.

## 1. Introduction

Several slow neutron spectometers based on the measurement of the slowing-down time of neutrons in lead [1] have been built by various groups during the past thirty years. In general, they have been used in measurements of neutron capture cross-sections, determination of some characteristics of fission, and acquisition of some data important for reactor physics [1-6] .

Although the energy resolution of those spectrometers has been rather poor (about 30-60 percent) and far from that obtained in the time-of-flight method, they do nevertheless have some advantageous features, such as their relatively high luminosity and ability to cover a wide enregy range (from 1 eV to about 30 keV). Moreover, they are fairly inexpensive.

The theory of the spectrometer has been presented in ref. [1] . We did not find any other theoretical formulation which enables the time and space distribution of the neutron density in a finite lead pile of the spectrometer to be calculated along reasonably simple lines.

The principal aim of this contribution is to present the experimentally derived characteristics of the lead slowing down neutron spectrometer which has been built at Lodz University, and to point out that the time-space distribution of neutron density in a lead pile is not quite consistent with the prediction of standart spectrometer theory.

## 2. Facility

The spectrometer is based on a pulsed fast neutron generator utilizing the $T(d,n)^4He$ reaction induced by 180-keV deuterons. The source of fast neutrons is displaced somewhat from the center of the lead pile having the dimensions: 1.2m×1.8m×1.4m. The pile is covered by a 0.5 mm thick sheet of cadmium to prevent any slow neutrons, back-scattered from floor and walls, from re-entering the assembly. In the lead pile three channels for detectors, targets and monitor have been introduced. Their dimensions are: 0.1m×0.1m and 0.05m×0.05m. In addition, one vertical hole (0.15m×0.15m) extending up to half the height of the pile has been made for the accelerator target tube.

The half-width of the periodically generated neutron bursts (with frequency 200-400 Hz) was 2.5 μs. Starting signals to the ion source at high voltage were transmitted optically by a light-pipe.

For the measurements of neutron density, $BF_3$ and He-3 neutron counters have been used. The energy distribution of slowed-down neutrons has been measured by registering the resonance capture gamma-rays in a $CaF_2$ scintillation counter. For measurements of time distributions of counts a 1024-channel time analyzer with 1-μs channel width has been used.

## 3. Results of measurements

The gamma-ray intensity from radiative capture of neutrons in a selenium targ t versus time after the neutron burst is shown in Fig.1. The energy resolution determined from the measurements with selenium and silver (5.22-eV resonance) amounts to about 60%.

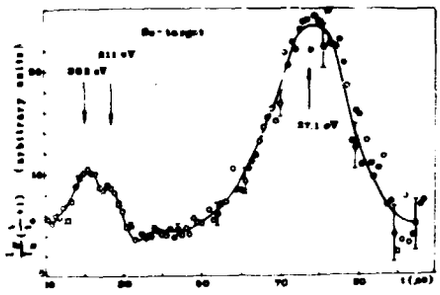

The commonly used calibration formula for the average neutron energy, E, as a function of the slowing-down time, t, is: $E=C(t+t_o)^{-2}$, where constant C and $t_o$ are characteristic for the spectrometer. Our measurements determined these to be respectively $C=(164\pm14)$ keV×μs$^2$ and $t_o=(0.35\pm0.3)$ μs.

Fig.1. Intensity of gamma-rays from radiative capture of neutrons in a selenium target versus slowing-down time. Results have been obtained from a $CaF_2$-scintillation counter and reduced to unit neutron flux.

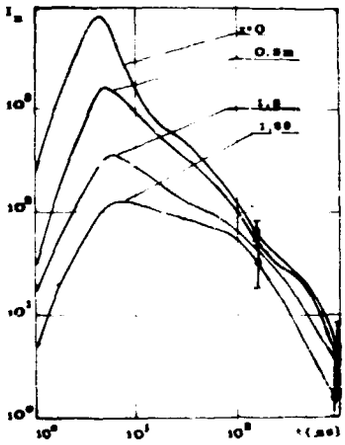

For a thin 1/v neutron counter the number of counts per time channel, $I_n$, is proportional to the instantaneous neutron density at the location of the counter (averaged over the region of the counter length). The Fig.2 illustrates the dependence of neutron density on the slowing-down time for various positions in the channel. In Fig.3 the space distributions of neutron density along the channel for various times is shown. When the cadmium cover of the lead pile was removed, a rise of the neutron density at the side of the pile was clearly discernible, especially for t>100us.

Fig.2. Curves of neutron counts intensity from 1/v neutron detector, proportional to the neutron densities, placed at various position in the lead pile channel as a function of slowing-down time.

## 4. Discussion and conclusions

The energy resolution of the spectrometer is inferior to those of others in the literature, where it achieved 30%. It is presumably caused by the quality of the lead used therein (an industrial type without any special purification). In spite of the cadmium cover, the floor and near-by walls probably additionally have some influence on the worsening of the resolution.

The obtained constant C is close to the values given by other authors. That calculated from the theory, taking into account the effective density of lead and $\lambda_s=0.028$ cm, is $C_{theor}=176$ keV×μs$^2$. The value of $t_o$ obtained from fitting is not highly accurate, as it is not very sensitive to the energy of low-lying resonances.

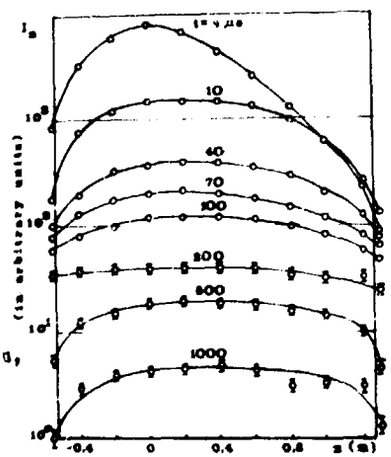

Fig.3. Spatial distribution of neutron density in the lead pile channel at various instants after the neutron burst.

From our results it appears that the conventional theory of the spectrometer [1] is not altogether accurate, especially for t 10≤μs, which can be important for energies exceeding 1 keV. According to the above mentioned theory, the dependence of neutron density on time is given by formula:

$n(t) \sim \left(\frac{t}{t_o} + 1\right)^{-\alpha} \exp\left(-\frac{t}{T}\right)$ where the leakage factor, $\alpha$, is constant for any given spectrometer and does not depend on the position in the pile. Hence the form of the space distribution is the same at all instants. In other words, the space and time coordinates in the solution for $n(x,y,z,t)$ should be separated.

In our case $\alpha_{calc} \approx 0.81$ but $\alpha_{exp}$, taken from the time interval 60-100 $\mu$s, changes from 0.3 for the periphery, to about 1.2 for the central zone. In this connection, the form of space distribution of neutron density changes with time, tending to be more flat. It seems that this conclusion holds even if one takes into account the neutrons partly transmitted through the cadmium cover which can re-enter the pile.

5. Acknowledgements

The authors would like to acknowledge the help and consultation provided by Dr E.A. Andreev and Dr A.A. Bergman.

References

1 A.A. Bergman, A.I. Isacov, I.D. Murin, F.L. Shapiro, I.V. Shtranikh and M.V. Kazarnovsky, Proc. Int. Conf. Peaceful Uses At. Energy, Geneva vol. 4 (1955) 135.

2 F. Mitzol and H.S. Plendl, Nukleonik 6 (1964) 371.

3 H. Wakabayashi, A. Sekiguchi, M. Nakazawa and O. Nishino, J. Nucl. Sci. Techn. 7 (1970) 487.

4 J.C. Chou and H. Werle, J. Nucl. Energy 27 (1973) 811.

5 M. Sawan and R. Zorn, Nucl. Sci. Eng. 54 (1974) 127.

6 R.E. Slovacek, D.S. Cramer, E.B. Bean, J.R. Valentine, R.W. Hockenbury and R.C. Block, Nucl. Sci. Eng. 62 (1977) 455.

# ПРИМЕНЕНИЕ ИНТЕНСИВНЫХ ФИЛЬТРОВАННЫХ ПУЧКОВ НЕЙТРОНОВ ДЛЯ ФИЗИЧЕСКИХ ИССЛЕДОВАНИЙ

Вертебный В.П.,
Институт ядерных исследований АН УССР, Киев, СССР

Дан обзор применений фильтрованных пучков для физических исследований и определения ядерных констант на атомных реакторах и ускорителях.

Даже средний по потоку атомный реактор на тепловых нейтронах является мощным источником не только тепловых, но и промежуточных и быстрых нейтронов. К сожалению, монохроматизация этих нейтронов или применение техники времени пролета к реакторным нейтронам затруднены. Новые возможности возникли с возникновением техники фильтрованных пучков промежуточных нейтронов /I/. В США, СССР, ЧССР и ФРГ, Англии и других странах были сделаны различные предложения по использованию фильтрованных пучков в ядерной физике. В обзорах /2/ приведены ссылки на оригинальные работы. Наибольшее применение получили фильтры из скандия (энергия нейтронов 2 кэВ), железа (24,5 кэВ), монокристаллов кремния (I44 кэВ, 55 кэВ и тепловые нейтроны). В опытах использовались хорошо сколлимированные квазимонохроматические пучки промежуточных нейтронов с потоком $10^6$ - $10^8$ н/см$^2$сек, имеющие небольшой фон быстрых нейтронов и гамма-лучей. Основные применения связаны с определением средних резонансных параметров, усредненных по большому количеству нейтронных резонансов. В /2/ можно найти примеры этих применений.

Отмечу дополнительно некоторые новые применения. Гнидак Н.Л., Павленко Е.А. и др. /3/ поставили опыты по исследованию резонансного самоэкранирования с применением самоиндикации на тонких образцах тантала /3/. В этих опытах определены не только средние полные и парциальные сечения, но и т.н. обобщенные дисперсии /4/:

$$\langle\sigma_t\sigma_s\rangle - \langle\sigma_t\rangle\langle\sigma_s\rangle, \quad \langle\sigma_t\sigma_\gamma\rangle - \langle\sigma_t\rangle\langle\sigma_\gamma\rangle$$

Используя связь этих величин со средними резонансными параметрами /4/, удалось определить в неразрешенной области все средние резонансные параметры - $S_0$, $R'$, $\langle\Gamma_\gamma\rangle$ и $D_0$. Работы /5, 6/ представляют пример успешного исследования гамма-спектров при радиационном захвате промежуточных нейтронов с помощью фильтров. Существенно уточнены схемы распада $^{128}I$, обнаружена аномальная зависимость от энергии нейтронов интенсивности жестких переходов в $^{238}U$, вызванных S - нейтронами. Работа /7/ представляет собою продолжение цикла совместных работ ОИЯИ и ИЯИ АН УССР по исследованию ( n,α) реакций на промежуточных нейтронах. В этих работах удавалось определять средние α - ширины, которые составляли $10^{-6}$ - $10^{-7}$ от радиационной ширины. Следует отметить, что возможно применение и других фильтров. Так в работе /8/ приводятся данные, свидетельствующие о возможности использования изотопов $^{58}Ni$, $^{60}Ni$, $^{64}Zn$ и $^{184}W$ для создания фильтрованных пучков нейтронов в интервале 0,09 - 5000 кэВ. Различные применения фильтров рассмотрены в работе /8/ где предлагается даже создать специализированный реактор. Фильтрованные пучки успешно использовались и на ускорителях. Фильтры обеспечивали малый фон /9, I0/.

## Литература

/I/ Simpson, O.D., Miller, L.G., Nucl. Instr. Meth. 68, 245 (1968)

/2/ Вертебный В.П., I Международная школа по нейтронной физике, Д3, 4-82-704, Дубна, стр. 66-86, I982, The IAEA Interregional Courses "Neutron Physics and Nuclear Data", Tashkent 1983

/3/ Вертебный В.П., Гнидак Н.Л., Новосёлов Г.М., Павленко Е.А., Пшеничный В.А., Сенченко Т.А., Трофимова Н.А., Нейтронная физика, т.3. Материалы 6 Всесоюзной конференции по нейтронной физике, Киев, стр. 28-32, I984.

/4/ Лукьянов А.А. - Замедление и поглощение резонансных нейтронов, М. Атомиздат, 1967, с. 360,

/5/ Мурзин А.В., Либман В.А., Кононенко И.В., Рубченко Н.А., Харакоз И.Н., Нейтронная физика т. 2, Материалы Всесоюзной конференции по нейтронной физике в Киеве, октябрь 1983 г. стр. 313-317, Атомиздат 1984, Логинов Ю.Е., Мартынов В.В., Мурзин А.В., Федоров Э.И., там же, т. 3, стр. 20-24,

/6/ Chrien, R.E., Kopecky, J., Nucl. Phys. A 414, 218 (1984)

/7/ Втюрин В.А., Мак А., Попов Ю.П., Салацкий В.И., Чадраабал И., Вертебный В.П., Долгов В.А., Кирилюк А.Л., Нейтронная физика т. 2, Материалы Всесоюзной конференции по нейтронной физике в Киеве, октябрь 1983 г., стр. 342-345, Атомиздат 1983,

/8/ Mill, A.J., Harvey, J.R., Nucl. Data for Science and Technology, Proc. Conf., Antwerp, 1982, p. 999 - 1004

/9/ Мурадян Г.В., Адамчук Ю.В., Щепкин Ю.Г., Нейтронная физика ч. I, Материалы Всесоюзного совещания, Киев, май 1971, изд. "Наукова Думка", Киев 1972, стр. 124-127.

/10/ Tsubone, I., et al., Nucl. Data for Science and Technology, Proc. Conf. Antwerp, 1982, p. 65-68; Nucl. Sci. Eng. 1984, 88, 579

# АНОМАЛЬНЫЕ ЗНАЧЕНИЯ МОМЕНТОВ ИНЕРЦИИ ЯДЕР, ПОЛУЧАЕМЫЕ ПРИ АНАЛИЗЕ СПЕКТРОВ НЕЙТРОНОВ ИЗ РЕАКЦИЙ $(p,n)$ И $(n,n')$.

О.А. Сальников, Г.Н. Ловчикова, С.П. Симаков, А.М. Труфанов
Физико-энергетический институт, Обнинск, СССР

Аннотация

В работе показано, что данные по моментам инерций, получаемые при анализе спектров нейтронов из реакций $(p,n)$ и $(n,n')$ для некоторых ядер имеют аномально низкие значения, находящиеся в противоречии с теоретическими представлениями.

Момент инерции ядра характеризует распределение массы ядра и агрегатное состояние ядерной материи, т.е. является величиной, имеющей фундаментальное значение для характеристики ядерных сил.

Теоретическое предсказание поведения момента инерции ядра в зависимости от энергии возбуждения основывается на модельных представлениях. Так, в модели ферми-газа – это постоянная величина, равная твердотельному моменту инерции, по модели сверхпроводимости момент инерции до критической энергии возбуждения растущая функция энергии возбуждения, достигающая твердотельного значения при энергии возбуждения $U \geq U_{крит.}$ .

Метод определения момента инерции основан на его связи с параметром спиновой зависимости плотности ядерных уровней $\sigma^2$ (дисперсии проекции углового момента ядра). Например, в модели ферми-газа:

$$\sigma^2 = \langle m^2 \rangle g \frac{t}{\hbar^2} = \frac{\mathcal{J} \cdot t}{\hbar^2} \qquad (I),$$

где $\langle m^2 \rangle$ – средний квадрат проекции углового момента нуклона в одночастичном состоянии вблизи поверхности Ферми, $g$ – плотность таких состояний, $t = \sqrt{U^*/a}$ – термодинамическая температура ядра, $U^* = U - \Delta$ , где $U$ – энергия возбуждения ядра, $\Delta$ – параметр, учитывающий четно-нечетные эффекты в плотности уровней, $a$ – параметр энергетической зависимости плотности ядерных уровней, $\mathcal{J}$ – момент инерции ядра, $\sigma$ – параметр спиновой зависимости плотности ядерных уровней.

$\sigma$ определяется подгонкой рассчитываемого с помощью модельных представлений

углового распределения испущенного ядром частиц к эксперименту, причем подгонка осуществляется изменением $\sigma^2$ до совпадения теоретического и экспериментального коэффициента анизотропии (отношения $A_2/A_0$, где $A_0$ и $A_2$ коэффициенты при полиномах Лежандра соответствующих порядков в разложении угловых распределений). При теоретических расчетах использовались как модель ферми-газа, так и модель сверхпроводимости.

В настоящее время имеются две группы экспериментов, дающие существенно различные результаты. Одна из них - определение моментов инерции делящихся ядер по угловому распределению осколков деления [I ÷ 3]. Эти работы показывают (см.рис.I [I]) хорошее согласие с предсказаниями модели сверхпроводимости: до критической температуры (критической энергии возбуждения) момент инерции $J_{эфф}$ растущая функция энергии возбуждения, а для $T(U) \geq T_{кр}(U_{кр})$ эффективный момент инерции становится равным твердотельному - $J_{тв}$. Для иллюстрации этого факта выбрана работа [I], т.к. в ней использовались нейтроны в том же диапазоне энергий (0,05 ÷ 7,2 МэВ), что и для изучения реакций (p, n) и (n, n') [4 ÷ 7].

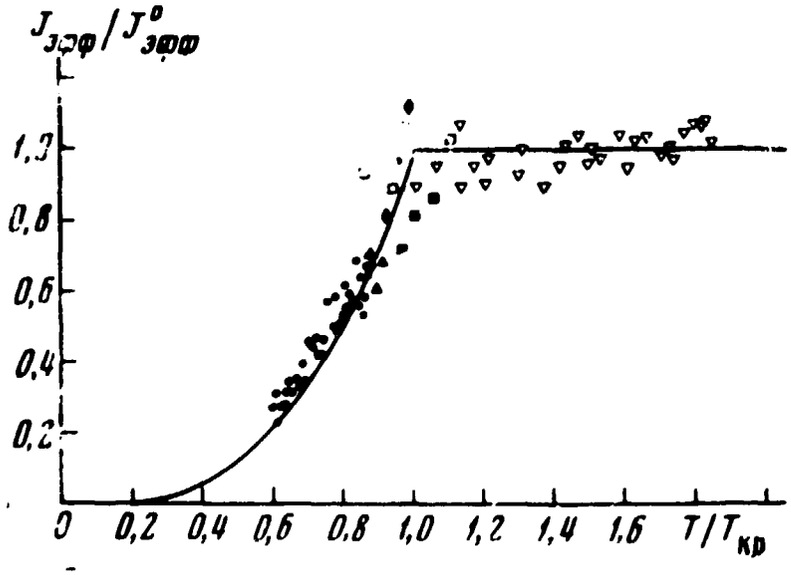


Рис.I. Отношение момента инерции ядра $^{239}Pu$ к его твердотельному значению $J_0$ в зависимости от ядерной температуры T [I].

Другая группа экспериментов - это извлечение значения моментов инерции при анализе угловых распределений нейтронов, испущенных в реакциях (p, n) и (n, n'). Здесь результаты неоднозначны: для одних ядер, таких как, например, цинк-65, ниобий-94, результаты практически совпадают с предсказаниями модели сверхпроводимости (см. рис.2), для других же - индий-113, олово-115, сурьма-117,119,120,122, воль-

...-зависимость значения эффективного момента инерции от энергии возбуждения, следуя по форме модели сверхпроводимости (излом в области $U \simeq U_{кр}$ ), отличается в области $U \geq U_{кр}$ в 2-7 раза (см. рис. 3 ÷ 4 и табл.I), и никакими уточнениями расчета эти результаты нельзя изменить.

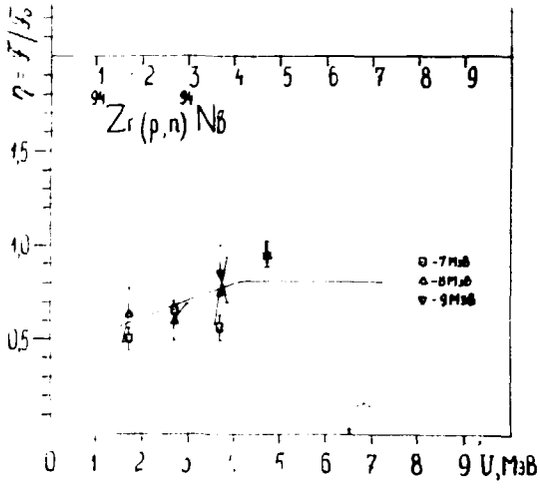


Рис. 2. Отношение момента инерции ядра $^{94}Nb$ к его твердотельному значению $\mathcal{J}_0$ в зависимости от энергии возбуждения. Результаты приведены для трех значений энергий налетающих протонов: 7,8 и 9 МэВ; —— расчет по сверхпроводящей модели ядра [4] .

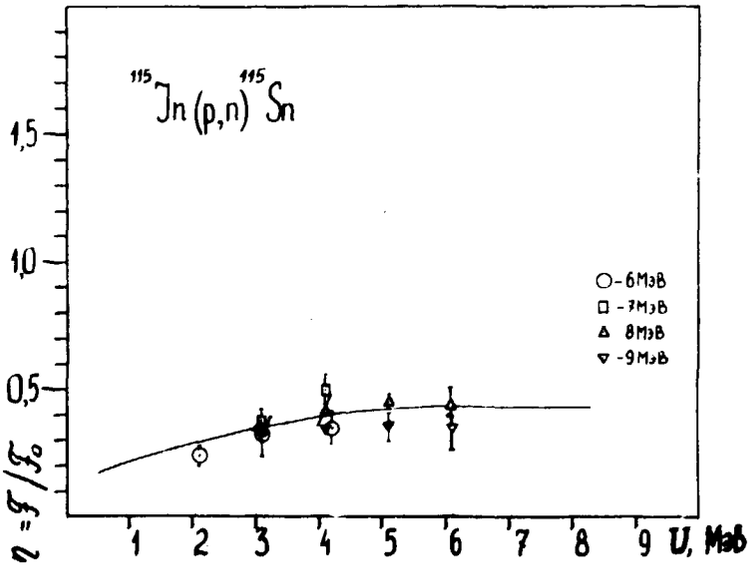


Рис. 3. Отношение момента инерции ядра $^{115}Sn$ к его твердотельному значению в зависимости от энергии возбуждения $U$ .
Результаты приведены для 4-х начальных энергий протонов.
Сплошная кривая - расчет по сверхпроводящей модели ядра [4] .

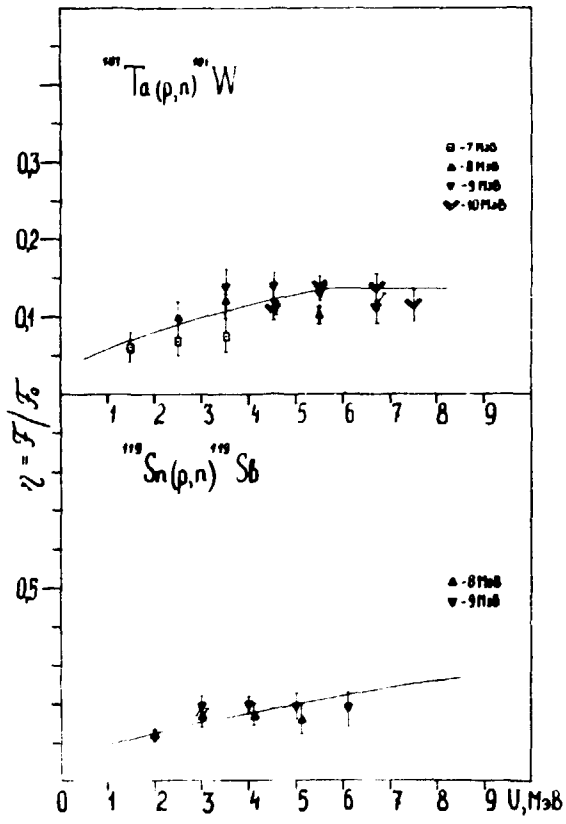


Рис. 4. Отношение моментов инерции ядер $^{181}W$ и $^{119}Sb$ к их твердотельным значениям. Сплошная кривая – расчет по сверхпроводящей модели ядра [4].

Таблица I.

| Элемент | $U_{min} \div U_{max}$, МэВ | модель ферми-газа: $a$, МэВ$^{-1}$ | $\Delta$, МэВ | $\eta_{ф}$ | $\Delta_0$, МэВ | модель сверхпроводимости: $U_{ф}$, МэВ | $\eta_{ф}$ | $\frac{a(U_{ф})}{\tilde{a}}$ |
|---|---|---|---|---|---|---|---|---|
| $^{65}Zn$ | I,7 + 5,7 | I0,7 | -0,4 | I,00 ± 0,24 | I2$\sqrt{A}$ | 7,4 | I,00 ± 0,25 | I,03 |
| $^{94}Nb$ | I,2 + 5,2 | II,39 | -0,7 | 0,77 ± 0,I2 | " | 4,I | 0,78 ± 0,I3 | 0,98 |
| $^{95}Tc$ | I,5 + 5,5 | II,75 | -0,9 | 0,55 ± 0,08 | " | 5,4 | 0,84 ± 0,I3 | 0,90 |
| $^{98}Tc$ | 0,5 + 5,0 | II,9 | -0,75 | 0,46 ± 0,05 | " | 4,I | 0,52 ± 0,05 | I,03 |
| $^{109}Cd$ | I,9 + 7,0 | I5,I | -0,2 | 0,48 ± 0.08 | " | 6,5 | 0,63 ± 0,II | I,02 |
| $^{113}In$ | I,4 + 7,4 | I8,25 | +0,7 | 0,47 ± 0,09 | I,38 | 9,0 | 0,59 ± 0,I2 | I,04 |
| $^{115}Sn$ | I,6 + 6,6 | I4,0 | +0,47 | 0,42 ± 0,05 | I,I8 | 4,9 | 0,45 ± 0,06 | 0,98 |
| $^{117}Sb$ | I,3 + 5,4 | 20,0 | +0,5 | 0,30 ± 0,I2 | I,39 | I0,8 | 0,42 ± 0,06 | I,03 |
| $^{119}Sb$ | I,5 + 6,6 | I8,6 | +0,36 | 0,2I ± 0,02 | I,3I | 8,8 | 0,27 ± 0,03 | I,03 |
| $^{120}Sb$ | I,5 + 4,5 | I6,8 | -0,5 | 0,3I ± 0,05 | I,I8 | 5,02 | 0,32 ± 0,03 | |
| $^{122}Sb$ | I,5 + 5,5 | I6,3 | -0,54 | 0,2I ± 0,02 | I,I9 | 4,9 | 0,24 ± 0,03 | I,08 |
| $^{181}W$ | I,0 + 8,0 | 20,3 | -0,25 | 0,I0 ± 0,02 | I2/$\sqrt{A}$ | 5,2 | 0,I3 ± 0,03 | 0,84 |

Примечания: I. Погрешность определения $a \pm 5\%$. 2. Значения $U_{\varphi}$ приведены с учетом поправки на четно-нечетные эффекты. $\tilde{a}$ - асимптотическое значение параметра плотности ядерных уровней при высокой энергии возбуждения.

Была неоднократно проверена программа расчета, с ее помощью получены все предельные случаи. Исследовано влияние параметров оптического потенциала входного и выходного каналов реакции на получаемые значения момента инерции. В выходном канале параметры нейтронного потенциала в плотности уровней определялись для каждого исследуемого ядра по наилучшему описанию интегральных спектров нейтронов во всем рассматриваемом диапазоне энергии. При расчетах угловых распределений нейтронов из реакции (p , n) исследовалось влияние задаваемой оптики входного канала на величину анизотропии ($A_2/A_0$) и, следовательно на получаемое значение момента инерции $J_{эфф}$. Оказалось, что максимальный разброс значений $\eta = \frac{J_{эфф}}{J_{rb}}$ при использовании различных наборов оптического потенциала как глобальных, рекомендованных Бечетти-Гринлисом [8] и Пэреем [9], так и индивидуальных, не превышает 10%. Бо́льшее влияние на угловые распределения оказывают принятые значения спина ядер-мишеней и структура низколежащих состояний, но они для изученных ядер хорошо известны.

Проведен тщательный учет оболочечных эффектов, уменьшающих плотность одночастичных состояний $g$ и величину среднего квадрата проекции одночастичного углового момента $\langle m^2 \rangle$, учтено влияние парных корреляций сверхпроводящего типа в модели сверхтекучего ядра. Все приведенные исследования показали, что перечисленные факторы не приводят к заметным изменениям моментов инерции исследованных ядер и, следовательно не могут объяснить данные экспериментов.

Одним из объяснений наблюдаемого несоответствия эксперимента и теории может быть присутствие в анализируемых спектрах нейтронов, обусловленных предравновесным испарением из составного ядра. Такие нейтроны имеют симметричное относительно угла $\theta = 90^0$ распределение и если их доля невелика, то их присутствие не исказит заметно энергетический спектр, и они могут быть приняты за нейтроны, покинувшие ядро в состоянии статистического равновесия. Но так как угловое распределение предравновесных нейтронов имеет бо́льший коэффициент анизотропии [10] , то это и может послужить причиной наблюдаемой аномалии. Если принять это предположение, то появляется инструмент для оценки этого вклада: сравнение наблюдаемой анизотропии с расчетной, использующей теоретические значения момента инерции, позволят установить этот вклад. В настоящее время этот эффект на пределе точности измере-

ний; даже если отнести всю наблюдаемую анизотропию к предравновесным процессам (считая равновесную часть спектра изотропной), то по оценке эта компонента $\leq 5\%$.

Однако имеются серьезные аргументы против такого предположения. Наблюдается совпадение моментов инерции, определяемых для одной и той же энергии возбуждения, но при разных начальных энергиях нейтронов или протонов, а вклад предравновесных процессов зависит от начальной энергии налетающих частиц. Моменты инерции, определенные для одних и тех же изотопов в различных реакциях $(p, n)$ и $(n, n')$ совпадают, а вклад нестатистических процессов должен быть для этих реакций различен.

Непонятно, почему для ядер в районе цинк÷ниобий без всяких предположений значения $\mathcal{J}_{эфф} \approx \mathcal{J}_{тв}$, хотя угловые распределения для них анизотропны (см. рис. 5, 6), а для вольфрама даже в предположении практически изотропного углового распределения момент инерции имеет $\mathcal{J}_{эфф} \approx 0{,}5\, \mathcal{J}_{тв}$.

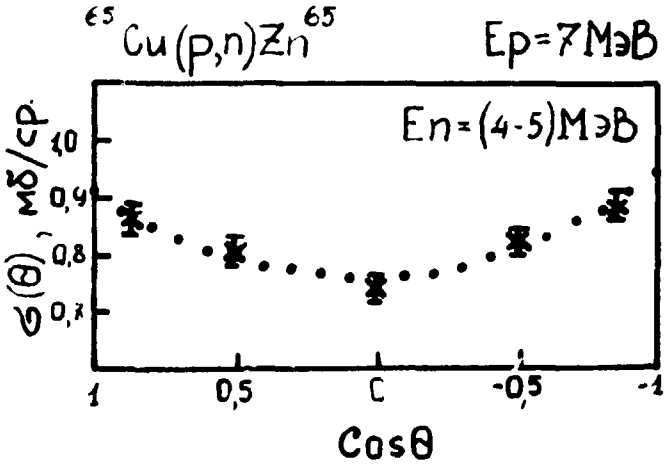


Рис. 5. Угловое распределение нейтронов с энергиями в интервале 4÷5 МэВ из реакции $^{65}Cu(p, n)^{65}Zn$ для энергии протонов 7 МэВ.

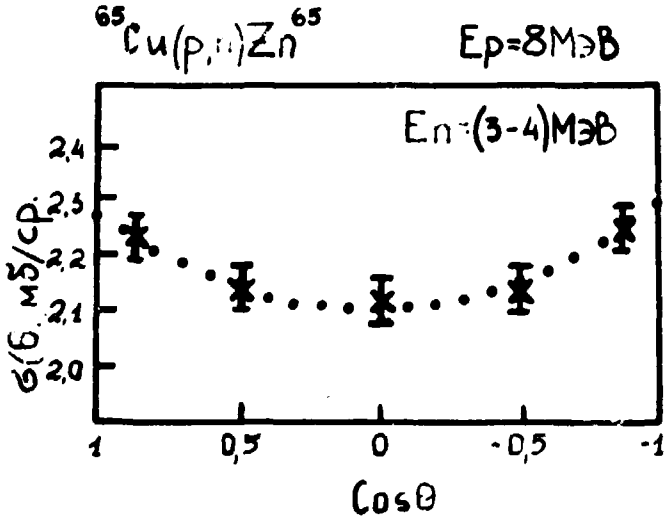


Рис. 6. Угловое распределение нейтронов с энергиями в интервале 3÷4 МэВ из реакции $^{65}Cu(p, n)^{65}Zn$ для энергии протонов 8 МэВ.

Вероятнее всего эти результаты являются следствием несовершенства имеющихся теоретических представлений о моментах инерции возбужденных ядер, недостаточности учета их индивидуальных свойств.

Для решения этой проблемы нужны усилия как теоретиков, так и экспериментаторов, т.к. точность оценки возможного вклада предравновесных процессов на границе чувствительности используемых методик.

# ЛИТЕРАТУРА


1. Д.Л.Шпак, Ю.Б.Остапенко, Г.Н.Смиренкин. Я.Ф., (1971),т.13, вып.5, с.950.
2. А.В.Игнатюк, М.Г.Иткис, Г.Я.Русанов, Г.Н.Смиренкин, А.С.Тишин, Я.Ф., (1977), т.25, вып.1, с.25.
3. А.В.Игнатюк, К.К.Истеков, Г.Н.Смиренкин, Я.Ф., (1982), т.36, вып.1, с.54.
4. А.М.Труфанов, Г.Н.Ловчикова, О.А.Сальников, Н.Н.Титаренко, Препринт ФЭИ-1484, Обнинск, 1983.
5. Симаков С.П., Ловчикова Г.Н. и др. Неупругое рассеяние нейтронов и плотность ядерных уровней. Ядерная физика, 1983, т.33, с.3.
6. А.М.Труфанов, Г.Н.Ловчикова, О.А.Сальников и др. Нейтронная физика, 1984, ч.III, с.235.
7. А.М.Труфанов, Г.Н.Ловчикова, О.А.Сальников и др. Нейтронная физика, 1984, ч.III, с.240.
8. F.D Becchetti, G.W. Greenless., Phys. Rev., 182(1969)1190.
9. F.G. Perey, Phys. Rev., 131(1963)745.
10. А.В.Игнатюк, В.П.Лунев, В.Г.Проняев. Известия АН СССР, серия физическая, 39 (1975) 21.

# МГНОВЕННЫЕ НЕЙТРОНЫ НИЗКОЭНЕРГЕТИЧЕСКОГО ДЕЛЕНИЯ АТОМНЫХ ЯДЕР.

Б.Ф. Герасименко, В.А. Рубченя
Радиевый институт им. В.Г. Хлопина, Ленинград

В работе приводится анализ механизма эмиссии мгновенных нейтронов низкоэнергетического деления атомных ядер. Расчеты проводились на основе метода Хаузера-Фешбаха в предположении эмиссии нейтронов из полностью ускоренных осколков и угловой изотропии нейтронных спектров в с.ц.м. В расчетах учитывался каскадный характер испускания нейтронов, учитывались распределения осколков по энергии возбуждения и спину, по кинетическим энергиям, по зарядам и массам. Для плотности уровней использовалось выражение, учитывающее оболочечную структуру ядер. Приведены результаты расчета спектров и распределения множественности мгновенных нейтронов для спонтанного деления калифорния-252 и деления урана-235 тепловыми нейтронами. Обсуждается чувствительность расчетов к вариациям параметров модели.

Характеристики мгновенных нейтронов деления (МНД) (спектры, среднее число нейтронов, распределения множественности) имеют важное значение при расчетах ядерных реакторов и других практических приложений. При этом необходимо знание характеристик МНД для различных нуклидов и энергий возбуждения, для которых измерения сильно затруднены. Имеющиеся к настоящему времени экспериментальные данные [1] довольно ограничены и недостаточны для практических потребностей. В связи с этим представляется важным разработка теоретических методов расчета характеристик МНД, с помощью которых можно получить недостающие данные или повысить надежность оценок и экстраполяций. С другой стороны, изучение МНД представляет возможность исследования процесса деления атомных ядер и механизма разрядки высоковозбужденных состояний осколочных нейтроноизбыточных ядер.

Результаты проведенных к настоящему времени исследований показывают, что МНД испускаются осколочными ядрами, а вклад нейтронов, образующихся в процессе разделения очень мал и находится, по-видимому, на уровне вероятности эмиссии легких заряженных частиц при тройном делении. Основная часть МНД испускается сильно нагретыми осколками по законам равновесной статистики. Обнаруженная в работе [2] так называемая изотропная в лабораторной системе доля МНД может быть связана с неравновесным механизмом эмиссии частиц. Соотношение между вкладом равновесного и неравновесного механизмов определяется скоростью перекачки энергии деформации осколков, в которой сосредоточена главная часть энергии возбуждения осколков при низкоэнергетическом делении, в тепловую энергию. На основании предложенной в работе [3] модели неравновесного механизма эмиссии МНД в результате неадиабатического изменения формы осколков непосредственно после разделения можно сделать вывод, что вклад таких нейтронов составляет не более 10% при разумных предположениях о распределении деформаций осколков и коэффициенте вязкости. Характерные времена эмиссии нейтронов с помощью такого неравновесного механизма меньше времени ускорения ядер-осколков, поэтому угловое распределение этих нейтронов не искажается переносной скоростью осколков. Для выделения неравновесных механизмов испускания МНД необходимы подробные расчеты равновесной составляющей МНД, чтобы из сравнения с

экспериментальными данными сделать надежные заключения о свойствах неравновесного компонента МНД. Кроме учета возможных механизмов разрядки ядер-осколков, при теоретическом анализе необходимо правильно учитывать распределения ядер по энергиям возбуждения, по кинетическим энергиям, по зарядам и массам. Трудности расчетов также связаны с недостаточным знанием свойств осколочных ядер, для которых экспериментальных данных практически нет.

Теоретические расчеты характеристик МНД в статистическом приближении проводились во многих работах, но не был произведен учет всех особенностей, связанных с характеристиками осколков деления. Анализ в работе [4] показал, что для согласования расчетов с экспериментальными данными необходимо уточнение описания плотности уровней осколочных ядер и сечения обратного слияния для нейтронов. В работе [5] использован простой вариант испарительной модели, в которой усреднение по распределениям параметров осколков заменено усреднением по треугольному распределению температуры для двух осколков, являющихся представителями легкой и тяжелой групп. Последовательные расчеты в рамках каскадно-испарительной модели проведены в работе [6]. Наиболее обоснованным подходом является использование статистической теории Хаузера-Фешбаха к расчету характеристик МНД [7]. В настоящей работе также использован метод Хаузера-Фешбаха с некоторыми изменениями по сравнению с работой [7], касающихся более точного учета каскадного характера эмиссии нейтронов, использования иного способа определения средней энергии возбуждения осколков, использования для плотности уровней выражения, учитывающего оболочечную структуру ядер [3]. Приведены результаты расчета спектров и распределения множественности МНД для наиболее важных случаев, а именно, спонтанного деления $^{252}Cf$ и деления $^{235}U$ тепловыми нейтронами.

Интегральный спектр мгновенных нейтронов деления составного ядра с массовым числом Ac, зарядом Zc и энергией возбуждения $E_c^*$ формируется из отдельных осколков:

$$N(E,A_c,Z_c,E_c^*)=\sum_{A,Z} Y(A,Z,A_c,Z_c,E_c^*)N(E,A,Z), \qquad (1)$$

где $Y(A, Z, A_c, Z_c, E_c)$ - независимые выходы осколков с массовым числом A и зарядом Z, нормированные на единицу. Энергетический спектр МНД из отдельных осколков $N(E, A, Z)$ по имеющимся представлениям состоит из двух компонентов:

$$N(E,A,Z)=\bar{\nu}_s N_s(E,A,Z)+\bar{\nu}_d N_d(E,A,Z). \qquad (2)$$

Здесь $N_s(E, A, Z)$ - спектр МНД, испускаемых статистически из полностью ускоренных осколков, $N_d$ - спектр МНД, испускаемых либо из неполностью ускоренных осколков статистически, либо с помощью неравновесных механизмов, $\bar{\nu}_s$ и $\bar{\nu}_d$ - среднее число равновесных и неравновесных МНД из отдельных осколков. ($\bar{\nu}(A,Z)=\bar{\nu}_s+\bar{\nu}_d$). В первой работе [2], обнаружившей неравновесный компонент $N_d$, авторы оценили его долю до 20% в интегральном спектре. Однако до настоящего времени количественно величина $\bar{\nu}_d$ не определена, но последние измерения [8] показывают, что $\bar{\nu}_d/\bar{\nu}$ меньше, чем оценено в работе [2]. В настоящей работе мы не рассматриваем неравновесный компонент $N_d$. Для равновесного компонента предполагается, что МНД испускаются изотропно из полностью ускоренных осколков. В этом случае спектр в лабораторной системе координат (Л.С.) простым образом связан со спектром в системе центра инерции (СЦИ) при данной кинетической энергии осколка Ек:

$$N_s(E,A,Z,E_K)=\frac{1}{\bar{\nu}_s}\int_{(\sqrt{E}-\sqrt{E_f})^2}^{(\sqrt{E}+\sqrt{E_f})^2}\frac{\Phi(\varepsilon,A,Z,E_K)}{4\sqrt{\varepsilon E_f}}\,d\varepsilon\,, \qquad (3)$$

где $E_f = Ек/A$. Здесь $\Phi_s(\varepsilon, A, Z, Ек)$ – спектр МНД в СЦИ при данной Ек, нормированный на $\bar{\nu}_s^f$. При расчете интегрального спектра необходимо усреднить по распределению Ек

$$N_s(E,A,Z)=\int_{E_K^{min}}^{E_K^{max}} P(A,Z,E_K)\,N(E,A,Z,E_K)\,dE_K\,. \qquad (4)$$

В процессе эмиссии нейтронов в результате отдачи первоначальное распределение по Ек искажается, но в рассматриваемом приближении этим можно пренебречь.

Спектр в СЦИ формируется в результате каскадной эмиссии нейтронов из возбужденных состояний осколков с начальным гауссовским распределением по энергиям возбуждения $P_0(E^*,A,Z,Ек)$

$$P_0(E^*,A,Z,E_K)=\frac{1}{\sqrt{2\pi\sigma^2_{E^*}}}\,e^{-\frac{(E^*-\bar{E}^*)^2}{2\sigma^2_{E^*}(A,Z,E_K)}}\,. \qquad (5)$$

Здесь $\bar{E}^*$ – средняя энергия возбуждения осколка при данном значении Ек, а $\sigma_{E^*}$ – дисперсия распределения по $E^*$. При усреднении по распределению (5) необходимо ограничиться максимальным значением $E^*_{max}$, которое принималось равным

$$E^*_{max}=\bar{E}^*(A,Z,E_K)+3\sigma_{E^*}(A,Z,E_K)\,. \qquad (6)$$

Величина $E^*_{max}$ определяет максимально возможное число нейтронов $\nu_{max}$, испущенных данным осколком, согласно неравенству

$$E^*_{max}(A,Z,E_K)-\sum_{i=1}^{\nu_{max}} B_n(A-i+1,Z)\leqslant B_n(A-\nu_{max},Z), \qquad (7)$$

где $B_n(A,Z)$ – энергия связи нейтрона. При использовании соотношения (6) вероятность эмиссии $\nu_{max}$-нейтрона меньше 0.01. Если распределение множественности нейтронов $W(\nu)$ нормировано на I, то спектр МНД в СЦИ определяется выражением

$$\Phi(\varepsilon,A,Z,E_K)=\sum_{\nu=1}^{\nu_{max}}\Big[1-\sum_{i=0}^{\nu-1}W(i)\Big]\cdot n_\nu(\varepsilon), \qquad (8)$$

где $n_\nu(\varepsilon)$ – энергетический спектр $\nu$-нейтрона, нормированный на I.

Энергетический спектр первого нейтрона определяется выражением

$$n_1(\varepsilon)=\int_{B_n+\varepsilon}^{E^*_{max}} P_0(E^*,A,Z,E_K)\,\varphi(\varepsilon,E^*,A,Z)\,dE^*, \qquad (9)$$

где $\varphi(\varepsilon,E^*,A,Z)$ – вероятность эмиссии нейтрона с кинетической энергией $\varepsilon$ из состояния с энергией возбуждения $E^*$.

После эмиссии первого нейтрона новое распределение энергии возбуждения находится из соотношения

$$P_1(E^*,A-1,Z,E_K)=\int_{B_n+E^*}^{E^*_{max}} P_0(E^*_1,A,Z)\,\varphi(E^*_1-E-B_n,E^*_1,A,Z)\,dE^*_1\,. \qquad (10)$$

Аналогично, спектр $\nu$-нейтрона определяется выражением

$$n_\nu(\varepsilon)=\int_{B_n(A-\nu+1,Z)+\varepsilon}^{E^*_{max}-\sum_{i=1}^{\nu-1}B_n(A-i,Z)} P_{\nu-1}(E^*,A-\nu+1,Z)\,\varphi(\varepsilon,E^*,A-\nu+1,Z)\,dE^* \qquad (11)$$

$$P_{\nu-1}(E^*, A-\nu+1, Z) = \int_{E_1^*+B_n(A-\nu+2,Z)}^{E^*_{max}-\sum_{i=1}^{\nu-1} B_n(A-i,Z)} P_{\nu-2}(E_1^*, A-\nu+2, Z)\varphi(E_1^*-E^*-B_n(A-\nu+2,Z), E_1^*, A-\nu+2, Z)dE_1^* \quad (12)$$

Распределение множественности МНД при $\Gamma_\gamma/\Gamma_n \ll 1$ определяются соотношениями

$$W(0) = \int_0^{B_n(A,Z)} P_0(E^*, A, Z)\, dE^*, \quad (13)$$

$$W(1) = (1-W(0))\int_0^{B_n(A-1,Z)} P_1(E^*, A-1, Z)\, dE^*, \quad (14)$$

$$W(\nu) = (1-\sum_{i=0}^{\nu-1} W(i))\int_0^{B_n(A-\nu,Z)} P_\nu(E^*, A-\nu, Z)\, dE^*. \quad (15)$$

Вероятность эмиссии нейтрона с учетом распределения состояний составного ядра по спину I представляется в виде

$$\varphi(\varepsilon, E^*, A, Z) = \sum_I \omega(I, E^*, A, Z)\frac{\Gamma_n(\varepsilon, A, Z, E^*, I)}{\Gamma_n^t(A,Z,E^*,I)+\Gamma_\gamma^t(A,Z,E^*,I)}, \quad (16)$$

где $\Gamma_n^t$ и $\Gamma_\gamma^t$ являются полной и радиационной ширинами соответственно, $\omega$ (I,E*,A,Z) - функция распределения по спину. Парциальная нейтронная ширина определяется выражением

$$\Gamma_n(\varepsilon, A, Z, E^*, I) = \sum_{I'} \rho(E^*-B_n(A,Z)-\varepsilon, A-1, Z, I')\sum_{\ell,j} T_{\ell j}(\varepsilon). \quad (17)$$

Здесь $\rho$ - плотность уровней составного ядра, $T_{\ell j}(\varepsilon)$ - коэффициенты прилипания для нейтронов. Полная радиационная ширина вычисляется по формуле

$$\Gamma_\gamma^t(A,Z,E^*,I) = \int_0^{E^*} dU \sum_{I'} T_\gamma(E^*-U, I')\rho(U, A, Z, I'), \quad (18)$$

где $T_\gamma$ - коэффициент прилипания для $\gamma$-квантов. Полная нейтронная ширина получается с помощью интегрирования парциальной ширины (17) по энергии возбуждения дочернего ядра. Для плотности уровней $\rho$ использовалась формула из работы [9], в которой учтено влияние нуклонных оболочек и парных корреляций. Распределение по спину в формуле (16) принималось таким же, как и распределение по спину для плотности уровней в работе [9]. Коэффициенты $T_{\ell j}$ рассчитывались по оптической модели с параметрами потенциала из работы [10], а коэффициенты $T_\gamma$ вычислялись в предположении дипольного $\gamma$-излучения, как и в работе [11].

Среднее значение энергии возбуждения осколка в выражении (5) принималось пропорциональным средней множественности МНД

$$\bar{E}^*(A,Z,E_K) = \bar{\nu}(A,Z,E_K)(\bar{B}_n+\bar{\varepsilon}+\bar{\delta}) + 1/2\,\bar{B}_n. \quad (19)$$

Здесь $\bar{\nu}$ и $\bar{\varepsilon}$ - средние значения числа и кинетической энергии МНД, которые в расчетах брались из экспериментальных данных, $\bar{\sigma}_n$ и $\bar{\delta}$ - средние по каскаду значения энергии связи нейтрона и поправки на четность в полуэмпирической формуле масс. Такое определение $\bar{E}^*$ дает согласованные значения рассчитанных величин $\bar{\nu}$ с экспериментальными в пределах экспериментальных ошибок. В тех случаях, когда известны экспериментальные значения дисперсии энергии возбуждения $\sigma_{E^*}$, они использовались в расчетах. В противном случае дисперсии энергии возбуждения парных осколков определялись из соотношений

$$\sigma^2 = \sigma^2_{E^*}(A_H, Z_H, \bar{E}^H_K) + \sigma^2_{E^*}(A_L, Z_L, \bar{E}^L_K)$$

$$\sigma_{E^*}(A_H, Z_H, \bar{E}^H_K)/\sigma_{E^*}(A_L, Z_L, \bar{E}^L_K) = \bar{E}^*_H/\bar{E}^*_L, \qquad (20)$$

где $\sigma^2$ - дисперсия кинетической энергии пары осколков, $\bar{E}^H_K$ и $\bar{E}^L_K$ - средние значения кинетической энергии осколков.

Распределение множественности нейтронов для пары осколков рассчитывались в предположении статистической независимости эмиссии нейтронов из парных осколков, поскольку полученные в работе [6] коэффициенты корреляции малы:

$$P_p(\nu) = \sum_{\nu_1}^{\nu} W_L(\nu_1) W_H(\nu - \nu_1). \qquad (21)$$

Полное распределение множественности на акт деления получено с помощью усреднения $P_p(\nu)$ по массовому распределению аналогично (1).

Из изложенного следует, что результаты расчета зависят от выбора необходимых параметров модели, поэтому нами были проведены расчеты с целью выяснения влияния используемых параметров на различные характеристики МНД. В работе [2] проведено сравнение рассчитанных спектров МНД в СЦИ с экспериментальными данными для выделенных масс и кинетических энергий осколков, которое показало, что рассмотренная модель в пределах экспериментальных ошибок описывает спектры МНД без неравновесного компонента. Расчеты [3] показали, что имеется сильная чувствительность вероятности эмиссии нейтронов с E>10 МэВ к вариации параметров начального распределения энергии возбуждения осколков (5).

С целью сокращения машинного времени, расчеты интегрального спектра МНД проводились таким образом, что усреднение по распределению кинетической энергии осколков заменялось выбором параметров начального распределения по энергии возбуждения, соответствующим средним значениям кинетической энергии осколков. На рис. 1 приведены результаты расчета интегрального спектра МНД для спонтанного деления $^{252}Cf$ в форме отношения к максвелловскому спектру с параметром T= 1,42 МэВ в сравнении с данными работы [4]. Средние значения кинетической энергии осколков $\bar{E}_K$, среднего числа нейтронов и средней энергии нейтронов в СЦИ $\bar{\varepsilon}$ взяты из работы [5], а дисперсии кинетической энергии пары осколков $\sigma^2$ и энергии возбуждения легкого осколка из работы [6]. Дисперсия энергии возбуждения тяжелого осколка определялась из первого равенства (20). Из рис. 1 видно, что теоретический спектр идет ниже максвелловского спектра при E<0,5 МэВ и при E>4 МэВ, но в пределах экспериментальных погрешностей хорошо описывает экспериментальные результаты. Аналогичные результаты для случая деления $^{235}U$ тепловыми нейтронами приведены на рис. 2. Здесь данные представлены по отношению к максвелловскому спектру с параметром T= 1,31 МэВ. Экспериментальные данные взяты из работ [7,8]. Параметры $\bar{E}_K$, $\sigma^2$ взяты из работы [9], $\bar{\nu}(A,Z)$ из работы [20]. Дисперсии энергии возбуждения осколков определялись из соотношений (20). С теми же исходными параметрами были рассчитаны рас-

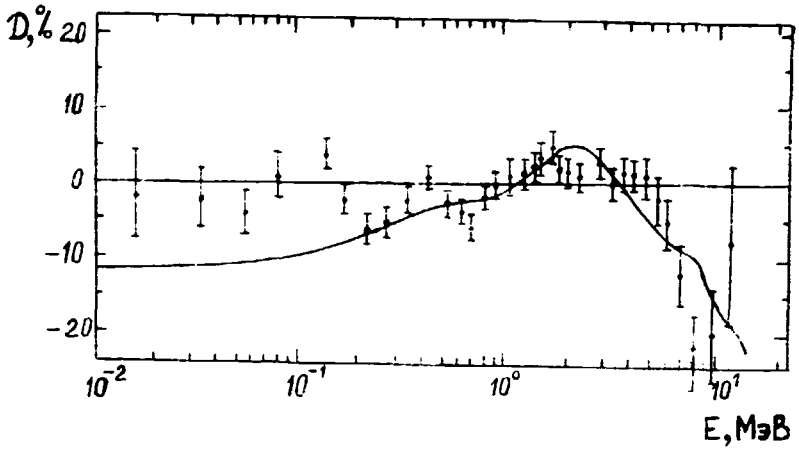


Рис. 1. Расчетный интегральный (сплошная кривая) и экспериментальный спектры (точки) МНД из работы [1] для спонтанного деления $^{252}Cf$ по отношению к максвелловскому спектру с T= 1,42 МэВ.

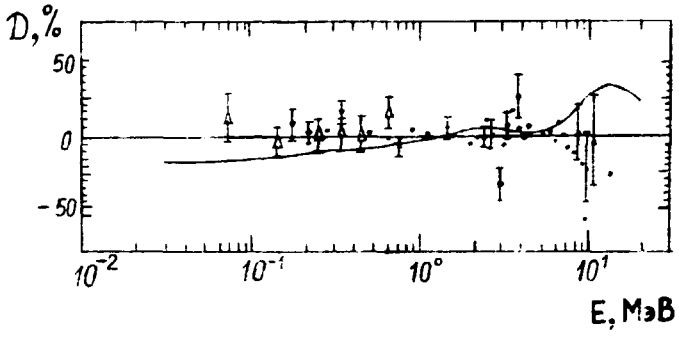


Рис. 2. Расчетный интегральный (сплошная кривая) и экспериментальный спектры МНД (Δ - работа [7], • - работа [8]) для деления $^{235}U$ тепловыми нейтронами по отношению к максвелловскому распределению с T= 1,31 МэВ.

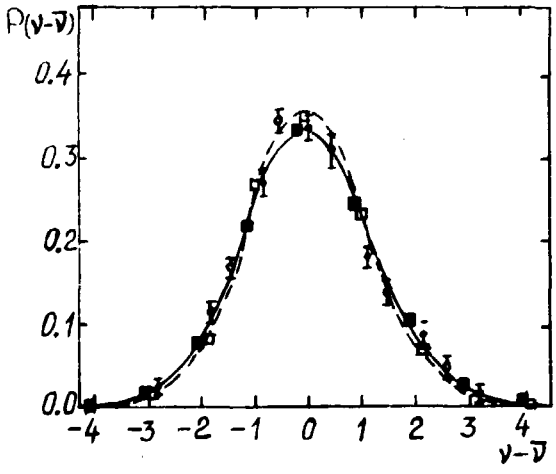


Рис. 3. Распределения множественности МНД: спонтанное деление $^{252}Cf$ (■ - расчет, • - эксперимент [2]), —— гауссовское распределение с расчетным $\sigma_\nu$); деление $^{235}U$ тепловыми нейтронами ( □ - расчет, ○ - эксперимент [2]), - - - - гауссовское распределение с расчетным $\sigma_\nu$).

пределения множественности для двух рассматриваемых случаев, результаты которых представлены на рис. 3 в сравнении с экспериментальными данными из работы [2]. Как видно из рис. 3, рассчитанные распределения множественности МНД хорошо описываются гауссовским распределением с параметрами $\sigma_\nu^2$= 1,46 для спонтанного деления $^{252}Cf$ и $\sigma_\nu^2$= 1,39 для деления $^{235}U$ тепловыми нейтронами.

Проведенное сравнение с экспериментальными данными показывает, что описание характеристик МНД в рамках статистической модели эмиссии нейтронов из полностью ускоренных осколков дает хорошее описание спектров МНД при E<15 МэВ. Наблюдавшийся в работе [8] повышенный выход нейтронов при E>20 МэВ не находит объяснения при статистическом описании при обычных предположениях о характеристиках осколков деления. Таким образом в рамках изложенного метода можно рассчитывать характеристики МНД для низкоэнергетического деления ядер, пока время жизни возбужденных осколков будет больше времени их ускорения. Детальное сравнение расчетов с дифференциальными ха-

рактеристиками МНД может дать возможность более точного определения роли неравновесного механизма эмиссии МНД.

ЛИТЕРАТУРА


1. Горбачев В.М., Замятнин Ю.С., Лбов А.А. - Взаимодействие излучений с ядрами тяжелых элементов. Справочник. М: Атомиздат, 1976.
2. Bowman H., Milton J., Tompson S., Swiatecki W. - Phys. Rev.,1962,v.126,p.2120.
3. Рубченя В.А. - препринт РИ-28, Л., 1974.
4. Кошер В.П., Савельева А.Е., Бихарева С.Б. - Атомная энергия, 1967, т. 23, вып. 4, с. 327.
5. Madland D.G., Nix J.R. - Nucl. Sci. Engng., 1982,v.81,p.213.
6. Märten H., Neumann D., Seeliger D. - Proc. of the IAEA Consultants'Meeting on the $^{252}$Cf fission neutron spectrum. Vienna: IAEA,1983,p.199.
7. Browne J.C., Dietrich F.S. - Phys. Rev.,1974,v. 10C,p.2545.
8. Батенков О.И., Блинов А.Е., Блинов М.В., Смирнов С.Н. - Нейтронная физика, М: ЦНИИатоминформ, 1984, ч. I, с. 339.
9. Игнатюк А.В., Смиренкин Г.Н., Тишин А.С. - ЯФ, 1975, т. 21, с. 485.
10. Becchetti F., Greenlees G. - Phys. Rev.,1969,v.182,N°4,p.1190.
11. Dietrich F.S., Browne J.C., O'Connell W.J., Kay M.J. - Phys. Rev., 1974,v.10C, N°2,p.795.
12. Батенков О.И., Блинов А.Е., Блинов М.В., Герасименко Б.В., Рубченя В.А., Смирнов С.Н. - Нейтронная физика, М: ЦНИИатоминформ, 1984, ч. I, с. 344.
13. Герасименко Б.В., Рубченя В.А. - препринт РИ-183, 1984.
14. Batehkov O.I., Blinov M.V., Boykov G.S., Vitenko V.A., Rubchenya V.A. - Proc. of the $^{235}$U fission cross-sections and on the $^{252}$Cf fission neutron spectrum. Vienna: IAEA,1983,p.161.
15. Пикасайкин В.М., Дытченко П.П., Кудаева Л.С. - ЯФ, 1977, т. 25, с. 723.
16. Nifenecker H., Signarbieux C., Poitou J. - Proc. of the Symposium on Physics and Chemistry of Fission. Vienna: IAEA,1974,v.2,p.117.
17. Bonner T.W., Ferrell R.A., Rinehart M.C. - Phys. Rev.,1952,v.87,p.1032.
18. Cranberg L., Frye G., Nereson N., Rosen L. - Phys. Rev.,1956,v.103,N°[illegible],p.662.
19. Milton J.C.D., Fraser J.S. - Can.J.Phys., 1962,v.40,p.1626.
20. Milton J.C.D., Fraser J.S. - Proc. of the Symposium on Physics and Chemistry of Fission. Vienna: IAEA,1965,v.2,p.39.
21. Terrell J. - Proc. of the Symposium on Physics and Chemistry of Fission. Vienna: IAEA,1965,v.2,p.3.
22. Märten H., Seeliger D., Stobinski B. - Proc. of the IAEA Consultants'Meeting on the $^{235}$U fission cross-sections and on the $^{252}$Cf fission neutron spectrum. Vienna: IAEA,1983,p.195.

# MEASUREMENT AND INTERPRETATION OF DOUBLE-DIFFERENTIAL NEUTRON EMISSION CROSS SECTIONS FROM LEAD AT 14 MEV

T. Elfruth, D. Hermsdorf, H. Kalka, D. Seeliger, K. Seidel, S. Unholzer
Technische Universität Dresden, Sektion Physik, DDR-8027 Dresden

Double-differential cross sections of the neutron emission from nuclei bombarded with 14 MeV neutrons are of increasing importance in connection with fusion reactor developments. The Pb-data have priority 1 in the World Request List /1/.

Emission spectra from Pb were measured with the pulsed-beam time-of-flight spectroscopy at the TUD DT-generator using a flight-path of about 5 m. The scattering arrangement spectrometer and data analysis were described in detail elsewhere /2, 3/. A typical feature of the scattering geometry chosen is the comparatively weak dependence of the incident neutron energy on the scattering angle ($E_0$ = 14.07...14.14 MeV). Cross sections were determined in the emission energy range from 2 to 14.8 MeV for scattering angles from $15^0$ to $165^0$ in steps of $15^0$. The data were corrected for geometrical uncertainties, nonlinearity, detector efficiency and neutron absorption within the scatterer. Multiple scattering corrections are in progress. The later are expected to be small due-to the comparatively small thickness (1 cm) of the ring scatterer. In Fig. 1 the derived preliminary DDCS are presented in a 3-dimensional plot with their statistical error bars. This presentation clearly shows the strong dependence of the angular distributions on the emission energy.

The DDCS at 3.1 MeV, 7,0 MeV and 11.1 MeV are compared with the recent measurement at the Osaka University /4/ as well as with the previous TUD experiment /5/ in Figs. 2, 3 and 4, respectively The figures show a general consistency between these three experiments at high emission energies, whereas remarkable differences occur at lower energies. Except the data point at $15^0$, the new TUD-data show an almost symmetric angular distribution around $90^0$, as it is expected from the dominating reaction mechanism,whereas the Osaka data show a forward-peaking, as it is usually expected for higher emission energies only.

In parallel to the experiments, theoretical calculations were carried out with the code AMAPRE ,6/ taking into-account preequilibrium and equilibrium statistical reaction contributions and with a DWBA code /7/ to calculate direct collective contributions. The code AMAPRE is based on the master equations of the exciton model and, therefore, both preequilibrium and equilibrium particle emission is obtained within the same concept. For preequlibrium angular distributions, the leading particle concept used. Till now the code AMAPRE allows the calculation of emission probabilities for the first nucleon only. Therefore, the spectra of secondary neutrons from (n,2n) processes had to be added. They were calculated with the Hauser-Feshbach code STAPRE /8/. The results of the calculations are inserted in Figs 2 - 4. At low emission energies the calculation reproduces the right order of magnitude of the experimental data as well as the slight asymetry of the angular distribution (Fig. 2). In the intermediate region the experiments are very well reproduced (Fig. 3). At high emission energy, the strong collective enhancement of the $3^-$ octupole vibration state in $^{208}Pb$ is evident.

Finally, the angle-integrated data are compared with calculations in Fig. 5. Again, the dominating influence of collective excitations at emission energies above 8 MeV is evident.

The reasonable description of the whole emission spectrum shows that the most essential reaction contributions are taken into account.

References


/1/ V. Piksaikin, World Request List for Nuclear Data, WRENDA 83/84, IAEA, INDC(SEC)-88/URSF, Vienna 1983

/2/ T. Elfruth et al., Proc. XIII. Internat. Symp. on Nuclear Physics, Gaussig, Nov. 1983, to be publ. by the IAEA

/3/ T. Elfruth et al., ZfK-530, June 1984, p. 13 and p. 14 and
H. Helfer et al., ZfK-530, June 1984, p. 126

/4/ A. Takahashi, OKTAVIAN-Report, A-83-01, June 1983

/5/ D. Hermsdorf et al., ZfK-277(U), 1975

/6/ H. Kalka, Diplomarbeit, TU Dresden, 1984

/7/ A.I. Ignatyuk, V.P. Lunev, priv. comm., 1984

/8/ M. Uhl, B. Strohmaier, Report IRK-76/1, 1976


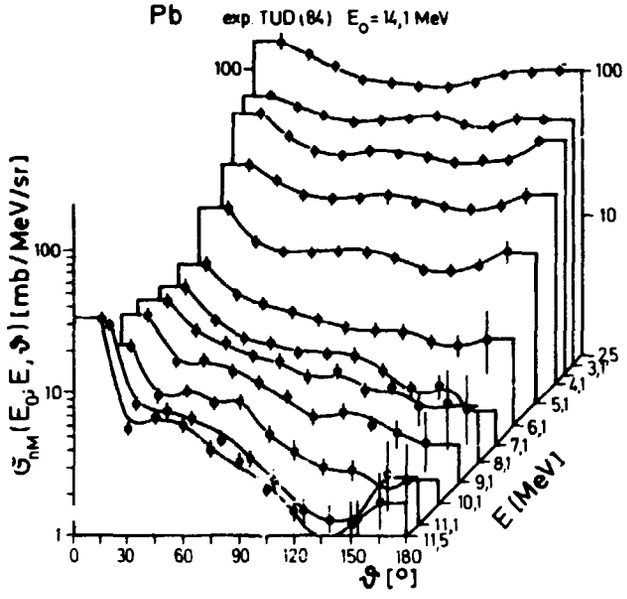


Figure 1

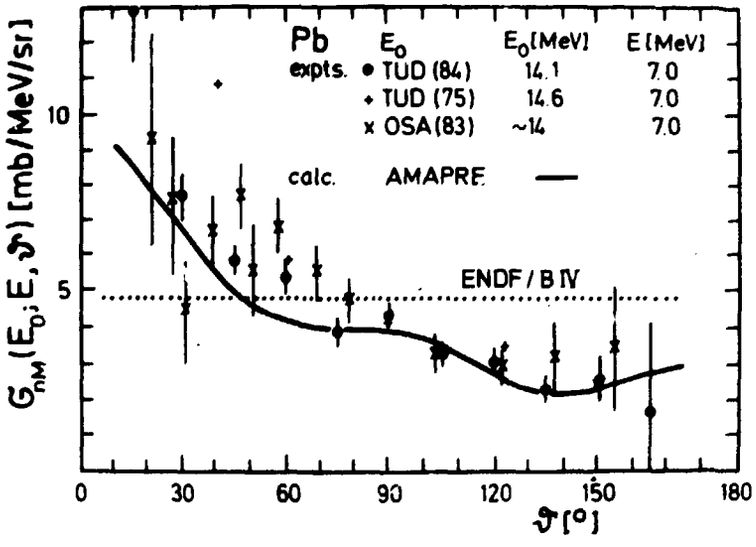


Figure 3

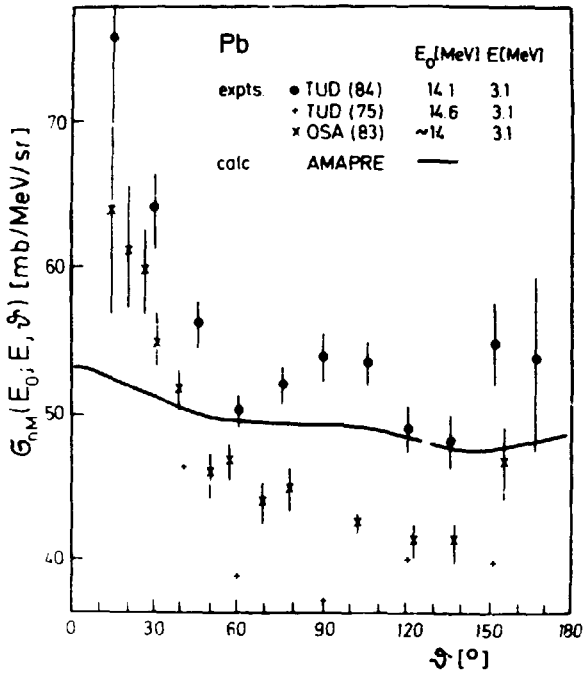


Figure 2

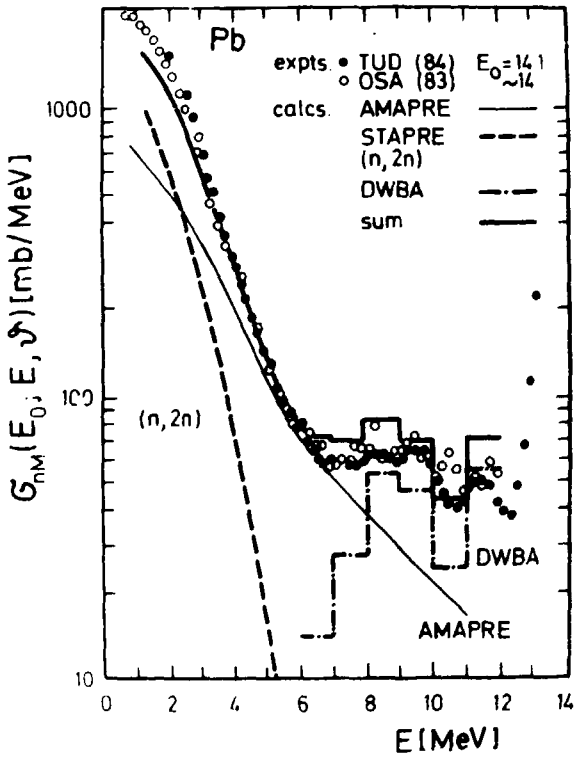


Figure 5

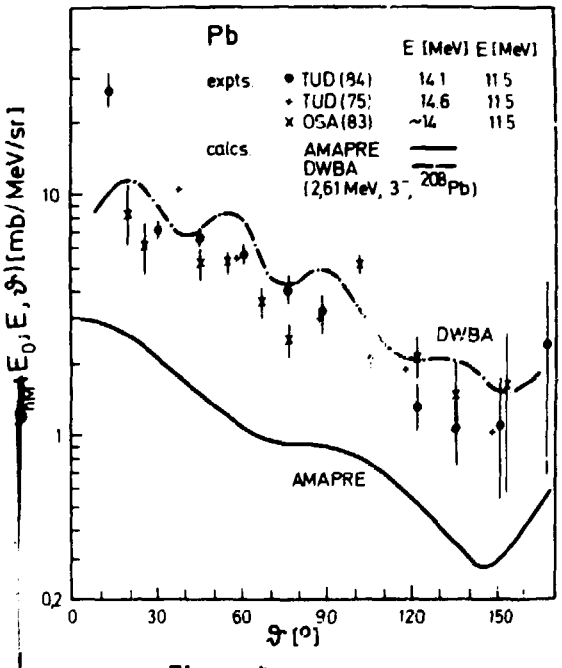


Figure 4

# COMPLEXITY OF ANGULAR DEPENDENCE OF SCATTERED FAST NEUTRONS - CONSEQUENCES AND RECOMMENDATIONS FOR MEASUREMENT AND APPLICATION OF DATA

D. Hermsdorf
Technical University Dresden, Section of Physics, GDR

Abstract

A state-of-art review is given on differential cross sections for fast neutron elastic and inelastic scattering.
Comparing the experimental accuracy achieved at present with data requests further improvements have to be necessarily envisaged in

i) carefully planning of experiments and more accurate raw data processing to reduce systematical errors and correlations;
ii) customers' processing codes to avoid any loss of information or accuracy by use of inappropriate numerical approximations and
iii) the computer-aided data storage format ENDF/B for a convenient representation of all verified factographical informations.

## 1. Introduction

Stimulated by the design and operation of very high intense sources of fast neutrons and their important applications for quite different purposes in technology, medicin, geophysics, biology etc. new demands for more accurate data of fast neutron elastic and inelastic scattering have been obtained. According to this 12.5 % of all data requests compiled in WRENDA 83/84 /1/ concern with angle differential and energy-angle-double-differential cross sections for a correct treatment of neutron transport in extended media including energy degradation and deposition by secondary charged-particles and γ-rays and radiation damage effects.

The experimental certainty achieved at present in very advanced measurements doesn't meet the required accuracy in general. Therefore it seems to be necessary to improve both the experimental technique and the processing of raw data to extract more reliable cross sections.

## 2. Considerations on the experimental accuracy

### 2.1. Uncertainties in measuring techniques and raw data processing for differential neutron scattering cross sections

Neutron scattering experiments have been carried out for nearly all nuclei and elements. However, the measuring technique has been improved and refined to a large extend. Nevertheless, if the data accumulated are compared to the demands for practical applications the inadequacy in accuracy for neutron inelastic scattering cross sections have to be pointed out. This is summarized in table 1

More illustrative than given numbers are examples for the experimental accuracy obtained at present shown in figs. 1, 2 and 3 taking data for elastic and inelastic scattering on $^{208}$Pb from refs. /2-6/.

Table 1: Comparison of requested and achieved accuracy for differential and integrated cross sections of fast neutron elastic and inelastic scattering.

| Quantity | accuracy (averaged) requested (according to /1/) | achieved (in advanced exp.) |
|---|---|---|
| $\sigma_{nn}(E,\vartheta)$ | 5 - 10 % | 5 - 15 % |
| $\sigma_{nn}(E)$ | 3 - 5 % | 3 - 10 % |
| $\sigma_{n,n'}(E,E_i',\vartheta)$ | 10 - 15 % | 15 - 50 % |
| $\sigma_{n,n'}(E,E_i')$ | 5 - 15 % | 10 - 20 % |

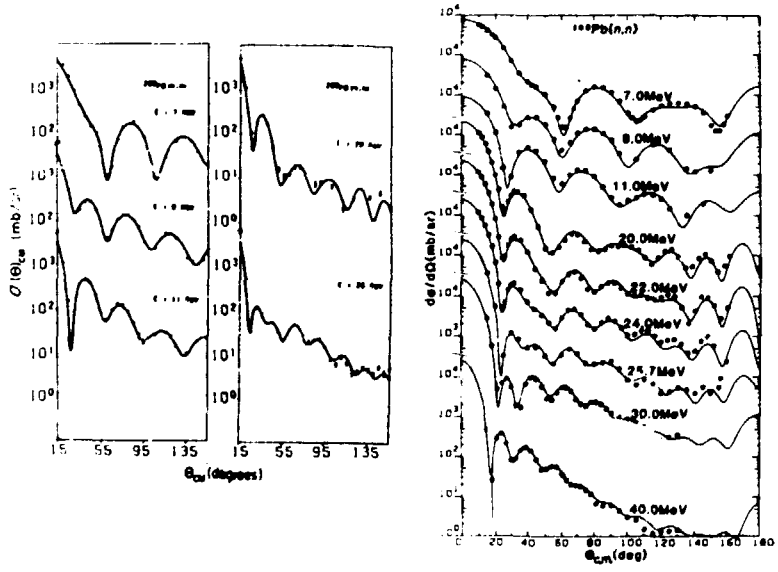


Fig. 1: Elastic scattering cross sections $\sigma_{n,n}(E,\vartheta)$ at different incidence energies E for $^{208}$Pb (taken from /2,3/).

Obviously, more accurate measurements can be performed by improvements of individual parameters of an experimental set-up like following

- optimized effect / background ratio;
- minimizing the overall time resolution;
- counting statistics;
- absolute monitoring;
- use of multi-detector arrangements;
- use of high-precision nuclear standards cross section for normalization or comparative measurements.

Such requirements are self-evident and need no further explainations.

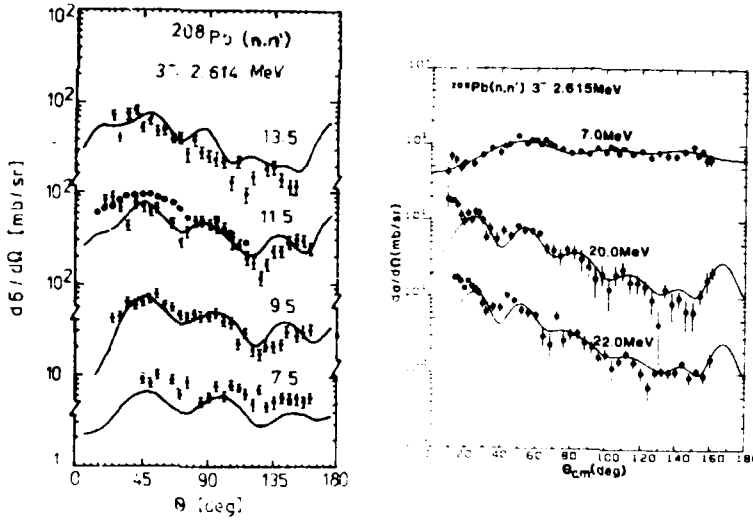


Fig. 2: Inelastic scattering cross sections $\sigma_{n,n_1'}(E,E_1',\vartheta)$ for excitation of the first $3^-$ level in $^{208}Pb$ (taken from /3,4/).

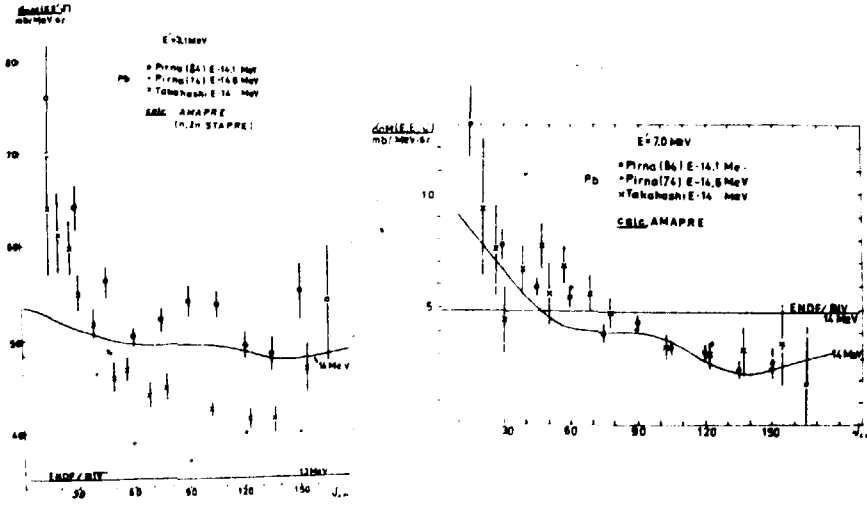


Fig. 3: Inelastic scattering cross section for excitation of level continuum $\sigma_{n,n'}(E,E',\vartheta)$ in $^{nat}Pb$ at emission energies 3 and 7 MeV (data taken from /5/ and /6/).

More crucial problems have to be solved to avoid systematical errors producing correlations as well as in angle and emission energy. Strong correlations between different angles of an angular distribution for a discrete level or between same angles of angular distributions of neighbouring levels can arise from

- incorrect definition of the angle relative to the beam axis; an accuracy of about 0.1 to 0.2° in dependence on the complexity of the angular shape is required for elastic scattering /7/;
- incorrect numerical procedures for peak area subtraction especially for complex (partially overlapping non-resolved) structures /8/;
- finite sample size corrections for discrete levels (generally for elastic scattering).

Strong correlations showing long range effects in neutron emission energy E' for inelastic scattering should be expected from

- inaccurate energy dependences of the detection efficiency $\mathcal{E}(E')$ resulting from either experimental problems in neutron detection (inclusively bias settings and stabilization, particle-γ-discrimination methods, light collection in big detectors etc.) or any calculational model (Monte-Carlo-method usually). At present, an accuracy in the order of 2 - 3 % can be obtained with reasonable effort. Any improvement requires tremendous expenses in both experimental arrangements or calculational models /9/;
- finite geometry corrections including down-scattering of neutrons within the sample. Several more or less sophisticated semi-empirical methods /5,10/ and Monte-Carlo-codes /11/ are in use at present.
  The uncertainty of such procedures can be estimated to be in the order of 3 % or more in dependence on the magnitude of the absolute correction factor.

In contrast to very-well documented and intercompared efficiency codes there is up to now no comparison of the results of different finite-size-correction codes applied on a typically experimental set-up. This should be recommended to get more reliability for a very important correction. All experimental problems should be mentioned here only. Most of them need further more deepened investigations. However, this is not the subject of the paper.

## 2.2. Uncertainties in determination of angle-integrated scattering cross sections

Generally, integral cross sections for elastic and inelastic neutron scattering are obtained by integrating the angular distributions over the solid angle.

The results can be checked partially within nearly the same order of accuracy by integral measurements performed to determine total cross sections $\sigma_{nT}$, non-elastic cross sections $\sigma_{nX}$ as well as neutron emission cross sections $\sigma_{n,n'}$ /12/.

However, the required accuracy of integrated cross sections is higher than for the differential quantities (see table 1). To obtain precise data from more uncertain differential measurements reliable numerical methods for the integration procedure have to be applied. Two main methods are widely in use:

i) fit of experimental data in terms of an Legendre-polynomial series and
ii) adjustment of parameters of nuclear reaction mechanism models by use of experimental data (no necessarily angular distributions only!).

### 2.2.1. Expansion of an angular distribution in terms of Legendre polynomials.

The dependence on the scattering angle $\vartheta$ can be represented by a series of Legendre-polynomials $P_l$ with coefficients $b_l$ according to

$$\frac{d\sigma(E,E',\vartheta)}{d\Omega} = \sigma(E,E',\vartheta) = \sum_{l=0}^{L_{max}} b_l(E,E')\, P_l(\cos\vartheta) \; . \qquad (1)$$

The integration over solid angle yields

$$\sigma(E,E') = 4\pi\, b_0(E,E') \qquad (2)$$

using the orthogonality of the $P_l$'s.

All coefficients $b_l (0 \leq l \leq L_{max})$ have to be extracted from the set of N experimental data $\sigma_i^{exp}$ and their uncertainties $\Delta\sigma_i^{exp}$ applying the $X^2$-method usually

$$\chi^2 = \sum_{i=1}^{N} (\sigma_i^{exp}(E,E',\vartheta_i) - \sigma(E,E',\vartheta_i))^2/\Delta\sigma_i^{exp^2} . \qquad (3)$$

This method is equivalent to a multi-parameter search including all problems of instability (or at least bad convergence conditions) and ambiguities in all parameters (at least strong correlations between $b_o$ and all other ones).

The set of $L_{max}+1$ parameters $b_l$ defined by minimizing the functional equ. (3) have to fulfil some additional conditions which are very helpful to exclude non-physical solutions. Such sensitive constraints are

- $\sigma(0^o)$; for elastic scattering this is equivalent to Wick's limit;
- $b_o$ should be independent on increase in $L_{max}$;
- $\Delta b_o$ should be at a minimal value;
- $L_{max}$ in equ. (1) should have a reasonable value from quantum-mechanical viewpoint; as reliable values may appear for elastic and inelastic scattering to discrete levels:

$$5 \leq L_{max} \leq 25 \text{ for } 2 \leq E \leq 20 \text{ MeV}$$

and for inelastic scattering to the continuum:

$$3 \leq L_{max} \leq 5 \text{ for } 2 \leq E' \leq 20 \text{ MeV}.$$

This procedure had been applied successfully for a great amount of differential data. Problems arise in such cases where

i) the angular range is insufficient to extrapolate as well as to very foreward and backward angles.
Generally, an investigated range

$$20^o \leq \vartheta \leq 160^o$$

can be considered to be sufficient /7/. In other cases any expansion according to equ. (1) diverges with increasing $L_{max}$.

ii) The number of experimental data points N is smaller than the necessary maximum degree $L_{max}$ $(N < L_{max})$ for convergency of the polynomial series.

iii) The number N is larger than the optimal value $L_{max}$ $(N > L_{max})$. A further increase in $L_{max}$ will also reduce $\chi^2$ usually but non-physically (or redundant and intercorrelated) higher-order coefficients $b_l$ are determined according to randomly fluctuating structures in the experimental data set. This is a direct consequence of an over-determination of the system of linear equations in equ. (3).

## 2.2.2. Theoretically based models to integrate differential data

Depending on the mechanism assumed to describe the neutron scattering there exist at least four models

i) the optical model (OM) for shape elastic scattering;
ii) the Hauser-Feshbach-formalism (HF) for compound-elastic and compound-inelastic scattering (to discrete levels and level-continuum also);
iii) the direct reaction models (DI) for inelastic scattering to discrete levels;
iv) the models for multi-step-compound- (MSCR) and multi-step-direct-reactions (MSDR) to describe inelastic scattering to both overlapping and discrete states.

### 2.2.2.1. Neutron elastic scattering

Already simple spherical OM potentials with seven parameters only have been successfully applied to describe experimental data sets in all details (see fig. 1).
For this purpose, several approved computer codes are available /13/. The codes ABACUS-2, ELIESE-2, ELIESE-3, CRAPONE and ECIS stand for several other. More recent OM parameter search codes have been developed but, unfortunatly most of them are unpublished and unavailable (RAROMP, GENOA, OPSTAT).
The application of such qualified models using verified computer codes (which have been checked by international computer code comparisons) provides for automatically correct constraints as $\sigma(0^o)$ Wick's limit) and $L_{max}$.

Unfortunatly, there is no direct way for

- determination of the uncertainty of the integrated cross section;
- determination of the uncertainties and correlations of all other Legendre coefficients $b_l$ $(l > 0)$.

### 2.2.2.2. Neutron inelastic scattering to discrete levels

Some models in use are distinguished according to different approaches for reaction mechanism and complexity of the excited state (collective, microscopic, direct, contribution from statistical modes etc.).

Generally, only a few parameters (deformations, strength of interactive forces) and the optical potential defined by independent data are necessary to obtain a very reasonable agreement in reproduction of the experimental data base.
At incidence energies below 7 - 8 MeV, contributions from compound-reaction mechanism estimated in terms of HF have to be added incoherently to improve the consistency with experimental angular distributions.

The achievable accuracy is fairly well (see fig. 2) but differences really appear caused by

- statistical and systematical errors in the experimental data obtained by different authors (see fig. 2 at 11.5 MeV);
- unexpected from theory pronounced foreward-directed inelastic scattering at higher incidence energies (see fig. 2 at 20 and 26 MeV) /3/.

### 2.2.2.3. Neutron inelastic scattering to level continuum

From experiments /5, 6, 14/ clearly asymmetric angular distributions have been verified for low emission energies already (see fig. 3 for E' = 3 MeV).
This can't be understood in terms of the H-F-formalism and more advanced MSCR models existing now by different modifications of the Exciton models (EM), which predict isotropic angular distributions of particle emission cross sections only.
On the other hand, there are only a few attempts for a practicable formulation of the MSDR /15, 16/. Some models and computer codes (ORION - TRISTAR-1 /17/ have been applied for nucleon-induced reactions around 50 MeV. At lower energies only a quite simple semi-empirical model, the "leading-particle-model" proposed by Agassi, Weidenmüller, Mantzouranis /18/ is able to predict with encouraging agreement the experimental well-established higher-order coefficients $b_l$ $(l > 0)$ (see fig. 4). Some computer codes exist (PRANG, PREM, AMARNE /19/) for calculation of angular distributions of inelastic scattering to the level continuum.
First results of an application of this model around 14 MeV have been published formerly /20/. One fact is of special far-reaching practical importance. The general structure of inelastic scattering cross sections to level continuum is relatively simple and can, therefore, be described with only very few low-order Legendre polynominals.

The first order coefficient (l = 1) is the dominant one which is responsible for the foreward peaking of neutron inelastic scattering cross sections also observed in angular distributions for excitation of low-lying levels (see fig. 2).

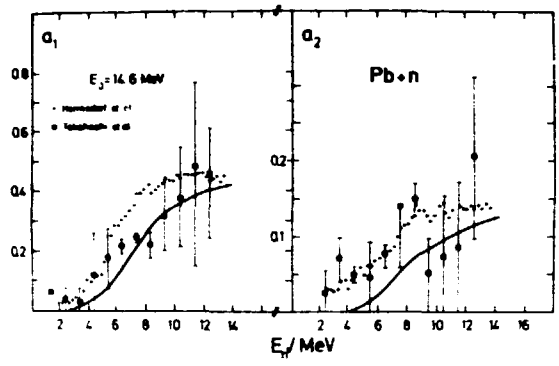


Fig. 4:
Coefficients of an expansion of the neutron emission cross section from Pb at 14 MeV in terms of Legendre polynomials. Experimental data has been taken from /5/ and /14/. Solid lines represent the calculated coefficients from code AMAPRE /19/.

From systematics of such averaged features Kalbach and Mann /21/ have derived a simple semi-empirical formalism to predict the coefficients $b_l$ by

$$b_l(E,E') = \frac{1}{2\pi}\,\frac{d\sigma(E,E')}{dE'}\,\frac{1}{1+\exp(A_l(B_l-E'))} \quad \text{for } l = 2,4,6$$

$$b_l(E,E') = \frac{1+r}{r}\,\frac{1}{2\pi}\,\frac{d\sigma(E,E')}{dE'}\,\frac{1}{1+\exp(A_l(B_l-E'))} \quad \text{for } l = 1,3,5 \qquad (4)$$

and with

$$A_l = 0.036 + 0.0039\,[\,l(l+1)\,]\ /\ \text{MeV} \quad \text{for } l > 0$$

$$B_l = 92.0 - 90.0\,[\,l(l+1)\,]^{-1/2}\ \text{MeV}. \qquad (5)$$

Using experimental data for r (the ratio of direct to total emission reaction mechanism) and the integral emission spectrum, the angular distribution can be estimated with a reasonable accuracy in comparison to most recent experimental data.

## 3. Recommendations for storage and application of angular differential data

### 3.1. Rules and procedures for storage in ENDF/B-format

The procedures and rules defined in ENDF/B-format manual /22/ are an internationally accepted and successfully used method for compact storage of neutron nuclear data.

By convenience in ENDF/B an angular distribution is defined in terms of Legendre polynomials $P_l$ also

$$\frac{d\sigma(E,E',\Phi)}{d\Omega} = \frac{\sigma(E)}{2\pi}\sum_{l=0}^{NL}\frac{(2l+1)}{2}\,f_l(E,E')\,P_l(\cos\Phi) \qquad (6)$$

with a normalised zero-order coefficient

$$f_0(E,E') = 1\ . \qquad (7)$$

Any upwards compatible development necessarily originated by use of data for other purposes than fission reactor calculations have to pay attention also for fast neutron physics data. Several proposals are in discussion /23/.
Having regard to those extensions also, following facts should be pointed out to be restrictive, unmotivated or at least inconvenient for a reasonable representation of fast neutron nuclear data in ENDF/B:

i) the number of Legendre polynomials NL (corresponds to $L_{max}$ in chapter 2) is restricted to $NL \leq 20$

   This is quite too low for elastic and inelastic scattering to discrete levels at energies $E > 14$ MeV and medium or heavy mass nuclei.

ii) the rule that NL should be an even number is of no physics justification.

iii) angular distributions to discrete levels should be given in a $P_l$-representation in the C-M-system. Considering such a lot of coefficients ($NL > 20$) to reproduce correctly an angular shape for elastic scattering, it may be more convenient and more exact to store highly structurized distributions in the $\mu$-representation (probability distribution) provided for data in L-S-system.

iv) for storage of energy-angle-differential data file MF6 is the only acceptable structure. According to a re-activation of MF6 proposed by Mac Farlane et al. /24/ several experiences have been obtained in using this rules. In author's opinion

   - problems my arise from truncation of the polynomial series at NL = 5 for inelastic scattering to discrete levels and
   - it is in contradiction to very fundamental rule of an arrangement of any variable in ascending order that in MF6 discrete level data have to coded first followed by inelastic scattering data to continuum (discontinuity in emission energy E'!).
   - including discrete levels in MF6 as well as the Q-value and the interpolation law (JNT) is questionable.

v) the introduction of a lumped reaction cross section type MT10 /23/ is advantageous but may be changed to a higher condensed type

   MT10 = MT4 + MT103 +...+ MT107 - discrete levels of MT700-series

   from reason of further simplification of data processing by customer's computer codes.

vi) proposals to introduce also covariance matrices for angular distributions in MF34 /23/ seems useful but have to be checked carefully in the next time.

## 3.2. Recommendations for use of angular differential data by customers

However, from customer's viewpoint the complexity of angular distributions is more or less restricted by that type of approximation applied in data processing codes for treatment of a definite problem.

So, neutron transport calculations will be carried out in $S_{16}$ - $P_3$ approximation generally. Comparing this with the investigations pointed out in chapter 2.2 it is really insufficient for any correct simulation of 14 MeV neutron transport.

Therefore, it has to be kept in mind:

i) any truncation of a polynomial series at $l < L_{max}$ result inevitably in falsified cross sections (i.e. partially negative values) and should be avoided carefully.

ii) sometimes not only the angular shape is in question but also their accuracy at any angle point.

Then necessarily the correlation between coefficients which can be determined from experimental data have to be taken into consideration. Because of the rapidly fluctuating Legendre polynomials $P_l$ rapidly destructive or constructive error components will appear from covariances. The total uncertainty is given by

$$\Delta\sigma(\vartheta) = \sqrt{\sum_{l=0}^{L_{max}} \mathrm{var}(b_l)\, P_l^2 + \sum_{\substack{l,l'=0 \\ (l\neq l')}}^{L_{max}} \mathrm{cov}(b_l, b_{l'})\, P_l\, P_{l'}} \qquad (8)$$

The application of equ. (8) preassumes the storage of covariance matrices for angular distributions also.

## 4. Summary

This paper is devoted to demonstrate the necessity of both the accurate evaluation of angular distributions of elastic and inelastic scattering of fast neutrons, their correct and convenient representation in a computer-readable data format and last but not least the very important fact of processing these data without any loss of accuracy and a reasonable effort by customer's computer codes.

Most of the considerations given here are relatively new for standard reactor physics applications. Therefore, having had some intense discussions new aspects should be investigated carefully to substantiate a generalization.

## References


/1/ V. Piksaikin (ed.), WRENDA 84/84, INDC(SEC)-88/URSF, Nov. 1983

/2/ J. Rapaport, T.S. Cheema, D.E. Baimun, R.W. Finlay, J.D. Carson, Nucl. Phys. A296 (1978) 95

/3/ R.W. Finlay, J.R.M. Annand, T.S. Cheema, J. Rapaport, Phys. Rev. C30 (1984) 796

/4/ G. Haouat, Proc. 2nd. Int. Symp. "Neutron Induced Reactions", Smolenice, 1979 p. 333, 1980

/5/ A. Takahashi et al., OKTAVIAN Report A-83-01, 1983

/6/ K. Seidel et al., Proc. XIIIth Int. Symp., Gaussig, 1983, to be published

/7/ T. Wiedling, Nucl. Instr. and Methods 173 (1980) 335

/8/ D. Schmidt, D. Seeliger, Report INDC(GDR)-18/L, 1982

/9/ H. Klein, Report PTB-ND-22, October, 1982

/10/ D. Hermsdorf, K. Seidel, Nucl. Instr. and Methods 112 (1973) 243

/11/ P.E. Koehler, Nucl. Instr. and Methods 224 (1984) 508

/12/ A. Chalupka, G. Staffel, H. Vonach, F. Wenninger, Proc. IXth Int. Symp., Gaussig, 1979, ZfK-410, p. 25, 1980

/13/ A. Prince, in "Nuclear Theory for Application", Trieste, 1979, IAEA-SMR-43, 1980, p. 149

/14/ D. Hermsdorf et al., Report ZfK-277(U), 1975

/15/ T. Tamura, T. Udagawa, D.H. Feng, K.-K. Kan, Phys. Lett. 66B (1977) 209

/16/ R. Bonetti, M. Camnasio, L. Milazzo-Colli, P.E. Hodgson, Phys. Rev. C24 (1981) 71

/17/ T. Tamura, T. Udagawa, M. Benhamon, Comp. Phys. Comm. 29 (1983) 391

/18/ D. Agassi, H.A. Weidenmüller, G. Mantzouranis, Phys. Lett. 56B (1975) 220

/19/ H. Kalka, diploma work, TU Dresden, 1983, unpublished

/20/ D. Hermsdorf, H. Kalka, D. Seeliger, Proc. XIIIth Int. Symp., Gaussig, 1983
D. Hermsdorf, H. Kalka, D. Seeliger, V.A. Ignatyuk, V.P. Lunev, Proc. 6. Int. Conf., Kiev, 1983

/21/ C. Kalbach, F.M. Mann, Phys. Rev. C23 (1981) 112

/22/ R. Kinsey, Report ENDF-102, Revised version, 1983

/23/ O. Schwerer, H.D. Lemmel, Report INDC(NDS)-156/G, April 1984

/24/ R.E. Mac Farlane et al., Report LA-UR-84-1026, 1984

# ANALYSIS BY RADIOACTIVATION USING 14.8 MEV NEUTRONS APPLIED TO EXPLORATION OF MINERAL RESOURCES

Chr.Miron-Gârlea, I.Gârlea, N.H.Roşu, O.Cărutaşu
Central Institute of Physics
76900 Bucharest, P.O.B. MG-6, Romania

A B S T R A C T

This paper presents a relative method of determination contents Nb, Zr and Ti in the geological samples, by 14.8 MeV neutron radioactivation. The quantities about 10 g have been irradiated at the TEXAS-9900 neutron generator of the Institute for Nuclear Physics and Engineering (INPE), Romania. They have been exposed with an absolutely calibrated fission chamber containing $^{238}U$. There were made reference detectors of materials as geological samples. The measurements have been performed by high resolution spectrometry, the both samples and reference detectors being measured in plane-contact. The method supplies the following possibility of detection: minimum content for: Ti up to 0.1%; Zr up to 0.05%; Nb up to 0.02% for an intensity of $10^{10}$ neutrons/s in $4\pi$.

## 1. I N T R O D U C T I O N

The determination of the content Zr, Nb and Ti in the geological samples rises the following problems:

- the natural complex of sample gives at exposure a complicate gamma spectrum, which has numerous gamma lines interfering;
- the samples contain very little amounts of the interesting elements (compared with the geological material);
- the reaction cross sections with thermal neutrons of these are small.

These reasons dictated the utilization of a fast neutron source [1] for irradiations.

## 2. METHOD DESCRIPTION

The interesting elements Zr, Nb and Ti have reactions of type (n,2n) and (n, p) with relative important cross sections [2] at 14 MeV. They lead to radioactive isotopes with life-time convenient for measuring and with well-known decay schemes, which permit gamma measurements. For these determinations of content has been chosen the following reaction:

$$^{90}Zr(n, 2n)^{89}Zr$$

with the cross section 0.786 b [1] and $T_{1/2}$ = 78.4 hours. The decay scheme is one given in reference [3] and the energy of used gamma line is 909.1 keV.

For Nb has been chosen the following reaction:

$$^{93}Nb(n, 2n)^{92}Nb$$

with the cross section 0.512 b [1] and $T_{1/2}$ = 10.2 days. The measured gamma line is that of 934 keV. For these elements have been obtained reasonable activities at the intensities available at the INPE neutron generator.

At the examination of the samples appeared the possibility of Ti determination by the reactions:

$^{47}Ti(n, p)^{47}Sc$ (cross section = 0.116 b, gamma line 159 keV)
$^{48}Ti(n, p)^{48}Sc$ (cross section = 0.053 b, gamma lines 983 keV)
1037 keV)
1311 keV)

They have $T_{1/2}$ = 3.4 days and respectively 43.7 hours.

In this relative method the both samples and a sealed fission chamber containing $^{238}U$, Saclay type [4], have been exposed. This fission chamber was used as neutron flux monitor. Our reference detectors, containing pure elements, have been exposed in the same conditions. Taking into account the well-known formula for activity calculation at the exposure in a neutron flux [5] and that there were the same conditions of measuring for the reference detectors and samples one can write:

$$m_s = \frac{A_{sat\ s}}{A_{sat\ r}} \times \frac{RR_r}{RR_s} \times m_r \qquad (1)$$

where:

$m_s$ - the exposed sample mass
$m_r$ - the reference detector mass
$A_{sat\ s}$ - the saturation activity for sample
$A_{sat\ r}$ - the saturation activity for reference detector
$RR_s$ - the reaction rate of fission chamber for sample exposure
$RR_r$ - the reaction rate of fission chamber for reference detector exposure .

The samples have been irradiated in the plastic capsules, with 30 mm diameter, 15 mm hight and 0.5 mm wall thickness. All capsules have been filled with powder, containing about 10 g. The irradiations have been performed with these capsules put on the window screen of the neutron generator and the fission chamber was placed on the sample. The spectrometry measurements [6] have been made by means of a Ge-Li 100 $cm^3$ crystal, in plane contact.

The reference detectors have been prepared in pure materials, with certified content. They have been exposed in the same conditions as the tested samples. After the exposure, the well-known ammounts of the reference materials have been homogeneously mixed with nonexposed geological material in order to obtain the identical conditions of measuring. This operation permitted to avoid the gamma self-absorption-in-sample correction [7].

## 3. RESULTS

The results are presented in Table I. There are given the used reactions the activities at the saturation for all formed isotopes, the sample and reference detector mass. The reference detectors are identified as NBY, ZR and TI. There are also given the reaction rates of the fission chamber-monitor for each exposure.

The geological samples which have been tested contained Al and Fe. These elements impeded us to perform the measurements in the first three days after the exposure , by the reactions:

$^{56}Fe(n, p)^{56}Mn$ $T_{1/2}$ = 2.6 hours
$^{27}Al(n, \alpha)^{24}Na$ $T_{1/2}$ = 15 hours.

Their gamma lines had high intensity and produced an important background.

In the Table I there are also given the associated errors for gamma activities. They are given by:

the error in background substraction for gamma peak areas;
the statistics and instrumental errors;
the weighting error
the error in determination of fission rates by means of fission chamber.

In Table II there are presented the concentrations in percents for tested geological samples and their associated errors. The incertitudes are principally generated by gamma line interference produced by the elements from the geological matrix.

TABLE II. Sample concentration

| Sample identification | Concentration (%) Zr | Nb | Ti |
|---|---|---|---|
| ZRO2 | 0.321 (± 2.5%) | | 3.152 (± 1.9%) |
| ZRO5 | 0.187 (± 3.6%) | | 2.093 (± 2.1%) |
| ZRO6 | 0.119 (± 5.8%) | | |
| ZRO9 | 0.021 (± 5.0%) | | |
| ZRO12 | 0.031 (± 5.4%) | | 0.309 (± 4.1%) |
| ZRO13 | 0.047 (± 4.7%) | | 0.503 (± 3.8%) |
| NB1 | 0.430 (± 1.6%) | 1.543 (± 1.7%) | 0.447 (± 2.3%) |
| NB2 | 0.424 (± 1.6%) | 1.400 (± 3.0%) | 0.461 (± 2.7%) |

The intensities available in this moment at INPE neutron generator permit a minimum content determination up to :

0.02% for Zr
0.05% for Nb
0.10% for Ti.

R E F E R E N C E S

1) I.Gârlea et al. - Revue Roum.Physique, No.5, p.45, Bucharest (1984)
2) S.M.Qaim - Handbook of Spectroscopy, vol.III, CRC Press, Florida (1981)
3) W.Zijp, J.Baard - Nuclear Data Guide for Reactor Neutron Metrology, EUR 7164EN (1981)
4) A.Fabry, I.Gârlea - Techn.Rev. IAEA-208, vol.II, p.291 Vienna (1978)
5) K.Bekurtz, K.Wirtz - Neutron Physics, Springer Verlag Berlin (1964)
6) I.Gârlea et al. - Studii şi Cercet.de Fizică, 30, No.10, Bucharest (1981)
7) I.Gârlea - Doctor Thesis, INPE - Bucharest (1979).

Table I. The saturation activities

| Identification | Mass (g) | Activities $^{90}Zr(n,2n)$ 909 keV | $^{93}Nb(n,2n)$ 934 keV | $^{48}Ti(n,p)$ 983 keV | 1037 keV | 1312 keV | Reaction rates |
|---|---|---|---|---|---|---|---|
| ZRO2 | 10.163226 | 2.401E2(±2.1%) | | 5.033E2(±1.3%) | 4.711E1(±1.4%) | 3.821E1(±1.5%) | 20.637±1.3% |
| ZRO5 | 11.478805 | 7.131E1(±3.5%) | | 2.287E2(±1.6%) | 2.154E2(±1.2%) | 1.758E2(±1.5%) | 12.579±1.4% |
| ZRO6 | 9.740030 | 1.067E1(±5.4%) | | 2.159E1(±3.4%) | 2.064E1(±2.4%) | 1.758E1(±3.4%) | 3.489±2.1% |
| ZRO9 | 9.673473 | 9.238E0(±3.6%) | | | | | 17.367±1.3% |
| ZRO12 | 7.852491 | 9.555E0(±5.2%) | | 2.055E1(±3.5%) | 1.849E1(±3.6%) | 1.490E1(±3.8%) | 10.836±1.6% |
| ZRO13 | 9.529585 | 1.486E1(±4.4%) | | 3.394E1(±3.3%) | 3.125E1(±3.3%) | 2.522E1(±3.3%) | 9.195±1.8% |
| NB1 | 9.229075 | 4.081E2(±1.2%) | 6.347E2(±1.4%) | 9.126E1(±1.9%) | 8.373E1 (±1.9%) | 6.923E1(±2.1%) | 28.884±1.0% |
| NB2 | 9.691500 | 2.775E2(±1.1%) | 2.281E1(±2.8%) | 6.490E1(±2.3%) | 6.010E1(±2.4%) | 4.861E1(±2.2%) | 18.930±1.2% |
| NBY | 0.135710 | | 3.965E2(±0.9%) | | | | 18.930±1.2% |
| TI | 2.895250 | | | 3.348E3(±0.7%) | 3.208E2(±0.5%) | 2.644E3(±0.4%) | 15.511±1.4% |
| ZR | 0.373063 | 2.748E2(±0.8%) | | | | | 20.637±1.3% |

NOTE: The masses of reference detectors (NBY, ZR, TI) is given in grames of pure element.

# NEUTRON CROSS SECTIONS MEASURED AT 14.8 MEV

Dr.I.Gârlea, C.Miron-Gârlea, H.N Roşu, M.Ion, V.Răducu
Central Institute of Physics, R76900, P.O.Box MG-6, Bucharest,
ROMANIA

Abstract

The integral cross sections for some reactions induced by 14.8 MeV neutron have been measured at the TEXAS 9900 neutron generator in the Institute of Nuclear Physics and Engineering (INPE). The tested reactions are $^{95}Nb(n,\alpha)^{90m}Y$, $^{90}Zr(n,2n)^{89}Zr$, $^{59}Co(n,p)^{59}Fe$, and $^{64}Zn(n,p)^{64}Cu$. Some before studied reactions have been also tested, using the same targets: $^{93}Nb(n,2n)^{92}Nb$ and $^{59}Co(n,2n)^{58}Co$. The cross section of $^{56}Fe(n,p)^{56}Mn$ reaction has been measured in order to verify the used method of measurement. The used reference cross section is that of the $^{238}U(n,f)$ reaction and it is 1.23 b. The flux monitoring has been performed by means of the fission chambers. A Ge-Li crystal and the associated electronics have been used for the absolute reaction rate determination.

## 1. *Introduction*

The needs of the nuclear data related to the technology of the fast reactors and fusion systems have given a strong impulse at the researches for the obtaining of the reaction cross sections in the range of high energy neutrons. In the frame of the international work sponsored by Nuclear Data Section of the International Atomic Energy Agency, the measurements at 14 MeV are performed under TC/INT Project and Coordinated Research Programme (CRP). This article presents the measurements performed under CRP (Research Contract No. 3818/RB).

## 2. *The cross Section Determination*

The exposures of the Nb, Zr, Zn, Co and Fe activation foils have been made at the INPE TEXAS-9900 neutron generator[1]. There were irradiated both the activation foil and a plate sealed fission chamber, Saclay type. The fission chamber deposit contains $^{238}U$ and it is absolutely calibrated [2], the calibration incertitude being 2.4%. The run to run monitor level system has three plate fission chambers (Ø 12 mm), placed at 120° arround the generator tube [1]. These chambers have been also calibrated in the same spectra: ΣΣ - ITN [3] and Thermal Standard Spectrum [4]. The monitor deposits contain $^{238}U$. The measuring procedure using fission chambers is given in the reference [5]. For the neutron flux monitoring has been used the method proposed in the paper [1].

The main operation characteristics of the neutron generator are:

- high voltage: 120 kV
- current: about 800 μA
- intensity: in the range $3.5 \times 10^9$ - $1.5 \times 10^{10}$ neutrons/s.

Thritium targets have Mo backings of 0.4 mm thickness. Ti deposits have about 1 mg/cm$^2$ thickness. The incident neutron energy was 14.8 MeV.

The absolute reaction rates have been measured by means of Ge(Li) crystal (100 cm$^3$) calibrated in the absolute efficiency [6]. The crystal resolution is 2.98 keV. The sample-crystal distance is 5 cm, for these measurements. The processing of the gamma peaks was made by means of SAMPO code [7], mounted on the PDP-15 computer. The used nuclear constants are given in the references [8,9].

The results are given in Table I. The cross sections measured at the INPE neutron generator are presented together the errors. The associated errors include:

- statistics and instrumental errors;
- uncertainties in the fission chamber deposit calibration;
- weighting error;
- error in background subsraction at gamma peak processing.

In the same table are also given some values indicated in the references (10,8), for comparison.

References

1) I.Gârlea et al - Int.rep. IRNE-RI-1388 (1983)
2) A.Fabry, I.Garlea - Techn.Rep. IAEA-208, vol.II, p.291, Vienna (1978)
3) I.Gârlea et al - Rev.Roum.Physique, No.2, 22 (1977)
4) I.Gârlea - Doctor Thesis, INPE-Bucharest (1979)
5) J.Grundl et al - Nuclear Technology, vol.25 (1975)
6) I.Gârlea et al - Studii Cercet.Fizică, 30, No.10 (1981)
7) J.T.Routti - UCRL 19452 (1969)
8) S.M.Qaim - Handbook of Spectroscopy vol.III, p.141, CRC Press, Florida (1981)
9) W.Zijp, J.Baard - Nuclear Data Guide for Reactor Neutron Metrology, EUR 7164EN (1981)
10) Edt.S.M.Qaim - Progress Rep. on Nuclear Data Research in FRG, Jülich, NEANDC-252U, vol.5 (1984).

Table I. The cross sections obtained at 14.8 MeV

| Reaction | Half live of product | E (keV) | η (%) | Cross sections (mb) This work | Cross sections (mb) Previous works |
|---|---|---|---|---|---|
| $^{93}Nb(n,\alpha)^{90m}Y$ | 3.19 h | 202.5<br>492.5 | 96.5<br>90.0 | 5.8 ± 0.3 | 5.5 ± 0.5 [8] |
| $^{93}Nb(n,2n)^{92}Nb$ | 10.16 d | 934.5 | 95.5 | 517 ± 37 | 512 ± 46 [8] |
| $^{90}Zr(n,2n)^{89}Zr$ | 78.4 h | 909.1 | 99.0 | 725 ± 44 | 768 ± 78 [8] |
| $^{59}Co(n,2n)^{58}Co$ | 70.8 d | 810.7 | 99.45 | 748 ± 52 | 720 ± 50 [8] |
| $^{59}Co(n,p)^{59}Fe$ | 44.6 d | 1099.3<br>1291.6 | 55.5<br>44.1 | 50.3 ± 3.4 | 73 ± 10 [8]<br>46.5 ± 2.3 [10] |
| $^{64}Zn(n,p)^{64}Cu$ | 12.8 h | 511 | 37.0 | 167 ± 14 | 160 ± 12 [8] |
| $^{56}Fe(n,p)^{56}Mn$ | 2.6 h | 846.6 | 99.0 | 111 ± 7 | 98 ± 7 [8]<br>111 ± 5.5 [10] |

# FAST NEUTRON SOURCES FOR THERAPY

J. Vincour and P. Bém
Nuclear Physics Institute, Czechoslovak Academy of Sciences,
250 68 Řež u Prahy, Czechoslovakia

The fast neutron beams and their sources for the therapy facilities should have the following properties:

1. Mean energy higher than 10 MeV in order to achieve a penetration equivalent to that of $^{60}$Co gamma range, low attenuation and scattering in the body. On the contrary, from the viewpoint of RBE it is desirable that the neutron energy lower than 10 MeV.

2. Intensity greater than $2.10^{11}$ n.sr$^{-1}$.s$^{-1}$ which corresponds to the dose rate at least 0.1 Gy.min$^{-1}$ at patient's position /~80 cm from the target/ for the treatment time per fraction not to exceed 10 minutes.

3. Adequate energy spectrum.

4. Small target spot /<2.5 cm/.

5. Suitable angular distribution of the neutrons emitted from the source. An anisotropic angular distribution is preferable.

Neutrons with such properties are produced only in the nuclear reactions on light nuclei with light ions accelerated on electrostatic linear accelerarors /the Cockroft-Walton or Van de Graaff types with maximum accelerating voltage of 600 keV/ or on cyclotrons [1].

Nearly monoenergetic neutrons in a wide energy range from 0.1 MeV to 25 MeV can be obtained by the reactions $^{3}$H/d,n/$^{4}$He, $^{1}$H/t,n/$^{3}$He, and $^{2}$H/t,n/$^{4}$He. The $^{3}$H/d,n/$^{4}$He reaction is most frequently used on the low energy accelerators. The neutron yield from the d-$^{3}$H reaction is limited by the power dissipation and by the tritium target life time. The reactions of tritium ions with hydrogen isotopes seen very promising. For example the $^{1}$H/t,n/$^{3}$He reaction [2] has a high cross section /650 mb for 6 MeV tritium laboratory energy/, it gives monoenergetic neutrons in wide energy range /up to 25 MeV/ and has a pronounced forward angular distribution which is very convient from the viewpoint of neutron shielding. At the same time the power dissipated in the target is 70-times lower as compared to d-$^{3}$H reaction for the same neutron yield.

The neutron beams of continuous energy spectrum are produced in the reactions $^{2}$H/d,n/$^{3}$He, $^{7}$Li/d,n/$^{8}$Be, $^{9}$Be/d,n/$^{10}$B, $^{7}$Li/p,n/$^{7}$Be and $^{9}$Be/p,n/$^{9}$B. The reactions of protons and deuterons with $^{9}$Be-nuclei are those most commonly used for producing therapy neutrons on cyclotrons owing to the properties of Be-target /high melting point and heat conduction, chemical indolance and mechnical stability/. Generally speaking, the reactions induced by protons are more advantageous than those by deuterons at the same cyclotron, it is due to

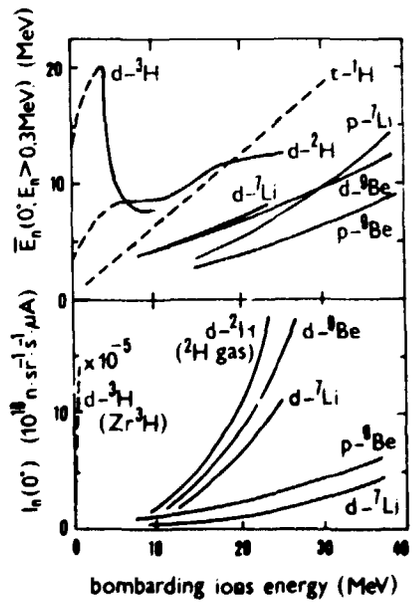


Fig.1. Average energies and intensities of the neutron beams emitted at 0° from the thick target in different reactions.

the fact that the proton as well as the neutron energies is roughly twice as high and also because the influence of the three-body break-up on the neutron energy is lower.

The average energies and the intensities of the neutron beams emitted at zero reaction angle from the thick target in different reactions as functions of bombarding ions energies are shown in fig.1. The dashed lines correspond to monoenergetic neutron sources. A surway of the parameters of neutron generators which have been used for therapy as well as those of the intensive neutron installations that are under construction is given in tab.1. The parameters of the facilities producing neutrons for therapy on the cyclotrons are given in tab.2. The intensive fast neutron sources in Czechoslovakia, listed also in tab.1 and 2., are used for nuclear physics and radiobiological studies rather than for radiotherapy.

Tab.1 Parameters of the d-$^3$H neutron sources for therapy

| Type | Laboratory | $U_d$/kV//$I_d$/mA/ | $F_n$/n.s$^{-1}$/ | $\dot{D}$/Gy.min$^{-1}$/ | Beam |
|---|---|---|---|---|---|
| RTNS-I | Lawrence Liver. Lab. | 400/20 | $6.10^{12}$ | 0.08/125cm | |
| RTNS-II | Lawrence Liver. Lab. | 400/150 | $4.10^{13}$ | | |
| INS TTF | Los Alamos | 180/200 | $10^{13}$ | | |
| INS | Los Alamos | 300/1000 | $10^{15}$ | | |
| Las. selen. | Washington | | $10^{14}$ | | |
| | Chalk River | 300/25 | $10^{13}$-$10^{12}$n.cm$^{-2}$s$^{-1}$ | | |
| DYNAGEN | NASA Lew. R. C. | 300/30 | $4.10^{12}$ | | isocentr |
| | Sandia N.L. | 200/200 | $10^{12}$ | 0.10/80cm | |
| " | Sandia N.L. | 200/4000 | $10^{13}$ | | |
| | Oak Ridge N.L. | 300/15 | $10^{15}$ | | |
| | Univ. Wisconsin | 200/14 | $1.3.10^{12}$ | 0.02/125cm | |
| | LBL Berkeley | 200/450 | $8.10^{12}$ | | |
| HILETRON | | 150 | $6.10^{11}$ | | isocentr |
| | | | | 0.01/125cm | |
| DYNAGEN | Hamburg | 500/8;5 | $2.3.10^{12}$ | 0.15/80cm | isocentr |
| | Julich | 200/1500 | $6.10^{13}$ | | |
| KARIN | Karlsruhe | 200/150 | $5.10^{12}$ | 0.20/85cm | isocentr |
| | Heidelberg | | | | |
| Lancelot | Valduc | 160/200 | $6.10^{12}$ | | |
| PHILIPS | Amsterdam | 280/8 | | 0.02/125cm | |
| DNO | Rijswijk | 270/6 | $0.6.10^{12}$ | 0.01/125cm | |
| | Manchester | | | | |
| | Glasgow | | | | |
| | Grenoble | | | | |
| SAMES 150 | Inst. Dozimetry,Prague | 150/2.5 | $10^{11}$ | | |
| | Inst. Physics,Bratislava | 300/10 | $10^{12}$ | under construction | |

Tab.2. Parameters of the facilities /cyclotrons,linacs/ for neutron therapy

| Type | Laboratory | React. | $E_i$/MeV//$I_i$/μA/ | $\bar{E}$/MeV/ | $\dot{D}$/Gy.min$^{-1}$/ | Beam |
|---|---|---|---|---|---|---|
| Lin. accel. | Fermilab. Batavia, | p-Be | 66 | 25 | | |
| TAMVEC | Houston | d-Be | 50 | 19,3 | | |
| NRL/HANTA | Washington D.C. | d-Be | 35 | 14,3 | | |
| NASA/CLANTA | Cleveland | d-Be | 25 | 10 | | |
| | Berkeley | p-Be | 42 | | | isocentr |
| | Univ. Washington | d-Be | 12 | 8 | | |

| Type | Laboratory | React. | $E_i$/MeV/ $I_i$/μA/ | $\bar{E}$/MeV/ | $\dot{D}$/Gy.min$^{-1}$/ | Beam |
|---|---|---|---|---|---|---|
| | Univ. Chicago | d-$^2$H | 8.3/180 | 6 | 0.30 | |
| Lin. accel. | FMIT Brookhaven N.L. | | | | | |
| | HEDL+LASL, Los Alamos | d-$^7$Li | 35/200mA | 15 | $\dot{I}$=2.10$^{16}$n.sr$^{-1}$.s$^{-1}$ | |
| | H.G.Hospital, Detroit | d-Be | 50/10 | | 0.7C/183cm | isocen. |
| MRC | Hammersmith, London | d-Be | 16 | 7 | | |
| MRC | Edinburg | d-Be | 15/100 | 6 | 0.43/125cm | isocen. |
| | Orléans | p-Be | 34 | | | |
| CGR | Buc | d-Be | 35 | | | isocen. |
| | C.Ant.Lacassaque,Nice | d-$^7$Li | 30 | | 0.04μA | |
| | Heidelberg | d-$^2$H | 11/40 | | | |
| | Essen | d-Be | 14.5 | | | |
| CYCLONE | Louvian | d-Be | 50 | | | isocen. |
| | Car Town | p-Be | 66 | | | |
| NIRS | Chiba | d-Be | 30 | 12 | 0.45 | |
| IMS | Tokyo | d-Be | 15 | 6 | 0.20 | |
| U-120 | Nucl.Phys.Inst.Dresden | d-Be | 12.5 | 6.2 | | |
| U-120 | Inst.Physics, Krakow | d-Be | 12.5 | 6.2 | | |
| U-120 | Inst. Physics, Kiev | d-Be | 13.6/30 | 6 | 0.24 | |
| | | d-$^2$H | | 11.5 | 0.09 | |
| U-120M | Nucl. Phys. Inst. Řež | d-Be | 20/10 | 7 | 0.09/125cm | |
| AN 2500 | Univ. Karlova, Praha | p-,α | 3.5/200 | | | |

References:


1. P. Bém, J. Vincour, F. Veselý: Produkce rychlých neutronů v jaderných reakcích na izochronním cyklotronu U-120M, ÚJF ČSAV, Report, listopad 1980.
2. M. Drosg: Proposal of a Novel High Intense Neutron Source of Radiation Therapy, Z. Physik A - Atoms and Nuclei 298,297/1980/.